NASA Space Engineering Research Center
for Utilization of Local Planetary Resources

Annual
Progress Report
1988-89

Director: T. Triffet Principal Investigators: K. Ramohalli, J. Lewis

UNIVERSITY OF ARIZONA
4717 E. Ft. Lowell Rd./AML
Tucson AZ 85712
TEL (602) 322-2304 FAX (602) 326-0938

TABLE OF CONTENTS

Page

III. SYSTEMS OPTIMIZATION

IV. DATA BASE DEVELOPMENT

OMIT ?
P-1-1

EXECUTIVE SUMMARY

EXECUTIVE SUMMARY

Consistent with the statement of work in the original proposal to NASA, several projects were begun in 1988. This report covers the progress on these projects and other accomplishments for the period from August 1988 through February 1989. The work planned for the period from March 1989 to March 1990 is also described.

All of the tasks outlined in the proposal were considered during one meeting of the NASA Technical Representative Committee and two meetings of the SERC Advisory Committee held at the Center. Based on advice from these committees and extensive discussions between the Center Director and the two Principal Investigators, those listed in the Table of Contents were selected, and their selection formalized through an internal summary document listing specific goals, measurable results, and faculty as well as student level of effort.

Though categorized as Propellant Processing, Material Properties, Systems Optimization, or Data Base Development, these projects actually represent beginning work in a number of distinct but closely related disciplines: (1) propellant and propulsion optimization, (2) automation of propellant processing with quantitative simulation, (3) ore reduction through chlorination and free radical production, (4) characterization of lunar ilmenite and its simulants, (5) carbothermal reduction of ilmenite with special reference to microgravity chemical reactor design, (6) gaseous carbonyl extraction and purification of ferrous metals, (7) overall energy management, and (8) information management for space materials processing. All yielded sufficiently promising results to recommend continuation during 1989-90.

Additionally, low levels of effort were devoted to the development of anhydrous cementing and construction materials from lunar soils, and to molten metal-molten salt separation research. The first of these has been redirected to feature melt binding methods and high purity iron characterization, the second to feature solvent extraction with recyclable organic chelating agents.

The technical highlights of the 1988-89 work are:

1. Extensive performance calculations for unconventional propellant combinations.
2. Evolution of a quantitative methodology for Figure-of-Merit (FoM) calculations for various space mission scenarios.
3. Design and construction of the process control hardware in one propellant processor.
4. Development of the fundamental criteria for automatic control of propellant processors.
5. Demonstration of significant gains through plasma processing of ores.
6. Demonstration of the relative merits of carbothermal reduction of ores.
7. System development for gaseous carbonyl extraction and purification research.
8. Proof-of-principle delineation of pinch technology for energy management.

Details of this work and other developments are provided in the following sections. Though still in its initial stage, the program has already made significant progress toward the overall goal of exploiting extraterrestrial resources for space missions (see Figures 1.1 and 1.2).

Several combinations of unconventional propellants were shown to have acceptable performance in the light of launch mass reductions. One specific propellant processor was acquired and automation procedures started; both hardware and software are under development. The systems analysis mission optimization program, even in its present simplistic configuration featuring a popular spreadsheet interfaced with an expert system, yielded valuable insight into the tradeoffs involved in performance and earth-transported resources. The chlorination processing of ores has shown promise in terms of rates and compactness of hardware, while pointing up the potential of free radical production. The carbothermal task group has not only evolved a flowsheet process model, but also built much of the equipment necessary to implement it on a laboratory scale. The carbonyl task group has made similar progress and placed orders for the required equipment. The "pinch technology" concept evolved by the energy management group promises to maximize the use of available energy.

To support the above and future work of the Center the following specialized items of equipment were acquired: (1) a variable ionization mass spectrometer, (2) a Baker-Perkins propellant processor, (3) an Inframetrics color-coded video with dedicated processor, (4) an IBM-compatible data acquisition and processing system, together with appropriate NASA (LeRC), Air Force, and industry propellant performance software.

A computing and communications network featuring high performance workstations (currently SUN 386i, IBM PS2/80, MACII) accessible to all investigators through ethernet links was also established at Center Headquarters. Transparency to SUN, VAX, MAX, and IBM systems is being stressed. Plans were also completed to install a microwave link between the University's local and national network and the Center's off-campus facility to facilitate more general access.

Another highlight of the startup program was the large number of distinguished visitors, most of whom came and presented seminars at no expense to the Center. Widespread faculty interest was generated and several high-quality students joined the program, due in no small measure to these seminars.

Twelve graduate students, including three women and four ethnic minority students, were supported during this period, and many applications for future participation were received--partly as a result of the seminars, and partly from the wide distribution of a flyer and poster describing the Center's mission.

Following the recommendation of the NASA Technical Representative Committee, an attempt was made to promote cooperation with other NASA SERCs. In terms of programmatic emphasis, those Centers that have the closest relation to our own are the ones at the Pennsylvania State University (space propulsion), University of Cincinnati (monitoring of rocket engine performance), and University of Colorado (space construction). A Program Coordination Task Group was initiated and a first meeting held at the Center which was attended by representatives of these Centers, as well as representatives from the Los Alamos National Laboratory, the Space Sciences Institute, and the California Space Institute.

It is perhaps worth noting that during this initial period of operation, well over two-thirds of the total direct-cost funding received from NASA was expended on support of the projects listed in the Table of Contents, together with nearly the same proportion of the matching funds received from the University of Arizona. Since all faculty investigator salary allowances and graduate fellowship stipends are included, preserving this ratio is believed to be the most effective way to maximize return on investment, both in terms of space processing research and space infrastructure development.

Several new projects are planned for 1989-90; these include:

1. Determination of Lunar Ilmenite Abundances From Remotely Sensed Data (R. B. Singer, Lunar and Planetary Laboratory)
2. Continuous Monitoring of the Lunar or Martian Subsurface Using On-Board Pattern Recognition and Neural Network Processing of Rover Geophysical Data (C. Glass and B. Sternberg, Mining and Geological Engineering Department)
3. Detection of Water on Near-Earth Asteroids (L. A. Lebofsky, Lunar and Planetary Laboratory)
4. Analysis of Near-Earth Asteroids and Cometary Cores (T. Gehrels, Lunar and Planetary Laboratory)
5. Production of Solar Reflectors From Lunar Materials for Solar Power in Space (R. J. Thibeault, Science Applications International, San Diego)

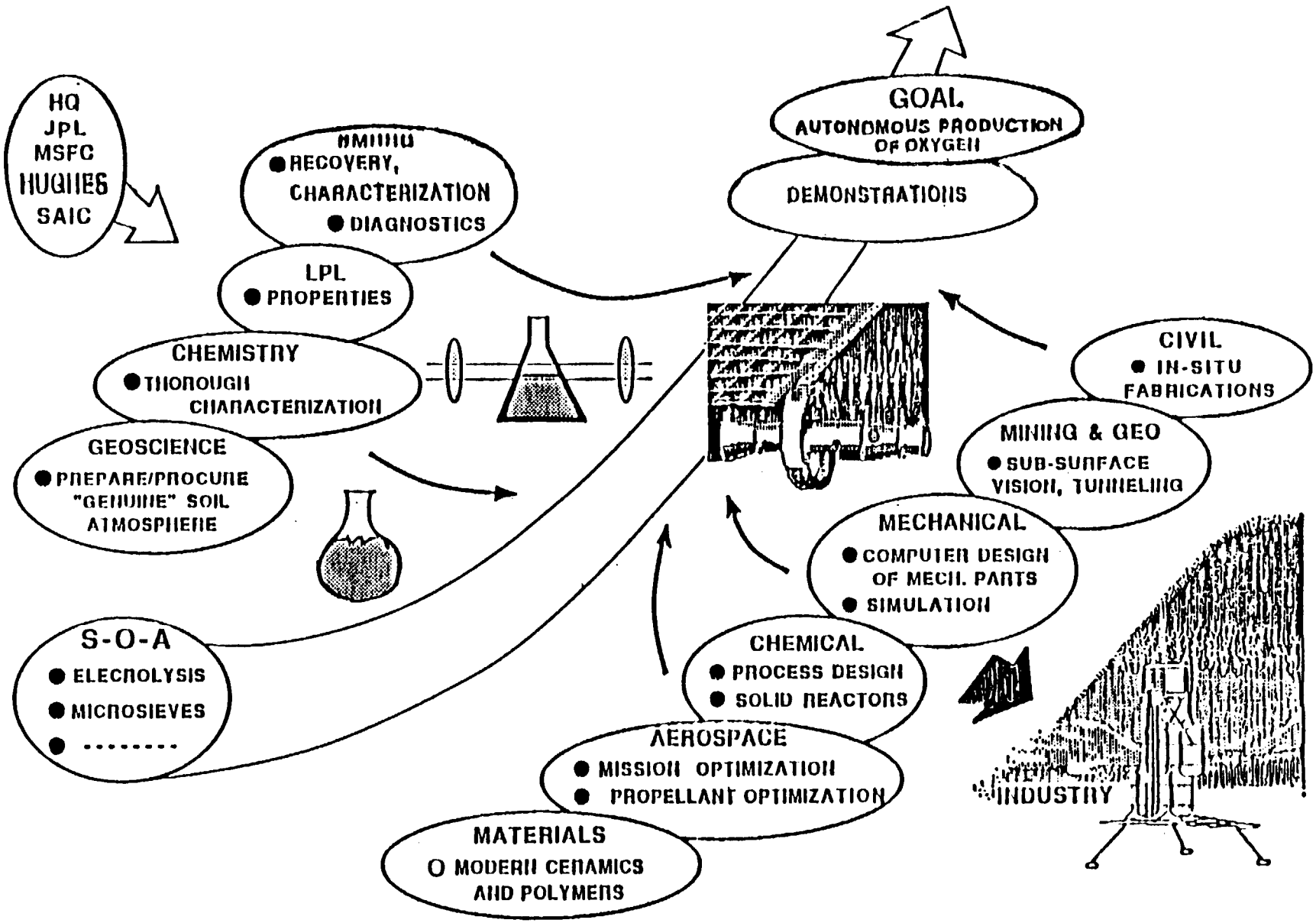

Figure 1.1. One concrete example.

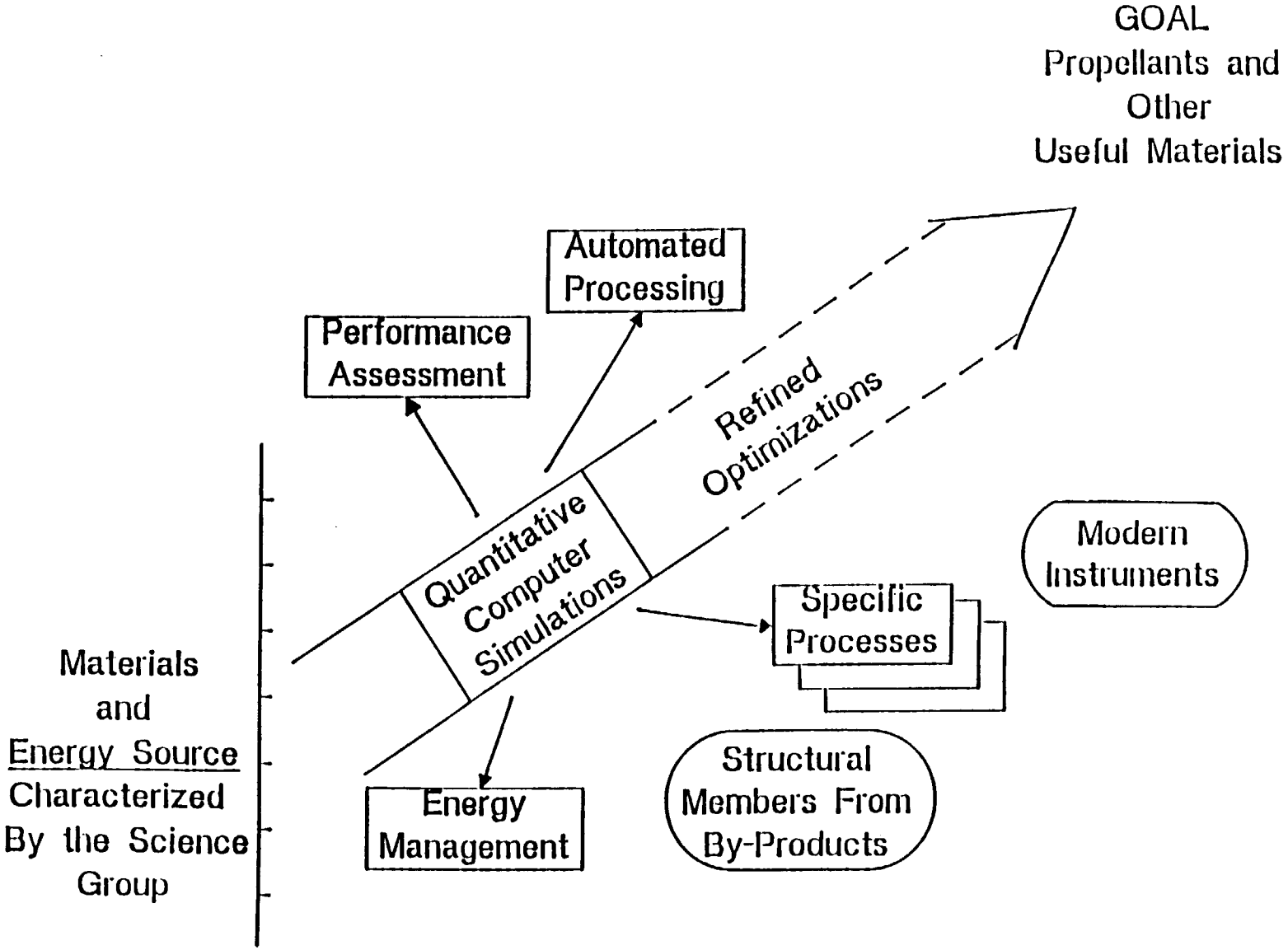

Figure 1.2. Engineering tasks.

I. PROPELLANT PROCESSING

Proof-of-Concept Automation of Propellant Processing

K. Ramohalli and P. Schallhorn
Department of Aerospace and Mechanical Engineering
The University of Arizona

Abstract

For space-based propellant production, automation of the process is needed. Currently, all phases of terrestrial production have some form of human interaction. A mixer has been acquired to help perform the tasks of automation. We have designed, built, and installed a heating system to be used with the mixer. Tests performed on the heating system verify design criteria. An IBM PS/2 personal computer has been acquired for future automation work. It is hoped that by the end of the next academic year, the mixing process itself will be automated. This is a concept demonstration task--proving that propellant production CAN be automated reliably.

Introduction

The research work deals with the autonomous production of propellants. Because 80% to 90% of a spacecraft's weight is propellant, it is advantageous to produce propellants in strategic locations en route to, and at, the desired mission destination. This will then reduce the weight of the spacecraft and the cost of each mission. Since one of the primary goals of the space program is safety, a totally automated propellant production system is desirable. This system would thereby eliminate the need for the constant human intervention currently required in production of many propellants. This enables the exploration of space to be more than the search for, and production of, propellants. As a proof-of-concept demonstration, one specific case was chosen for this study--composite propellant production; the principle is more important than the application.

Background

Currently, composite solid propellant production is done with constant human intervention. Using a control room, man has total control over all aspects of the propellant production. This is fine on Earth, but it is too costly in space. Thus, the need for automated composite propellant production exists.

Approach

We are currently completing testing of a heating system, which was designed by the student (Paul Schallhorn), for the one-pint mixer that is to be used for this project. Because composite propellant production requires mixing the ingredients at two

constant temperatures (160 and 140°F), a self-contained water-heating system is required for space-based operation. Such a system is shown in Figure 1.1. This system provides the required temperatures and only needs an electric power source to drive the pump motor and heat the water heaters. This is not unrealistic considering that electricity is also required for the mixer and controlling computer.

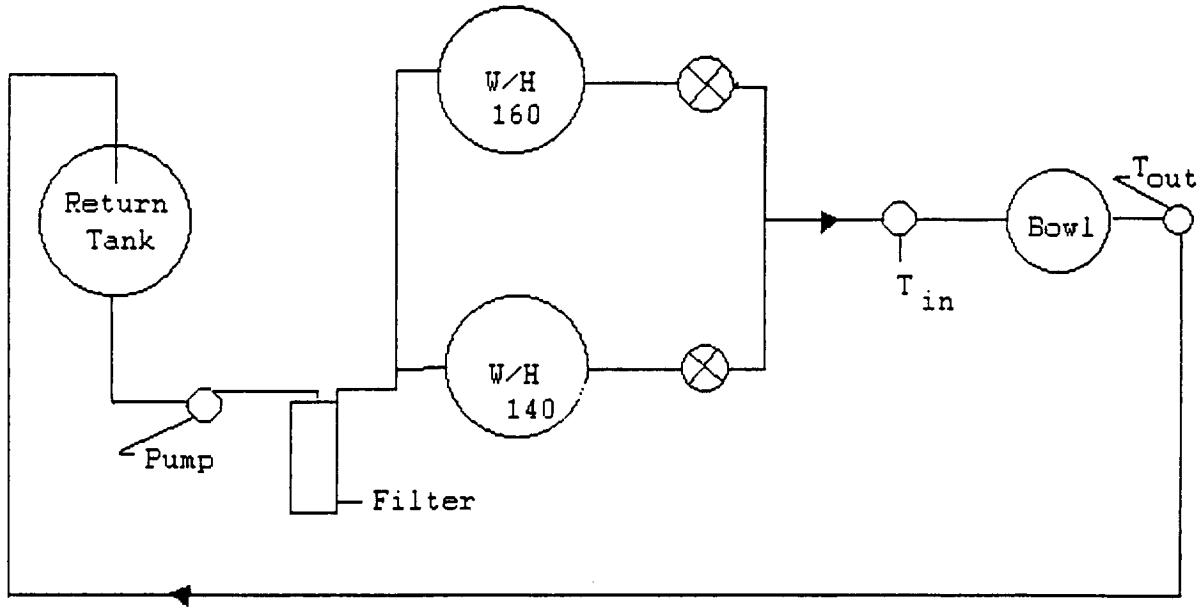

Figure 1.1. The heating system.

One approach, therefore, is to use a personal computer to control the introduction and mixing of the composite propellant ingredients to the mixer (making sure that temperature is constant on the walls of the bowl, detecting local "hot spots" within the mixture, and taking in-situ measurements of the viscosity of the mixture to check if it is within an acceptable range). Then, pump the mixture, via computer programs, into a cast which will be placed in an oven for curing and then stored for future use.

Results to Date

The major results to date are as follows:

1. A used Baker-Perkins PX-2 mixer was acquired; this introduces a factor of 6 cost reduction (see Fig. 1.2 for the complete mixer setup). A heating system was required for its operation.
2. In September 1988, Schallhorn designed the heating system to be used for the mixer (see Fig. 1.1). It was determined that the minimum volumetric flow rate for the heating system for a 1-degree temperature drop acrosss the mixer

operating at steady state was 2.5 gallons per minute. Therefore, we selected a pump with a volumetric flow rate of 4.4 gallons per minute to ensure a negligible temperature drop across the mixer bowl. Since only two temperatures are needed, it was logical to have two separate reservoirs, each at one of the required temperatures. We chose to have both reservoirs be hot water heaters. Because we only had 120-volt a/c power available, we had to choose the most efficient heater size on the market. As we began to search for heaters for the project, it was discovered that the same heating element was commonly used in different-sized 120-volt water heaters. This made it clear that for maximum water heating, the smaller the water heater, the more advantageous. That was the basis for the selection of two 10-gallon water heaters (see Fig. 1.3). The system uses distilled water to eliminate the possibility of scale buildup in the system. To further ensure the cleanliness of the water in the system, a filter is placed in the system immediately following the pump (see Fig. 1.4).

3. Acquisition of the components of the heating system was begun in October 1988. By the middle of November, all of the components were in and the heating system was assembled.
4. Initial verification of the temperature profile of the heating system was begun in December 1988. Verification of the heating system continued through March 1989, including verification of flow rate and the time required to heat the system from a cold start.
5. In August 1988, research was begun to determine which personal computer to purchase for this project. By the end of September, an IBM PS/2, Model 80 was selected, with an Intel 80386 microprocessor operating at 20 MHz, a 115-megabyte hard disk drive, and 2 megabytes of RAM. The computer was ordered at the end of September, along with the following peripherals: a 14-inch monitor, a 80387 math coprocessor, a modem, a 5.25-inch external diskette drive, additional memory, a mouse, and a Hewlett Packard Laserjet II printer. Due to shipping problems from IBM, the computer did not arrive until late in January, and the peripherals did not arrive until early February. By the middle of February, the computer system was operational. This computer system will be used on various other NASA Center projects, also.

Summary and Future Work

In summary, this task strongly suggests that there is a need for automated production of propellants for space-based propellant production. We have also seen

ORIGINAL PAGE
BLACK AND WHITE PHOTOGRAPH

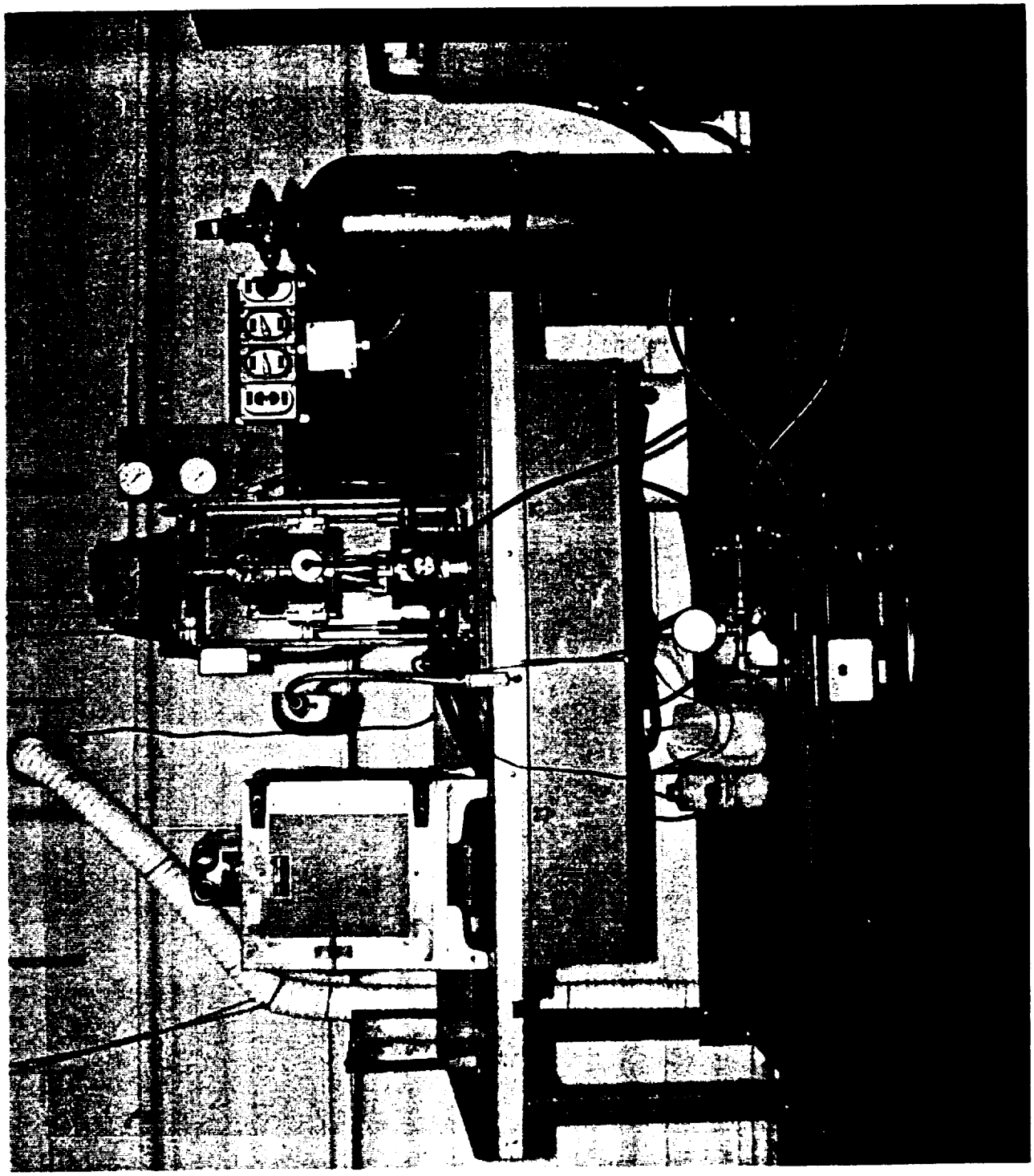

ORIGINAL PAGE
BLACK AND WHITE PHOTOGRAPH

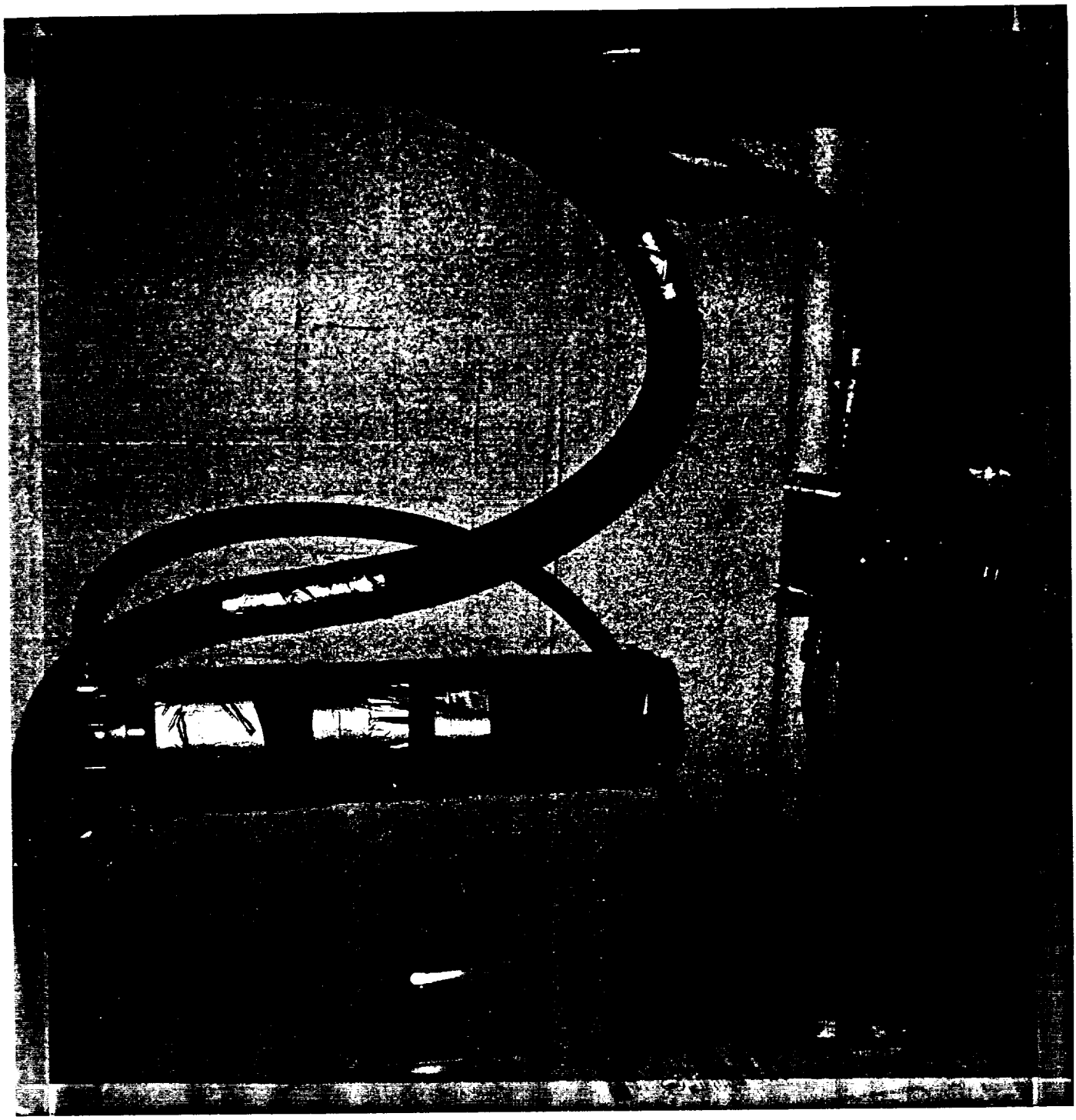

that there is no current system to produce composite propellants without human intervention. A mixer has been acquired to help perform this task. We have designed and built a heating system to be used in conjunction with the mixer to maintain constant mixing temperature. The heating system has been, and is continuing to be, tested under operational conditions for design verification. We have acquired an IBM PS/2 personal computer for the computer portion of the automation.

For the 1989-90 academic year, the student plans to begin his Ph.D. research, which will consist of the actual automated propellant production. During the year, we will begin to automate the mixing process itself. It is hoped to have the computer control the addition of each ingredient from a "hopper" (yet to be built) to the mixer at required times and have the computer control the mixing of the ingredients for the required amount of time. We also plan on building and installing the in-situ viscosity measuring device for future integration into the automation system.

Acknowledgments

We would like to take this opportunity to thank University of Arizona technician Gary Hopkins for his help in assembling the heating system. We would also like to acknowledge Richard Wilson, who is doing the automatic controls portion of the heating system.

Extraction of Volatiles and Metals From Extraterrestrial Ores

J. S. Lewis
Lunar and Planetary Laboratory
The University of Arizona

During the start-up phase of this project, we have concentrated upon planning our laboratory efforts for the second fiscal year. The principal motivating purpose of our work has been to identify extraterrestrial materials, processes, and products associated with the production of propellants in space, including the most complete possible conversion of the feedstocks for propellant production into useful products with the minimum feasible expenditure of energy. We have tentatively identified and are beginning laboratory research on several processes that promise very large increases in the mass of useful products at the cost of only modest increases in energy consumption. Processes for manufacturing propellants then become processes for making propellants plus metals and refractories. It is the overall yield of useful materials per unit expended energy that matters, not simply the yield of propellants.

Three tasks have been undertaken to date:

1. *Literature search and compilation of a dBase III data base on space materials processing.* This work is being done mainly by an undergraduate, Leo Masursky, with many of the references being supplied by graduate students working for various SERC projects. The data base is roughly half finished. Completion of the data base is expected this summer. Thereafter, a low level of effort should suffice to keep it current. The data base is designed with numerous subject flags to permit efficient searches on any of a large number of subjects. This is the heart of a computerized annotated data base to be prepared by Dr. Andy Cutler. Andy has assisted us in the design of the data base.
2. *Gaseous carbonyl extraction and purification of ferrous metals.* This work is being carried out principally by a graduate student, Mike Nolan, and Professor Lewis. Our activities during the first fiscal year have been concentrated on planning and equipment design of our carbonyl apparatus. Orders have gone out for a number of crucial components of the gas system. Renovations of the lab space have been completed, and the lab is now occupied. The gas line is being designed to have the capability of mixing several gases in precisely measured proportions, including both carbonyls and inert carrier gas (nitrogen or argon); compressing the mixtures to a presssure of 10 atmospheres; and regulating temperatures over the range 0 to 250°C. We have also drawn up plans for extraction experiments on native meteoritic metal alloys, magnetic separates from lunar fines, cathode metal

deposits from the lunar magma electrolysis scheme (Haskin), and the byproduct elemental iron from reduction of lunar ilmenite (Shadman).

3. *Characterization of lunar ilmenite and its simulants.* This work is the principal responsibility of a graduate student, Melinda Hutson. During the past year, she has completed a literature search on the chemical and physical properties of lunar and meteoritic ilmenite and of schemes for beneficiation of ilmenite from lunar regolith (see Appendix A). Certain achondritic (basaltic) meteorites contain either large crystals or large concentrations (not both) of ilmenite which has a chemical composition similar to, but not identical with, lunar ilmenite. The meteoritic ilmenite is free of ferric iron, the component of terrestrial ilmenite whose presence invalidates its use as a lunar simulant. Museum catalogs have been examined to identify the best sources for the most promising meteorites, and samples are on order. Experiments will be conducted by Shadman on lunar, synthetic, and meteoritic ilmenite to determine which, if any, are satisfactory kinetic and thermodynamic simulants of real lunar ilmenite. With Joaquin Ruiz, we are preparing a proposal for Apollo 17 lunar regolith samples to be used in studying the physical properties of lunar ilmenite and in designing and testing beneficiation schemes for extraction of ilmenite from typical lunar feedstocks.

Production of Oxygen From Lunar Ilmenite

F. Shadman and Y. Zhao
Department of Chemical Engineering
The University of Arizona

Abstract

The overall objective of this project is to develop a novel carbothermal reduction process for production of oxygen from lunar ilmenite. The specific objective is to use a reaction sequence in which a wide variety of carbonaceous compounds (including carbonaceous wastes) can be used as reducing agents. During the first phase of this work, two reactor systems were designed, constructed, and operated to investigate the fundamentals of the reactions important in this process. One system is a small fluidized bed, and the other is a thermo-gravimetric reactor system. Preliminary experiments on synthetic ilmenite are conducted to study the effect of carbon type, carbon loading, temperature, and gas flow rate. Results indicate that a reaction path based on carbon gasification can be employed to promote the overall kinetics. A unique temperature and concentration-programmed reaction procedure is being developed for rapid parametric study of the process.

Introduction

Oxygen is a consumable material which needs to be produced continuously in most space missions. Its use for propulsion, as well as life support, makes oxygen one of the largest volume chemicals to be produced in space. Production of oxygen from lunar materials is of particular interest and is a very attractive possibility.

There is a significant amount of oxygen on the moon, although very little is readily available as water or gaseous oxygen. The only practical source of oxygen on the lunar surface is igneous materials, which contain typically 40-50% oxygen as oxides. Minerals present in these rocks include ilmenite (the most abundant opaque material in lunar rocks), anorthite, and olivine. The igneous rocks have been pre-crushed to form regolith, the lunar equivalent of soil, by meteoritic bombardments. This reduces the need for crushing and simplifies the mining and separation problem greatly.[1,2]

Extraction of oxygen from iron oxide present in lunar ilmenite is of particular interest because it is energetically more favorable than extraction from silicon, aluminum, titanium, calcium, or magnesium oxides. Iron oxide reduction is also attractive because of its potential for producting iron as a co-product. A number of processes have been suggested for oxygen production from ilmenite in lunar regolith. Table 1.1 shows a list of these processes. Most of these processes require imported

reagents to be recycled in the process. Therefore, low loss per mass is a critical factor and requirement for process feasibility.

Table 1.1. Selected proposed processes.

Hydrogen reduction
Low-temperature carbothermal reduction
Slagging (high-temperature) carbothermal reduction
Slag electrolysis
Leaching: Fluoroacid
HCl
Caustic
Carbo-chlorination
Vaporization/rapid quenching, arc electrolysis, plasma reduction, alkali metal thermal cycling, vapor-phase pyrolysis, etc.

Among the proposed processes, the hydrogen and carbothermal reductions of ilmenite appear very promising. Hydrogen reduction has a relatively simple process configuration; the individual steps are relatively well studied. However, the major problem is the large heating and cooling loads required to condense the water and then heat the hydrogen to its reaction temperature. Handling and storage of large amounts of hydrogen is also a problem. Hydrogen reduction of lunar ilmenite has been studied by several investigators.[3] Carbothermal reduction of terrestrial ilmenite has also been extensively studied, but the application to lunar ilmenite is still an open area for investigation.[4]

Even though a considerable body of literature has been published on various aspects of the reduction of terrestrial ilmenite, the mechanism of transformation and the rate-controlling step in the overall reduction have not been clearly established. Most studies on terrestrial ilmenite show that both hydrogen reduction reactions take place in two main stages. In the first stage, the ferric iron component of the ilmenite was rapidly reduced to ferrous iron. In the second stage, which was much slower than the first stage, the ferrous iron was reduced to the metallic state. During the carbothermal process, terrestrial ilmenite starts to react at about 860°C at the contact points between the reactants. Up to 1020°C, solid-state reduction appears to be the main reaction mechanism, while above this temperature, a rate increase has been observed and has been contributed to a change in the mechanism to a gaseous reduction of ilmenite by

regenerated CO.[5,6] It has been reported that the reaction rate between synthetic ilmenite and graphite is increased significantly by the addition of ferric chloride, which promotes the nucleation of iron, and is decreased by the addition of rutile.

The above mechanisms and the available kinetic information are not directly applicable to lunar ilmenite, which is very different from terrestrial ilmenite in both physical and chemical properties. Moreover, the emphasis in reduction of terrestrial ilmenite has been on metal oxide recovery and not on oxygen production. However, the existing technical background on carbothermal processing of terrestrial ilmenite indicates that its application to lunar ilmenite should be pursued. In comparison with the hydrogen reduction, the carbothermal process has a more complicated flow configuration, but is energetically more favorable, and can potentially use a wide variety of carbonaceous compounds as reducing agents. A comparison of the primary features of the carbothermal and hydrogen reduction processes can be made using Tables 1.2 and 1.3.

Table 1.2. Hydrogen reduction.

Advantages
Simple flow sheet
Relatively well-known chemistry
Continuous operation
Disadvantages
Low hydrogen utilization
Problems in hydrogen transport, handling, and storage
High heating/cooling demand
No useful co-products (low integration value)
Key Research Areas
High-temperature water dissociation
High-temperature ceramic membranes
Sensitivity to the physical and chemical properties of the feed
Process design

Table 1.3. Carbothermal reduction.

Advantages
Known technology for terrestrial ilmenite
Available carbonaceous makeup
Almost 100% utilization of carbon
Useful co-products (high integration value)
Ease of carbon transport, storage, and handling
Disadvantages
More complex flow sheet
More solid handling in continuous operation
Key Research Areas
Reaction kinetics and mechanism for lunar ilmenite
Ceramic membranes application
CO_2 reverse fuel cell
Sensitivity to the physical and chemical properties of the feed
Process Design

Objectives

The overall objectives of this study can be described as follows:

- Study of the mechanism and kinetics of carbothermal reduction of simulated lunar ilmenite; determination of the rate-limiting steps; investigation of the effect of impurities, particularly magnesium; search for catalysts suitable for enhancement of the rate-limiting steps.
- Development of new reduction methods which are based on the use of a waste carbonaceous compound as a carbon source for the process; development of a novel carbothermal reaction path which utilizes gasification of a carbonaceous solid for reducing gaseous species (hydrocarbons and carbon monoxide) to facilitate the reduction reaction kinetics and make the process more flexible in using various forms of carbonaceous feeds.
- Development of advanced gas separation techniques, including the use of high-temperature ceramic membranes.
- Development of an optimized process flow sheet for carbothermal reduction and comparison of this process with the hydrogen reduction scheme, as well

as a general comparison with other leading oxygen production schemes; use of new and advanced material processing and separation techniques.

Method of Approach

In the first phase of the work, the emphasis has been on the development of experimental methods for studying the kinetics and mechanism of reduction of simulated lunar ilmenite. The experimental facilities and procedures are summarized below.

Experimental Apparatus. Two reactor systems have been designed, fabricated, and put into operation during the past 9 months: A mini-fluidized bed reactor for quick response times and a thermo-gravimetric reactor system with an electronic microbalance for the continuous measurement of rate and sample conversion. Schematic diagrams of these two reactor systems are given in Figures 1.5, 1.6, and 1.7. The components of these two reactor systems are described below.

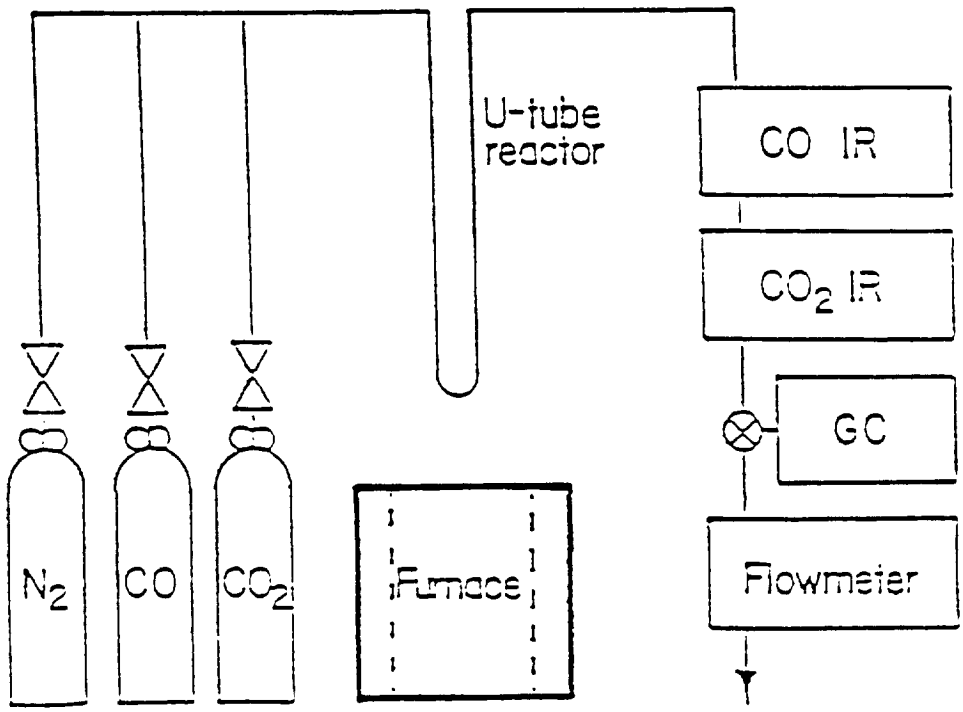

Figure 1.5. Mini-fluidized bed reactor system.

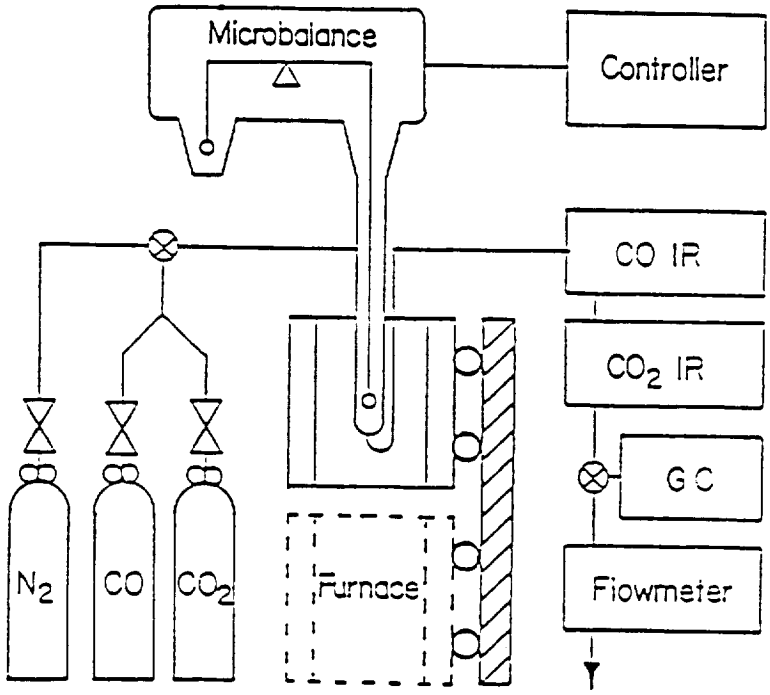

Figure 1.6. Micro-gravimetric reactor system.

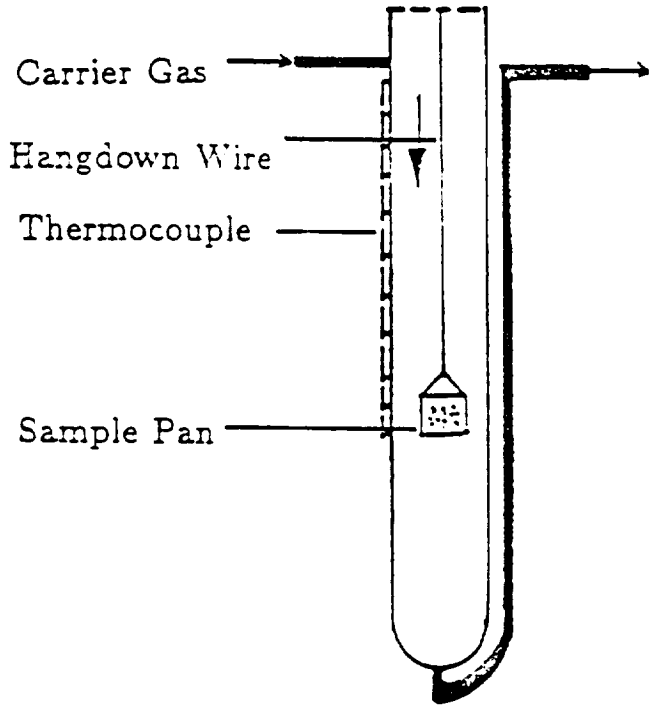

Figure 1.7. Schematic of the quartz reactor.

a. Gas Preparation Section: This includes a UHP nitrogen delivery system with critical flow elements for mass flow control.
b. The Mini-Fluidized Bed Reactor: This is a quartz reactor with a U configuration. The reactor is mounted on the stand and can be moved vertically in and out of an electric furnace. A chromel/alumel type K thermocouple is placed adjacent to the fluidized bed to monitor the temperatures independently during the course of an experiment. The ilmenite particles are supported by a stainless steel screen fitted inside the reactor. This reactor has low dead volume and a very rapid response.
c. Thermo-Gravimetric Reactor: In this reactor system, the sample is suspended on one arm of an electronic recording balance. A specially designed quartz reactor, which surrounds the sample with ports for inlet and dilution gas entry, is mounted vertically on wheels. This configuration allowed rapid start-up and quenching of the experiments for accurate measurement of initial and instantaneous rates. The furnace is equipped with a PID controller for both steady and temperature-programmed reactions.
d. Gas Analysis Section: This includes nondispersive infrared analyzers for measurement of carbon monoxide and carbon dioxide, as well as a gas chromatograph for a more complete gas analysis.
e. Other facilities used in our experimental study include an X-ray diffraction spectrometer, Mossbauer spectrometer, and scanning electron microscope with EDX.

Experimental Procedure. The work so far has focused on the study of the mechanism and kinetics of reactions important for carbothermal reduction of lunar ilmenite. The samples used have been synthetic ilmenite (iron titanate) obtained from CERAC, Inc., with a purity of 99.9% and particle size between 63 and 74 microns. To simulate lunar ilmenite, it was important to make sure that the iron in the sample was only Fe^{++}. To confirm this, Mossbauer spectroscopy was performed on the synthetic ilmenite. A typical Mossbauer spectra of the sample is shown in Figure 1.8. The results indicate that the amount of impurities, including Fe^{+++}, was less than 0.8% on a metal basis.

In each experimental run, a well-characterized mixture of ilmenite and carbon with known particle size and composition was placed in the reactor while the furnace was heated to a desired temperature. The gas flow inside the reactor was then stabilized and maintained for purging the reactor and the sample while the furnace temperature approached the pre-set value. To start the run, the reactor was lowered into the furnace

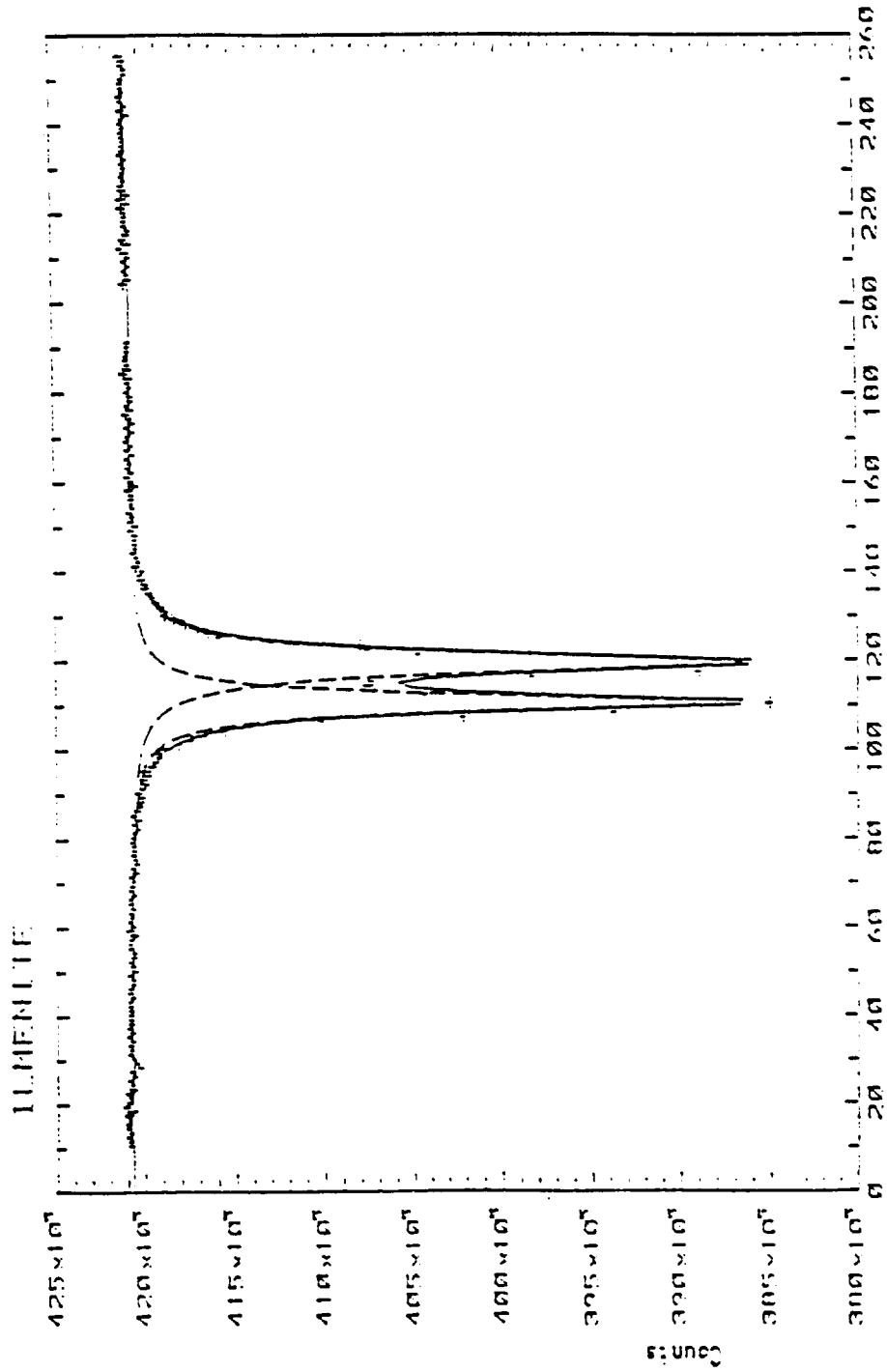

Figure 1.8. Mossbauer velocity spectrum for synthetic ilmenite particles.

(in the fluidized bed system) or the furnace was raised around the reactor (in the thermo-gravimetric system). The course of the reaction was studied by monitoring the gas composition and the sample weight in the gravimetric reactor.

The other methods used for characterization of the starting ilmenite were scanning electron microscopy and X-ray diffraction spectroscopy. Application of these techniques to samples at different levels of conversion can help us to understand the morphological and phase changes that occur in the samples during the course of reaction.

Discussion of Results

Due to the heterogeneous nature of the reduction reactions, the kinetics of the process depend on the physical structure of the solid. Figures 1.9 and 1.10 are the micrographs of the original synthetic ilmenite. The small particles on the surface are tiny chips generated during the grinding process. Figures 1.11 and 1.12 show partially reacted samples and, in particular, the porosity developed during the reaction. The SEM micrographs show a significant change in the structure and porosity of the particles as the reduction reaction proceeds. It appears that the new products formed on the surface of the particles have a lower melting point compared with that of ilmenite (melting point of iron titanate is 1327°C). Further characterization of this phase change is in progress.

So far, two types of experiments have been performed in the reactor systems. Most of the results are tests of the accuracy, reproducibility, and calibration of the newly developed reactor systems. More recently, however, experiments for determining the kinetics and mechanisms have been started. Among the first type of experiments are tests of the differential nature of the reactors. This is important to make sure that the kinetics are characteristics of the reaction and not the reactor geometry; this is an important point often neglected in similar studies. As an example, tests with different sample mass were conducted and the initial rates were compared. The results are shown in Table 1.4. The fact that the initial rate did not change significantly with sample size confirms that the reactor is differential and that the rates are intrinsic values. Similar results were obtained when flow rate was varied.

One of the important process parameters is the optimum carbon/ilmenite ratio in the reactor. The preliminary results are shown in Figure 1.13. It appears that the initial rate increases slightly with an increase in the carbon content. The significant difference is in the rate profile. As carbon content decreases, the variations in rate with time and conversion become more significant. The variations in rate are very important in the design of a large-scale reactor.

Figure 1.9. The surface microstructure of synthetic ilmenite (particle size ≅ 70 μm; sample coated with Au/pd); specimen tilt, 30°; magnification, 600X; left bar length, 10 μm.

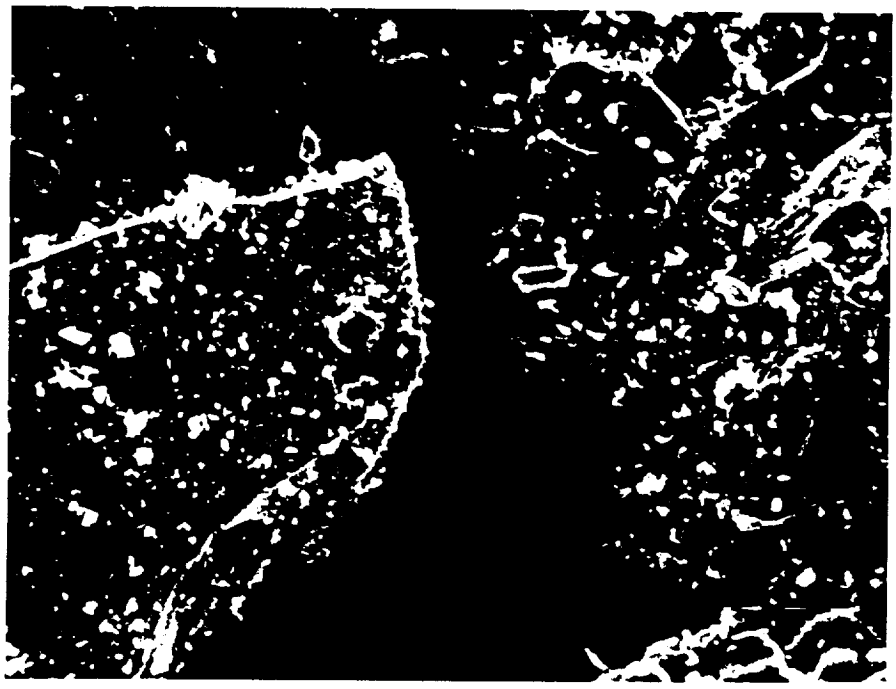

Figure 1.10. The surface microstructure of synthetic ilmenite (particle size ≅ 70 μm; sample coated with Au/pd); specimen tilt, 30°; magnification, 1030X; left bar length, 10 μm.

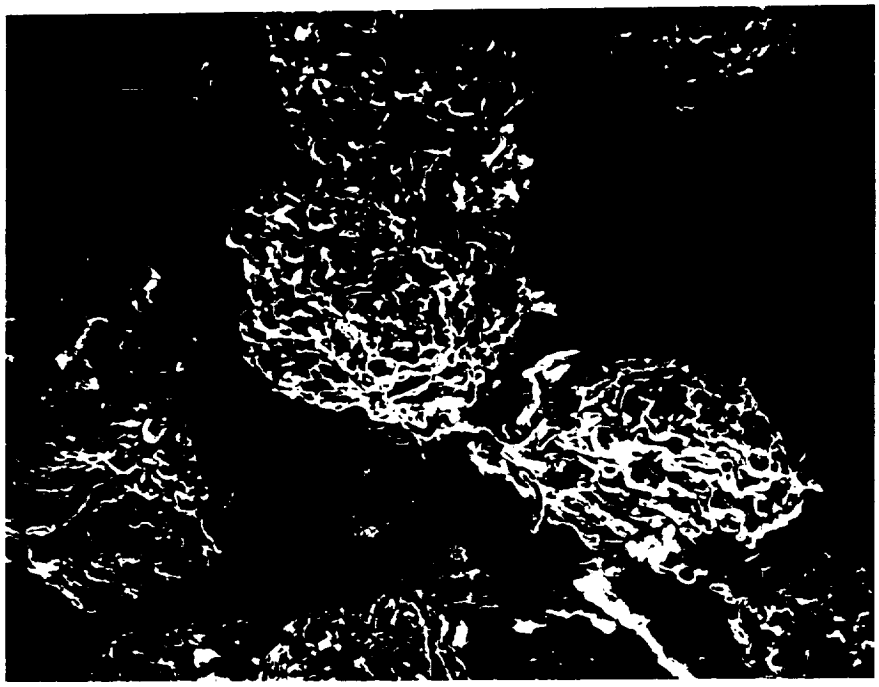

Figure 1.11. The surface microstructure of the reduced synthetic ilmenite (particle size ≅ 70 μm; sample coated with Au/pd); specimen tilt, 30°; magnification, 490X; left bar length, 10 μm.

Figure 1.12. The surface microstructure of the reduced synthetic ilmenite (particle size ≅ 70 μm; sample coated with Au/pd); specimen tilt, 30°; magnification, 1050X; left bar length, 10 μm.

Table 1.4. Effect of sample mass on reaction kinetics (temperature = 1120°C; flow rate = 75 cc/min).

Run Number	Sample Size (g)	Carbon Content (wt%)	Initial Rate (g CO/g ilmenite·s)
1	0.986	20	3.3×10^{-4}
2	0.498	20	3.1×10^{-4}

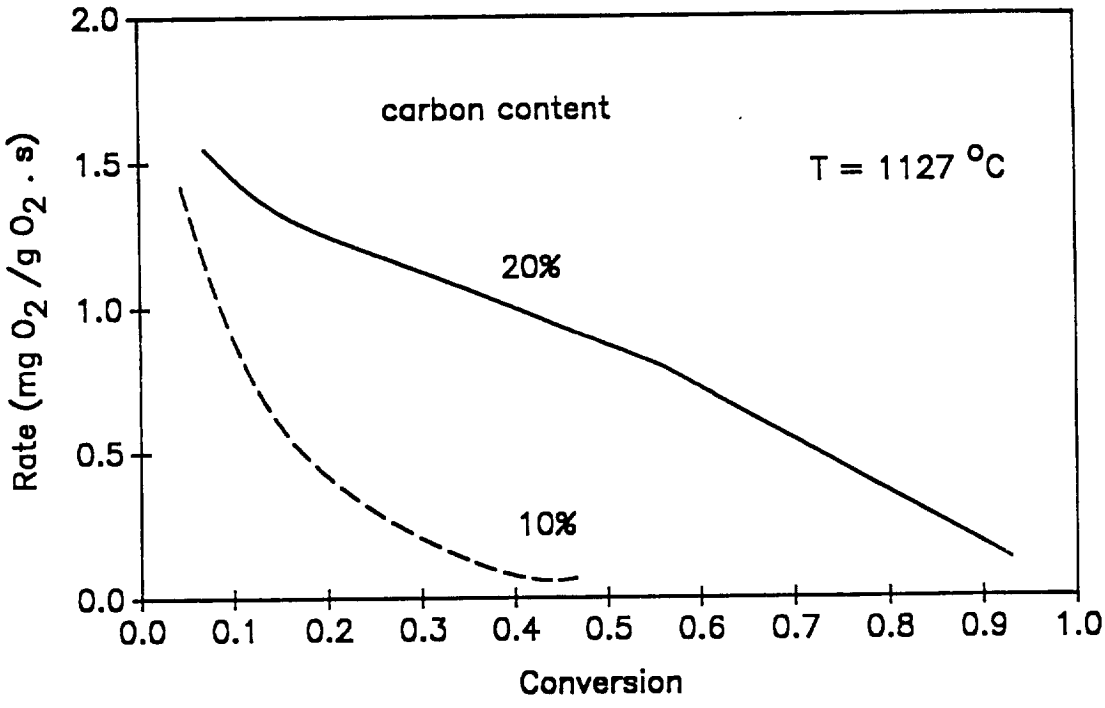

Figure 1.13. Effect of carbon content on ilmenite reduction kinetics.

Another important finding is the influence of carbon type on the kinetics of the process. As shown in Figure 1.14, the reaction rate and even product distribution for two types of carbon are quite different. It seems that carbon forms with higher surface activity give a higher overall reduction rate. These preliminary results indicate that the gasification of carbon is an important (and possibly rate-determining) step in the overall process. Therefore, the use of a catalyst to promote this reaction should be investigated. One of the objectives of this study is to find a suitable catalyst to promote the gasification reaction.

The chemical reactions taking place during the carbothermal reduction are as follows:

$$C + FeTiO_3 = CO + Fe + TiO_2 \quad (1)$$

$$CO + FeTiO_3 = CO_2 + Fe + TiO_2 \quad (2)$$

$$CO_2 + C = 2CO \quad (3)$$

Reaction 1 is expected to start at the points of contact between carbon and ilmenite. However, the desirable path which will be emphasized in this project is a combination of Reactions 2 and 3. This path does not require solid contact and can use a wide variety of carbonaceous compounds for ilmenite reduction.

Finally, a new temperature and concentration-programmed reaction is being developed to investigate the mechanism of the reduction reaction. This technique is suitable for studying the effect of various reaction conditions on rate using relatively few experiments. One example showing the effect of temperature on rate is shown in Figure 1.15.

References

1. W. N. Agosto, "Electrostatic Concentration of Lunar Soil Ilmenite in Vacuum Ambient," in *Lunar Base and Space Activities in the 21st Centry*, W. Mendell, Ed., Lunar and Planetary Institute, Houston, 1986.
2. R. J. Williams, D. S. McKay, D. Giles, and T. E. Bunch, "Mining and Beneficiation of Lunar Ores," in *Space Resources and Space Settlements*, NASA SP-428, J. Billingham, W. Gilbreath, and B. O'Leary, Eds., U.S. Government Printing Office, Washington, 1979.
3. M. A. Gibson and C. W. Knudsen, "Lunar Oxygen Production Vis Fluidized Bed Iron Oxide Reduction," 1988 Annual Meeting of American Institute of Chemical Engineers, Washington, 1988.

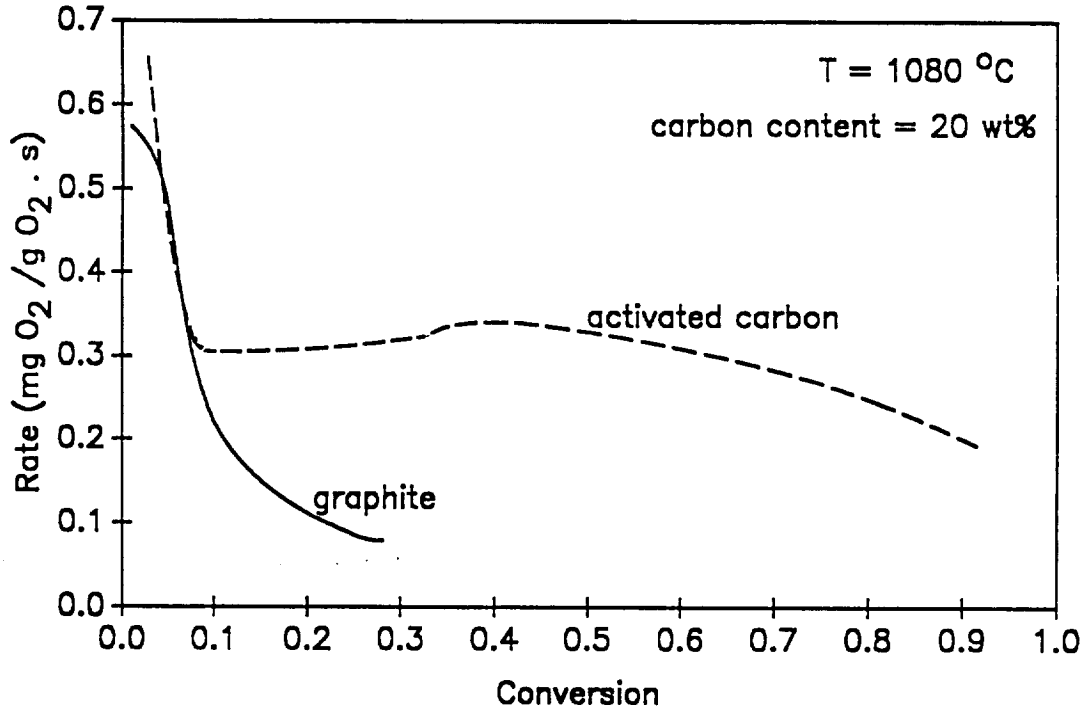

Figure 1.14. Effect of carbon type on ilmenite reduction kinetics.

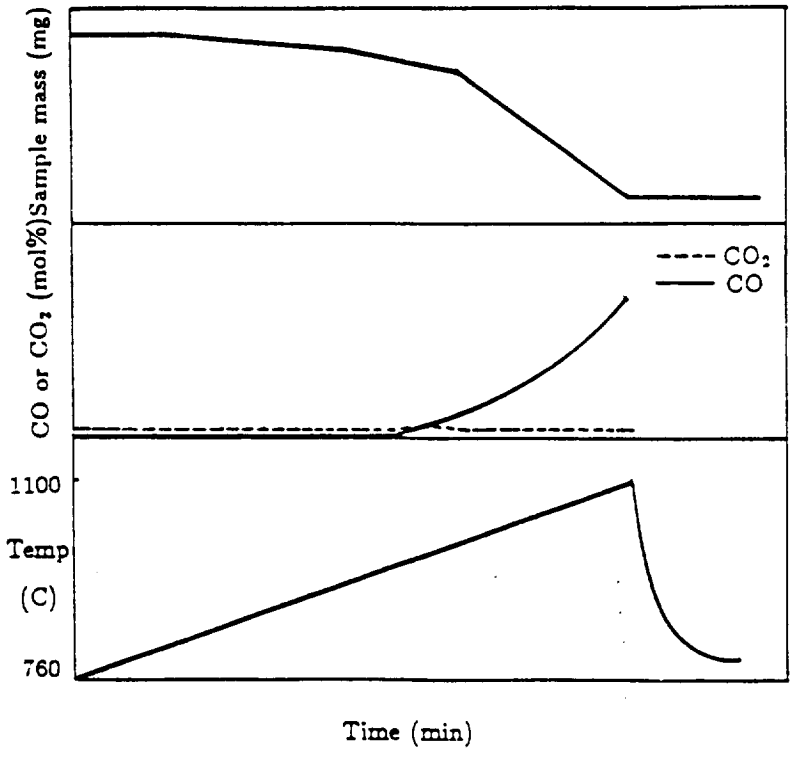

Figure 1.15. Temperature-programmed reaction results.

4. A. H. Cutler and P. A. Krag, "Carbothermal Scheme for Lunar Oxygen Production," in *Lunar Base and Space Activities in the 21st Centry*, W. Mendell, Ed., Lunary and Planetary Institute, Houston, 1985.
5. D. G. Jones, *J. Appl. Chem. Biotechnol.* **25**, 561-582, 1975.
6. M. I. El-Guindy and W. G. Davenport, *Met. Trans. Am. Inst. Min. Eng.* **1**, 1929-1970, 1970.
7. K. G. Suresh, V. Rajakumar, and P. Griereson, *Met. Trans. B* **18B**, 713-718, 1987.

Chlorination Processing of Local Planetary Ores for Oxygen and Metallurgically Important Metals

D. C. Lynch
Department of Materials Science and Engineering
The University of Arizona

Abstract

The use of chlorine to extract, reclaim, and purify metals has attractive possibilities for extraterrestrial processing of local planetary resources. While a complete cyclic process has been proposed for the recovery of metallurgically significant metals and oxygen, this progress report focuses on the chlorination step of the cycle. An experimental apparatus for reacting refractory materials, such as ilmenite, in a microwave-induced plasma is being built. Complex equilibria calculations reveal that stable refractory materials can, under the influence of a plasma, undergo chlorination and yield oxygen as a by-product. These issues and the potential advantages for plasma processing in space are reviewed. Also presented in this report is a discussion of the complex equilibria program used in the analysis.

Introduction

On Earth, the use of chlorine to extract, reclaim, and purify metals has long been an attractive possibility.[1-5] In space, plasma chlorination has even greater possibilities. Those possibilities include the production of oxygen and chloride metal vapor. The latter can be either reduced or decomposed to its metal and chlorine states for recycling. In addition, a plasma chlorinator is versatile. It can be used to process a number of different ores, and it can also be used to decompose metal chloride vapor or waste products from other processes.

Our immediate goal is to complete construction of the plasma reactor and begin testing. The unit will, for the next year, be the center of focus for our experimental program. The reactor has been designed to meet both our immediate needs and to serve as a service facility for other investigators participating in Center activities who may wish to determine if a plasma can enhance their research.

In the same spirit of cooperation, we have assembled a software package for complex equilibria calculations and an extensive data base. The software package is based on Outokumpu's HSC program. The data base is oriented toward the extractive metallurgical industry and has already found considerable use in this work. The HSC program has been interfaced with LOTUS 123 for manipulation of data, Grapher and Energraphics for data plotting, and Inset to cut and insert results from any program into

another. The entire package is up and running, and we plan to put together a brief description regarding its operation.

Background

The general advantages to chlorination processing are the large number of elements that form chlorides, the reactivity, volatility and solubility of metal chloride products, and the reducibility of metallurgically important chlorides to metal.[1] Almost all of the elements in the periodic table form chlorides, except for a few noble gases. In addition, chlorides tend to volatilize or have comparatively low melting points. Both physical phenomena provide a means for separation and subsequent refining.

Metal chlorides, while easily produced by reaction of chlorine with the metal, are difficult to form from metal oxides.[2] This difficulty is usually overcome by employing a CO-Cl_2 gas mixture or by reacting the oxide with Cl_2 in the presence of solid carbon. In carbochlorination, carbon monoxide acts as a reducing agent, forming CO_2, while the chlorine oxidizes the metal, forming a volatile chloride. In this manner, a new surface is continually exposed for reaction. This process is certainly viable, and one worth considering for space application. However, there are technical complexities with carbochlorination that may be ignored on Earth, but cannot be overlooked with regard to space application.

A number of chlorinated oxy-carbon compounds are stable at elevated temperatures. Landsberg et al.[6] conducted an extensive study of the relationship between various metal oxide carbochlorination reactions and C-Cl-O compound by-products. They found and quantified 136 identifiable C-Cl-O by-product compounds produced during carbochlorination of oxides of titanium, zirconium, and aluminum at reaction temperatures between 600 and 1000°C. In an economic setting, such as that which can be anticipated for a space base, the loss of scarce reactants and oxygen in an unwanted by-product cannot be tolerated.

"Cold" plasma chlorination can eliminate this problem, enhance reaction rates, minimize reactor size, and yield oxygen as a by-product. In addition, a plasma chlorination reactor is versatile. A single reactor could be used to process more than one ore, and it could also be used in the thermal reduction of chloride vapor.

Approach

"Cold" plasma processing of metallurgical materials is a natural progression of technological development within the extractive industry. High-temperature or "thermal" plasmas are used in many industrial applications in the extractive industry, including such areas as process heating and melting, thermal decomposition, smelting,

and refining.[7,8] Those applications rely primarily upon plasma heating to achieve conventional results that could be achieved with other heating sources. A "cold" plasma, unlike conventional heating sources, can significantly enhance reaction rates and form compounds, ions, and reactive species that cannot be produced by normal means.

In spite of their name, "cold" plasmas are not necessarily cold. Depending upon the gas composition and pressure, a "cold" plasma can exist at molecular temperatures up to 2000 K. The term "cold" is attached to those plasmas wherein there is a significant difference between the molecular and electron temperatures, the latter often being thousands of degrees greater than the former. The reactive nature of a "cold" plasma is a direct result of the difference in the two temperatures.

Both the reactive nature and the thermodynamic character of a "cold" plasma are represented by the sketch in Figure 1.16. In this sketch, the chemical potential of both reactants and products are plotted against an arbitrary variable to represent potential reactions. In a normal gas solid reaction, reactants combine to yield products and an overall reduction in the chemical potential of the system. In a "cold" plasma, energetic free electrons collide with gas molecules, leading to ionization and/or dissociation of those molecules. Depending on the initial gas composition, the excitation process can produce novel reactants, such as monatomic chlorine.[9,10] In addition, there occurs a substantial increase in the overall chemical potential of the reactants, which, in turn, allows a number of extra potential reactions, including the formation of metastable phases not attainable under non-plasma conditions.

Reaction rates can be substantially increased in a "cold" plasma. The high chemical potential of ionized and dissociated molecules reflects the reactive nature of these molecules. The presence of broken bonds, partially filled orbitals, and unbalanced charge makes these molecules highly reactive and can substantially enhance kinetic processes. It is these characteristics of a "cold" plasma, and how they can be used to enhance extractive processes, which are the focus of this investigation.

Results to Date

Experimental Apparatus. The primary effort in the past eight months has involved design and construction of the experimental apparatus. A schematic diagram of the apparatus is presented in Figure 1.17. The system includes a microwave source, an applicator where the plasma is generated, a gas delivery system, a mass spectrometer for monitoring the extent of the reaction, an optical pyrometer for monitoring the temperature of the solid specimen in the plasma, a specimen holder that both rotates and allows for vertical translation of the solid specimen, and a vacuum system.

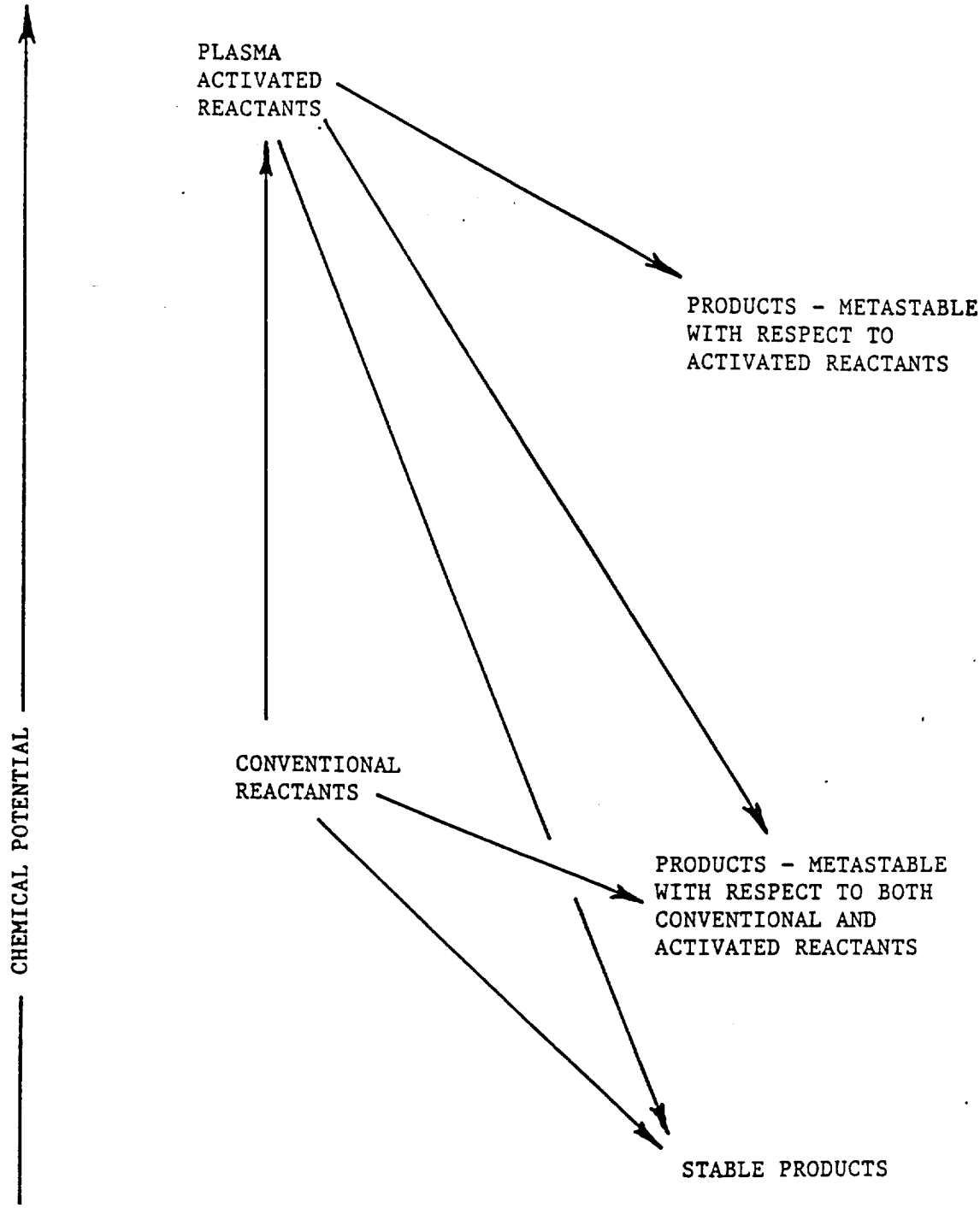

Figure 1.16. Schematic representation of chemical potential for conventional and plasma-assisted reactions.

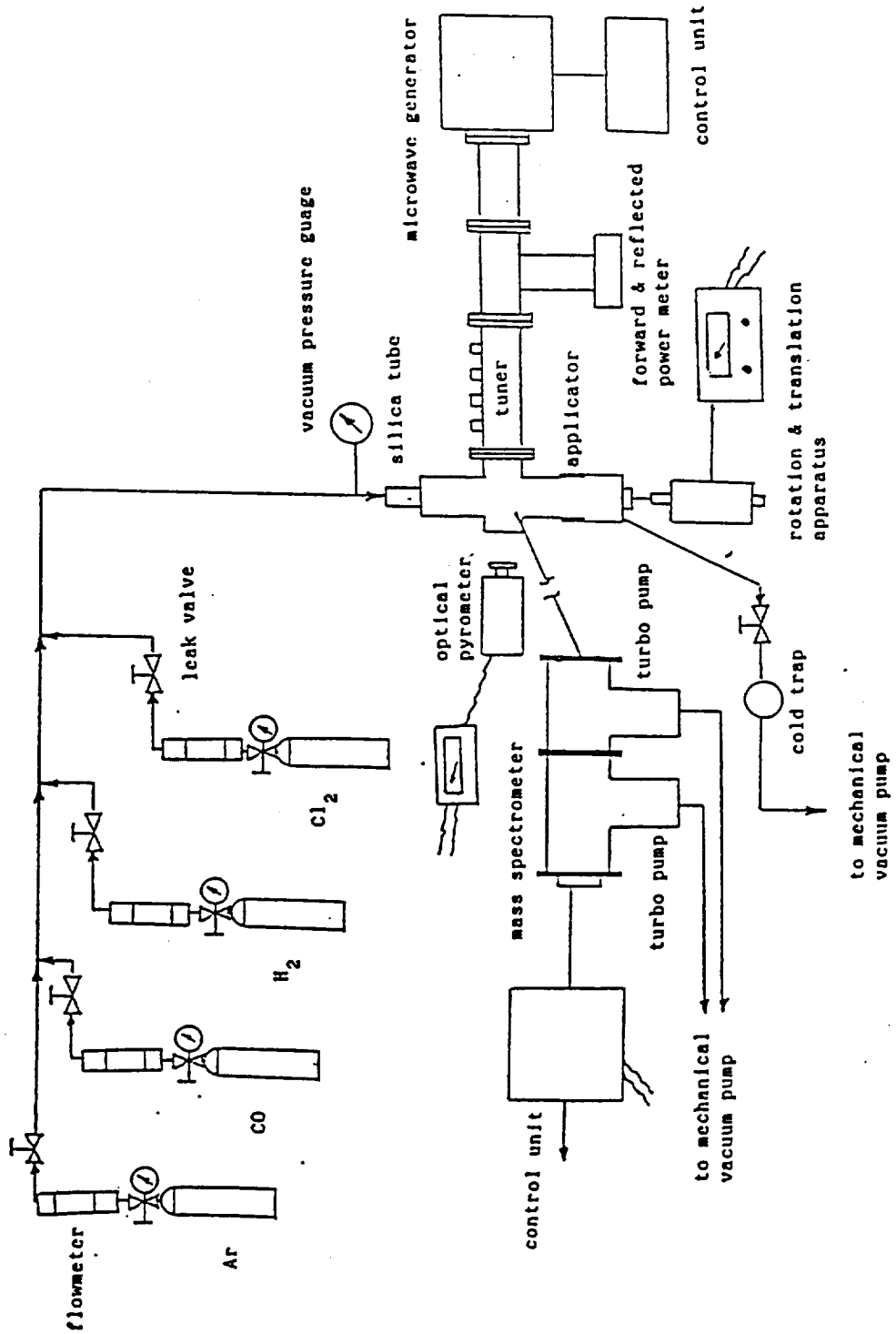

Figure 1.17. Experimental apparatus. Note: Mass spectrometer is rotated 90° and mass spec capillary sampling tube is not to scale.

The microwave generator was moved from a southside industrial site to the Arizona Material's Laboratory, where it has been set up and is now operational. The gas delivery system is in place; the specimen holder has been constructed, tested, and deemed operational. The reaction chamber, which is housed in the applicator, has been designed and built, while the applicator has been redesigned to accommodate the mass spectrometer.

In addition to these activities, we are in the process of completing arrangements for specimen preparation. This activity has involved construction of a vacuum system for sealing specimens in silica ampules and setting up a sintering furnace. Specimens prepared from powders will be isostatically pressed and then sealed in a silica ampule under vacuum before sintering at approximately 1000°C. The solid specimens formed in this manner will be characterized using a BET apparatus to determine surface area and pore volume, with visual confirmation of those results provided through use of a scanning electron microscope.

We are currently awaiting arrival of the mass spectrometer and mechanical pumps. The mass spectrometer, an EXTRELL C-50 Quadropole, was ordered last Fall. The instrument is currently being tested by the manufacturer, and the expected shipping date is March 17, 1989. Three corrosion-resistant pumps are on order and are expected to be shipped before the end of March 1989. Upon receipt of this equipment, we will complete construction of the apparatus and begin experimentation.

Thermodynamic Calculations. In many systems, chlorination is limited by the dissociation of diatomic chlorine. In Figure 1.18, the equilibrium partial pressure of monatomic chlorine in equilibrium with the diatomic species is plotted assuming the sum of the partial pressures of both the monatomic and diatomic species equals 1 atm. Also in Figure 1.18, the partial pressure is compared to the partial pressure of monatomic chlorine that can be achieved in a "cold" plasma. The latter value, based on a total plasma pressure of 0.1 atm and total dissociation of diatomic chlorine, intersects the equilibrium-calculated curve at 1560 K. Depending upon the concentration of monatomic chlorine in the plasma, it is possible to enhance the chlorination kinetics greatly.

The chemistry which takes place in a plasma is usually quite complex and involves a large number of elementary reactions which are initially generated by collisions between energetic free electrons and gas molecules.[10,11] While we cannot model the thermochemistry of the plasma at this early stage, we are in a position to estimate its potential impact on chlorination processing. The impact is estimated through complex equilibria calculations, using the computer program described earlier.

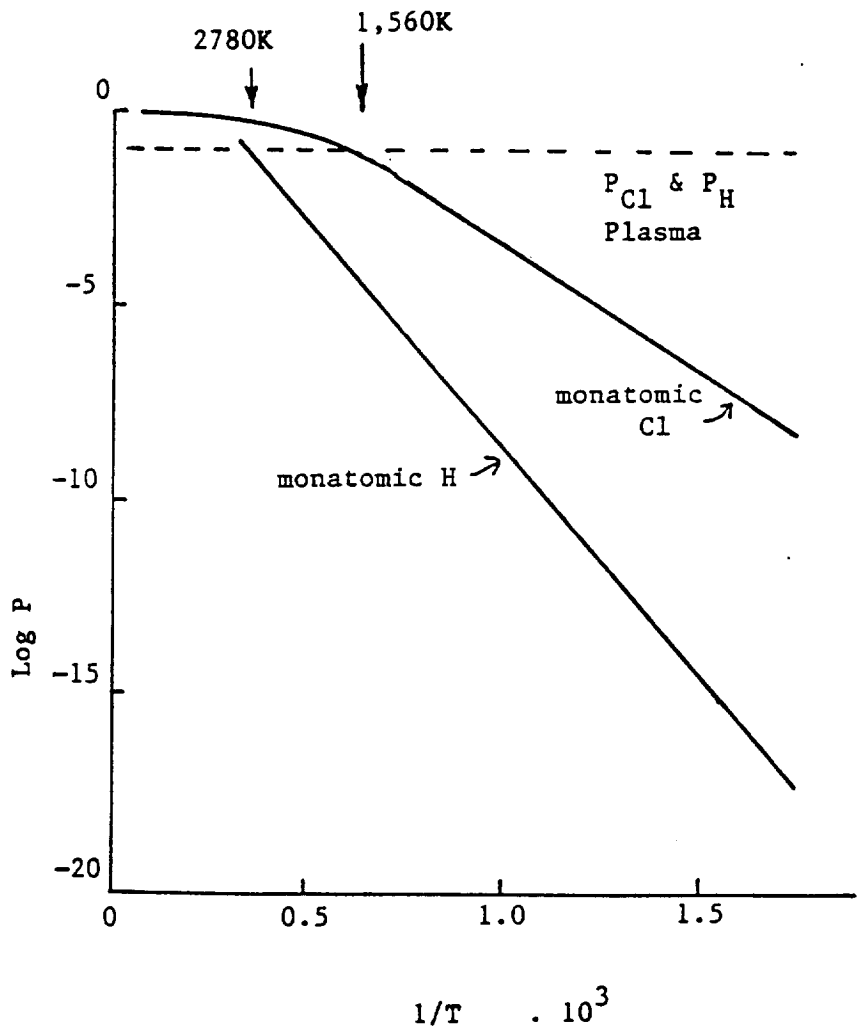

Figure 1.18. Comparison of the partial pressures of monatomic chlorine and hydrogen produced by thermal heating (total pressure 1 atm) and plasma (total pressure 0.1 atm).

The chlorination of ilmenite has been modeled using the system presented in Table 1.5. It has been assumed that, in plasma processing, diatomic chlorine is completely decomposed. Accordingly, the results presented below regarding the plasma represent the best-case scenario and do not take into consideration the effect of the plasma on other reactants and products. Moreover, it is important to remember that the results presented in this section are based on thermodynamic calculations and thus represent only what is energetically possible. Kinetic processes may also limit what can be achieved.

Table 1.5. System used for thermodynamic calculations.

Vapor Phase		
Cl_2 and/or Cl, O_2, ClO, ClO_2, FeCl, $FeCl_2$, $FeCl_3$, Fe_2Cl_6, TiCl, $TiCl_2$, Ti_2Cl_6, $TiCl_4$, TiOCl, $TiOCl_2$, TiO		
Solids		
$FeTiO_3$	TiO_2	$TiCl_2$
$TiCl_3$	$TiCl_4$	FeO
Fe_2O_3	Fe_3O_4	$FeCl_2$
$FeCl_3$	FeOCl	

Ilmenite reacts with chlorine at 1100°C. The extent of this reaction is represented in Figure 1.19 as a function of the moles of chlorine available per mole of ilmenite. The results in the figure and the raw data reveal that the iron is volatilized as chlorides while elemental oxygen is released. The process continues until iron is eliminated, leaving only rutile (TiO_2) remaining in the solid. At this point, the reaction stops for all practical purposes.

The extent of the chlorination of ilmenite in a plasma can be enhanced, as the results shown in Figure 1.20 reveal. Even after all the iron has been volatilized, the chlorination process continues. Titanium chlorides are volatilized and elemental oxygen is released. A comparison of Figures 1.19 and 1.20 reveals that the chlorine may be better utilized in a plasma reactor.

The potential for plasma chlorination is dramatically illustrated in Figure 1.21. Rutile, as noted earlier, is not readily chlorinated under standard conditions. The results in Figure 1.21 reveal that rutile, a highly refractory material, may readily be reacted in a plasma. It is this reactive nature that holds exceptional promise for the use of "cold" plasmas in the processing of local planetary resources.

Summary and Future Work

The investigation is in its initial stage. Considerable effort has been expanded in the design and construction of the plasma reactor. This initial work is expected to continue for three to four months. Upon completion of the apparatus, a number of preliminary experiments will be undertaken.

The preliminary experiments will focus on the power absorbed by the plasma, which will be evaluated as a function of the gas content (chlorine versus inert gas content, as well as the choice of inert gas), the total pressure, reactor size, and power

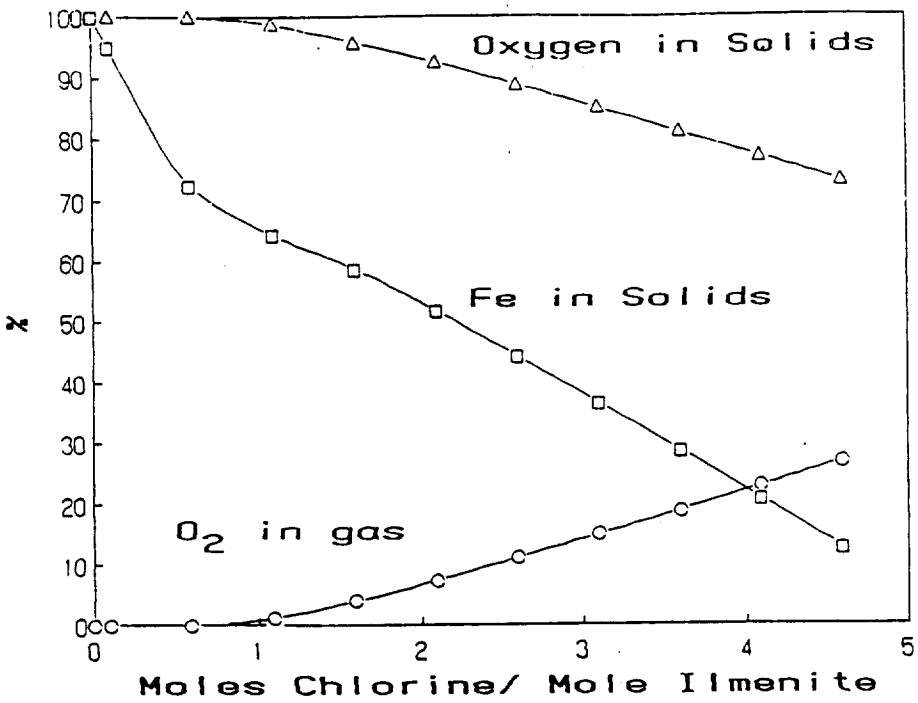

Figure 1.19. Extent of reaction of ilmenite with chlorine under conventional heating at 1100°C and total pressure of 0.1 atm.

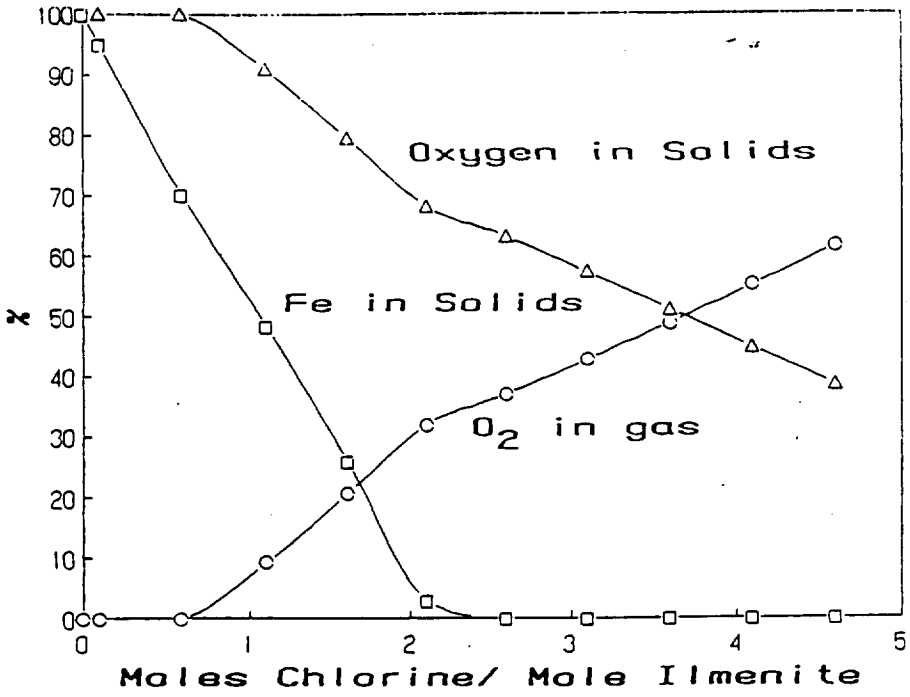

Figure 1.20. Monatomic chlorine in a plasma can readily react with ilmenite at 1100°C and a total pressure of 0.1 atm.

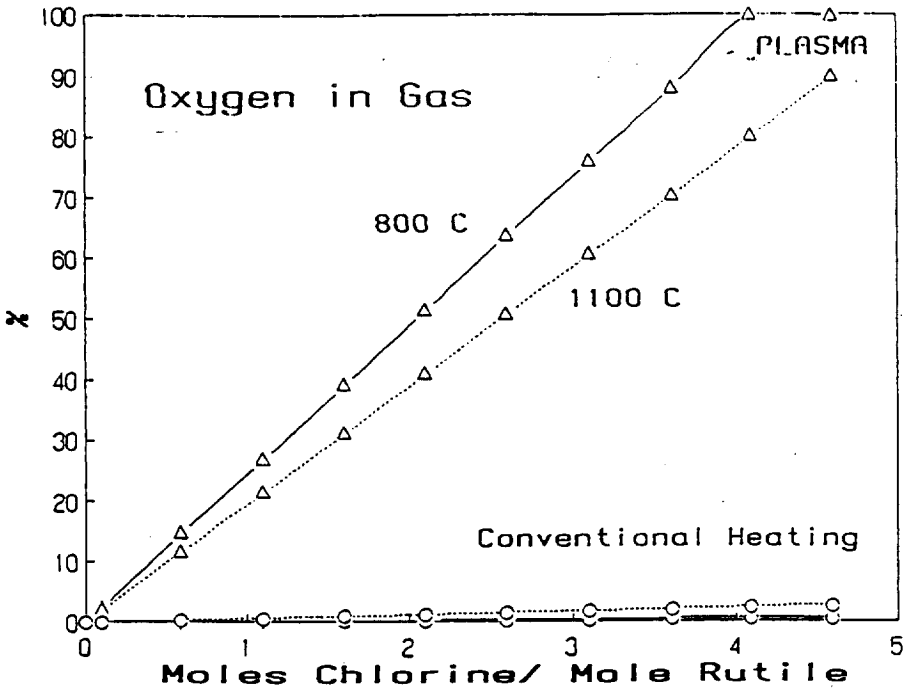

Figure 1.21. A plasma can effectively chlorinate refractory oxides.

provided. The apparatus is equipped with meters to measure both the forward and reflected power, the difference being the absorbed power. The level of absorbed power reflects the extent of radical formation. The results of this work will be used to identify optimum conditions for the chlorination reaction. This work is expected to take no longer than two months.

Chlorination studies will begin upon completion of the initial power studies. The kinetics of chlorination will be examined as a function of temperature, chlorine content in the gas, total pressure, power level, and plasma density. These experiments are expected to be in progress throughout the remainder of the year.

Student Participants

Mr. Daniel Bullard and Mr. Robert Ortega, both U.S. citizens, are working on this project. Daniel, who joined our research group in January, completed his undergraduate program at the University of Wisconsin at Milwaukee in December, where he received a double degree in Materials Engineering and Chemistry. Robert is in his last year of undergraduate study at the University of Arizona. Upon completion of his Bachelor's degree in May, he plans to commence graduate work. Robert began working on the project in December.

References

1. A. Landsberg and F. E. Block, *A Study of the Chlorination Kinetics of Germanium, Silicon, Iron, Tungsten, Molybdenum, Columbium, and Titanium*, USBM RI 6649, 1965.
2. I. Barin and W. Schuler, "On the Kinetics of the Chlorination of Titanium Dioxide in the Presence of Solid Carbon," *Metall. Trans. B* **11B**, 199-207, June 1980.
3. A. Landsberg, C. L. Hoatson, and F. E. Block, "The Chlorination Kinetics of Tungsten, Molybdenum, and Their Alloys," *J. Electro. Chem. Soc.* **118**, 1331-36, August 1971.
4. A. Landsberg, C. L. Hoatson, and F. E. Block, "The Chlorination Kinetics of Zirconium Dioxide in the Presence of Carbon and Carbon Monoxide," *Metall. Trans.* 3, 517-23, February 1972.
5. A. Landsberg, "The Chemical Reactivity and Equilibria of Au, Pt, Pd, Ir, Rh, Re, Mo, and W With Chlorine," private communication, May 1988.
6. A. Landsberg, R. D. Wilson, and W. Burns, "Conditions Affecting the Formation of Chlorinated Carbon Compounds During Carbochlorination," *Metall. Trans. B* **19B**, 477-82, June 1988.
7. W. H. Gauvin, M. G. Drouet, and R. J. Munz, "Developments in Plasma Processes for Extractive Metallurgy," *J. Metals* **39**, 14-17, December 1987.
8. C. W. Chang and J. Szekely, "Plasma Applications in Metals Processing," *J. Metals* **34**, 57-64, February 1982.
9. F. H. Dorman and F. K. McTaggart, "Absorption of Microwave Power by Plasmas," *J. Microwave Power* **5**, 4-16, January 1970.
10. A. T. Bell, "An Introduction to Plasma Processing," *Solid State Tech.*, pp. 89-94, April 1978.
11. A. T. Zander and G. M. Hieftje, "Microwave-Supported Discharges," *Applied Spectroscopy* **35**, 357-71, April 1981.

Oxygen and Iron Production by Electrolytic Smelting of Lunar Soil

L. A. Haskin
Department of Earth and Planetary Sciences and
McDonnell Center for the Space Sciences
Washington University

Previous work has shown that Fe^0 and O_2 can be derived by electrolysis from silicate melt of a composition typical of lunar soils (Lindstrom and Haskin 1979). In the present study, our goal is to refine further the conditions necessary to optimize production and to determine efficiencies of production (how much product is derived for a given current) and purity of products. These depend on several factors, including potential imposed between electrodes, configuration and surface area of the electrodes, composition of the electrolyzed silicate melt, and oxygen fugacity. We have designed experiments to measure the dependence on these variables of three parameters that must be known before production by electrolysis can be optimized. These parameters are:

Limiting Current = f[anode surface area (ASA), cathode surface area (CSA), distance between electrodes (d), electrolyte composition (X), potential between electrodes (E)]

Actual Current = f[ASA, CSA, X, E, reduction potentials of electroactive species (E^0), diffusion rates of electroactive species (D)]

Efficiencies of Production = f(X, E, fO_2) .

The limiting current is the maximum current the electrolyte can sustain at a given potential. It is related to the intrinsic conductivity of the bulk electrolyte. The conductivity has been measured previously for several compositions (Lewis 1985), and the limiting current can be calculated from these values.

For a direct current to flow through the electrolyte, oxidation and reduction of electroactive species must take place at the anode and cathode. Therefore, the actual current depends on reduction potentials and concentrations of electroactive species in the melt, as well as the electrode surface areas, and in general will be somewhat less than the limiting current. Once this dependence is understood, the actual current can be optimized to the limiting current by adjusting ASA, CSA, and E. Because different reactions are occurring at the anode and cathode, the effect of ASA on the current is not necessarily the same as the effect of CSA. Therefore, it is necessary to measure their effects independently. We did this by using a three-electrode experimental set-up, one electrode to establish a reference potential and the other two as working electrodes. This permitted the total potential to be divided into the potential driving

the anodic reaction plus the potential driving the cathodic reaction. In this way, we have determined the dependence of current on ASA, CSA, E, and X.

We have developed a method for measuring O_2 yield and, therefore, O_2 production efficiency. The amount of O_2 produced is based on the difference in sample weight before and after the experiment. We have found a simple relationship which explains most of the variation in production efficiency for O_2. Mainly, efficiency decreases in proportion to the competing oxidation of Fe^{2+} to Fe^{3+}.

Determination of efficiency of Fe production has proven more difficult because of the solubility of Fe^0 in the Pt wire loops used to hold the samples and the reduction of Si^{4+}. However, we have estimated Fe efficiencies indirectly from the differences in current at various potentials. Experiments were designed to determine the difference between "background" current flow (related to reductions other than Fe) and total current flow. These values were determined by measuring current flow as a function of potential for both a silicate melt containing Fe and a silicate melt in which a molar-equivalent amount of electro-inactive MgO had been substituted for FeO. We found that Fe efficiency increases regularly with increasing FeO concentration and decreases with increasing potential. The decrease in efficiency with increasing potential is related to the increasing amount of Si^{4+} that is reduced at higher potentials, suggesting that the purity of the Fe product also decreases with increasing potential.

In summary, we have determined the three relationships above for several compositions over a range of potentials from 0 to about 1 volt. With this information, the three equations can be solved simultaneously to optimize ASA, CSA, E, X, and fO_2 for optimum production rate or production efficiency. Furthermore, because these relationships are general, rather than specific to a preconceived electrolytic set-up, these data will be applicable to whatever electrolytic set-up further research finds to be most practical.

An abstract describing these results which was published in *Lunar and Planetary Science XX* follows.

Some Effects of Composition on Efficiencies for Production of O_2 and Fe^0 From Silicate Melts by Electrolysis, R. O. Colson and L. A. Haskin, Department of Earth and Planetary Sciences and McDonnell Center for the Space Sciences, Washington University, St. Louis, Missouri

Several experiments have been conducted aimed at determining the efficiencies for production of O_2 and Fe metal by electrolysis of silicate melts. Efficiency of O_2 production [defined as the moles of O_2 produced/(moles of electrons passed through the melt/4)] is calculated from the amount of O_2 produced and the measured total

current flow. The amont of O_2 produced is determined from the difference in sample weight before and after the experiment. Efficiency of Fe metal production was determined by a combination of theoretical treatment and experiment. Experiments were designed to determine the difference between "background" current flow (related to reductions other than Fe) and total current flow. These values were determined by measuring current flow as a function of potential for both a silicate melt containing Fe and a silicate melt in which a molar-equivalent amount of electro-inactive MgO has been substituted for FeO. Because the duration of these Fe-efficiency experiments is short and the species being reduced are not significantly depleted, these estimates correspond to the case in which the melt being electrolyzed is continuously "refreshed" and well stirred (except that oxidation products from the anode are not reduced at the cathode).

Efficiencies of production will be influenced by the presence of reducible or oxidizable species other than the species of interest. For example, O_2 production is expected to be made less efficient by the concurrent oxidations of $Fe^{2+} \rightarrow Fe^{3+}$ and $Fe^0 \rightarrow Fe^{2+}$ (we have found a significant amount of Fe^0 to be soluble in the silicate melt, similar to solubilities of Ni^0, Co^0, and Zn^0 found by Semkow et al.[1]). Fe^0 production is expected to be made less efficient by reductions such as $Fe^{3+} \rightarrow Fe^{2+}$, $Si(^{4+}) \rightarrow Si^0$, $Cr^{3+} \rightarrow Cr^{2+}$, and $Ti^{4+} \rightarrow Ti^{3+}$; however, Cr and Ti are not present in the experiments of this study. We expect the efficiencies of O_2 or Fe production to decrease as the relative amounts of competing species increase and as electrode potentials approach the reduction potentials of the competing reactions. Therefore, it is useful to look at efficiences as a function of (1) electrode potential, (2) oxygen fugacity, and (3) melt composition (in specific, Fe concentration).

O_2 Efficiency.—O_2 efficiencies as a function of electrode potential are shown in Figure 1.22. The low point in the oxygen efficiency curve is near the reduction potential for Fe^{3+} which, as expected, is the region of minimum efficiency. (Based on Fe^{3+} reduction potentials, we estimate about 35-65% of the Fe^{2+} is oxidized at these potentials.) At low potentials, a small amount of Fe^{2+} is oxidized to Fe^{3+} (we estimate 5-10%) and at higher potentials the amount of Fe^{2+} that is oxidized is small compared to the amount of oxygen because oxygen is much more abundant in the melt than Fe.

O_2 efficiency as a function of fO_2 at constant potential and constant total Fe concentration is shown in Figure 1.23. The efficiency is lower at lower fO_2, consistent with the higher concentration of Fe^{2+} at the lower fO_2 and, therefore, a larger fraction of current is related to the oxidation of Fe^{2+}. For this change in oxygen fugacity, the fraction of current attributable to $Fe^{2+} = Fe^{3+}$ increases by 65%, and calculations based on the report of Sack et al.[2] indicate an increase of 55% in Fe^{2+} concentration. If we

assume that all the current is related to oxidation of either oxygen ions or Fe^{2+}, we can choose the equation $\%Fe^{2+}/\%O_2 = X(Fe^{2+})/X(O^{2-})$ to represent relative amounts of the current attributable to each oxidation, where $\%Fe^{2+}$ is the percentage of the current attributed to the oxidation of Fe^{2+} and $X(O^{2-})$ is the effective concentration of oxidizable oxygen (which we assume is constant for the series of compositions between diopsidic and hedenburgitic melts used in this study). The equation can be modified (assuming $\%Fe^{2+} + \%O_2 = 100\%$) to yield $\%O_2/(100 - \%O_2) = X(O^{2-})/X(Fe^{2+})$. This relationship predicts that as Fe^{2+} concentrations increase, O_2 efficiency will decrease. This is the relationship observed and shown in Figure 1.24.

Fe Efficiency.--Figure 1.25 plots cathodic current as a function of electrode potential for several compositions. The "background" current is for a composition in which MgO has been substituted for FeO. This current is related primarily to the reduction of Si^{4+}. If we assume that no current is lost to electronic conduction,[3] then the figure gives a rough estimate of the relative amounts of the total current that can be attributed to the Fe^{2+} and Si^{4+} reductions at various potentials and Fe concentrations. However, for these compositions and potentials, most, if not all, of the reduced Fe is dissolved in the melt or Pt electrodes and does not exist as (readily extracted) pure metallic Fe. Threshold potentials for the precipitation of pure metallic Fe can be calculated from the data presented in Grove.[4] Threshold potentials so calculated are plotted as a function of Fe concentration in Figure 1.26. Comparison of Figures 1.25 and 1.26 indicates that in the range of potentials we have studied, pure metallic Fe can only be precipitated at concentrations of Fe > 35 mole%FeO and, at those concentrations, the amount of Fe reduced will be very large compared to the amount of Si^{4+} reduced. These results indicate that high efficiencies of O_2 and Fe production can be achieved by electrolysis, but not in bulk melt of the same composition. High efficiencies of O_2 production are favored by low Fe concentrations, and high Fe^0 production efficiencies are favored by high Fe concentrations.

Acknowledgments.--We gratefully acknowledge partial support for this work from UA/NASA Center for Utilization of Local Planetary Resources.

References

1. K. W. Semkow, R. A. Rizzo, L. A. Haskin, and D. J. Lindstrom (1982) GCA 49,1897-1908.
2. R. O. Sack, I. S. E. Carmichael, M. Rivers, and M. S. Ghiorso (1980) Contr. Min. Pet. 75, 369-376.
3. D. J. Lindstrom, L. A. Haskin, and K. W. Semkow (1986) LPSC XXVII.
4. T. L. Grove (1981) Contr. Min. Pet. 78, 293-304.

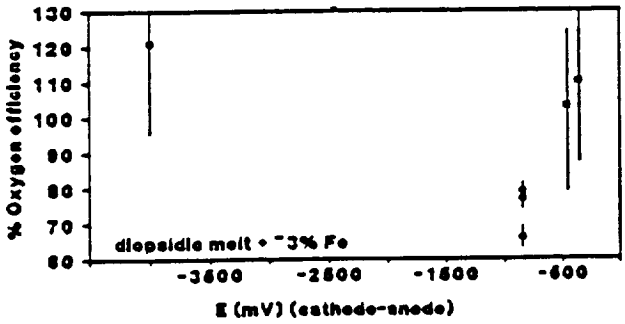

Figure 1.22

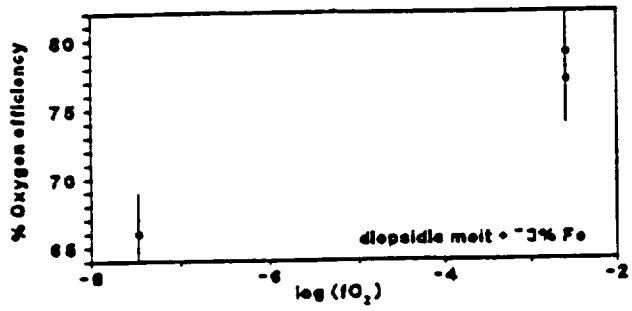

Figure 1.23

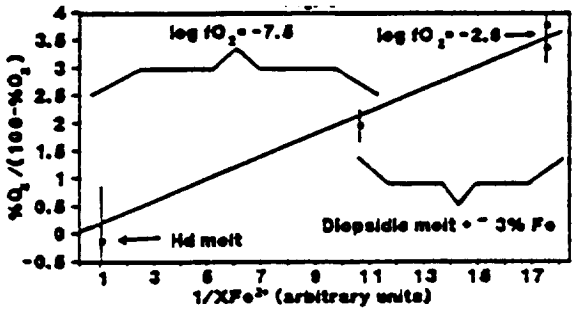

Figure 1.24

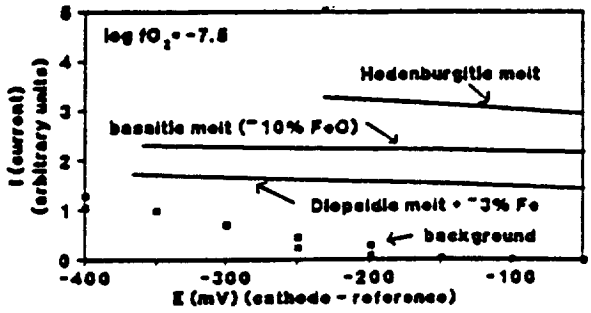

Figure 1.25

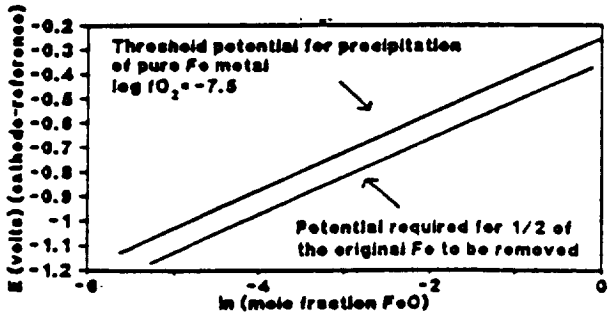

Figure 1.26

II. MATERIAL PROPERTIES

An Investigation of Some Mechanical and Thermal Properties of Lunar Simulant Materials Heated at 2.45 GHz

T. T. Meek
Department of Materials Science and Engineering
University of Tennessee

During the time period from September 1, 1988 to February 28, 1989, work has progressed in the following areas. Lunar simulant material has been fabricated to simulate Apollo 11, Apollo 15, and Apollo 16 soils. Table 2.1 shows the approximate compositions which these soils simulate. Samples of each soil simulate were fabricated into right circular cylinders of approximately 1.27 cm diameter by 1.27 cm length. Each sample was then placed into a microwave reaction cavity and heated using 2.45 GHz radiation to a particular processing temperature at which it was held for a prescribed length of time. Figures 2.1 and 2.2 show examples of two microwave heating programs for these simulant samples. Upon completion of thermal processing, each sample had its top and bottom surfaces polished to a surface roughness of approximately 4 μ inches RMS.

Table 2.1. Simulated compositions (weight percent).

	A11 (10089, 4)	A15 (15999, 126)	A16 (69999, 75)
SiO_2	42.03	46.52	45.26
TiO_2	7.48	1.40	0.58
Al_2O_3	13.59	17.10	26.22
FeO	15.74	12.05	5.82
MnO	0.20	0.17	0.07
MgO	7.86	10.42	6.39
CaO	11.98	11.17	14.76
Na_2O	0.44	0.43	0.45
K_2O	0.14	0.20	0.13
Cr_2O_3	0.30	0.27	0.12
P_2O_5	0.11	0.20	0.13
S	0.13	0.07	0.07

Samples were then thermally shocked using an apparatus consisting of a tube furnace vertically oriented so that a sample could be suspended in it while being heated and then be allowed to drop, after some prescribed amount of time, through the furnace into a water quench.

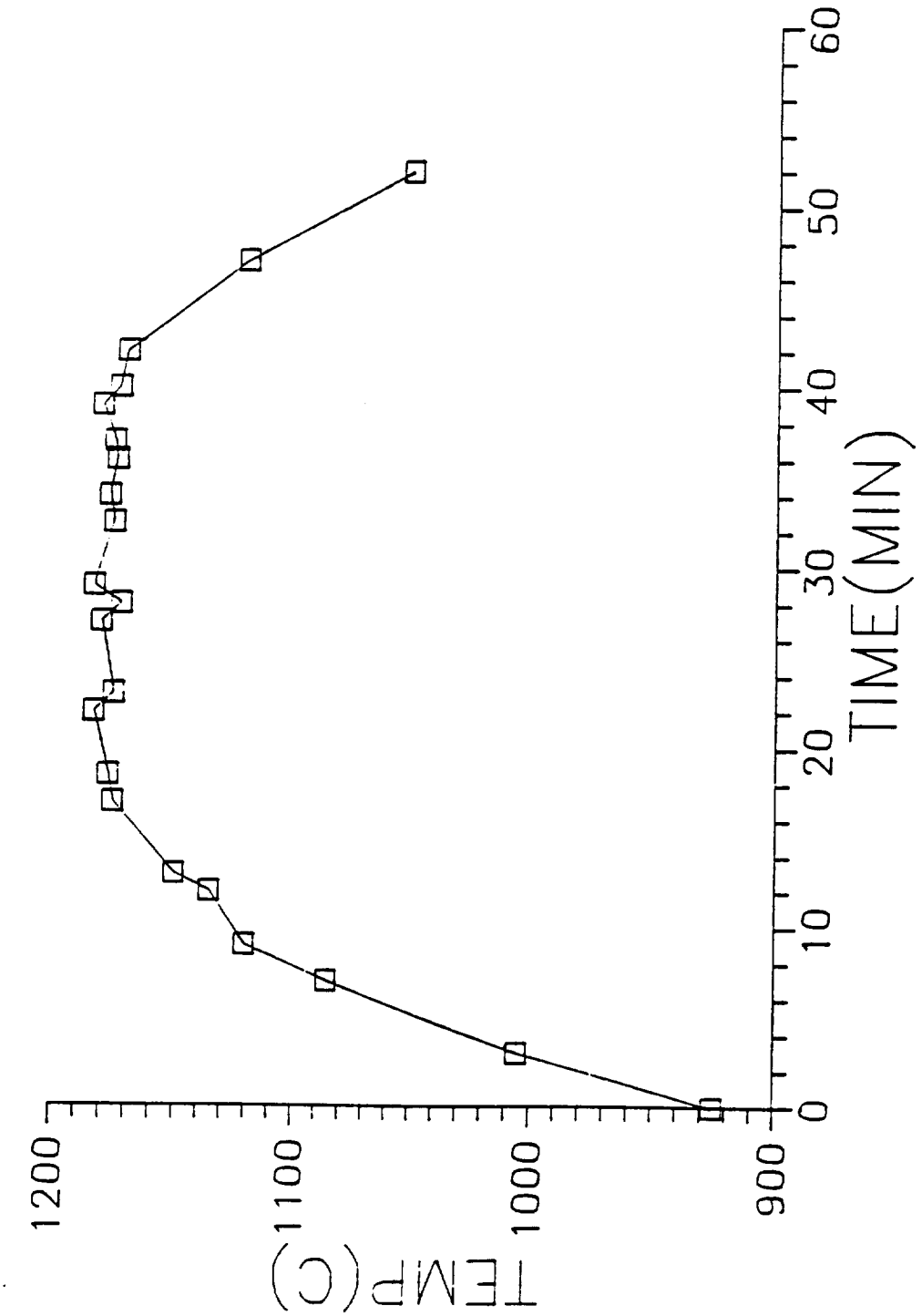

Figure 2.1. Time versus temperature for samples 2D and 4D.

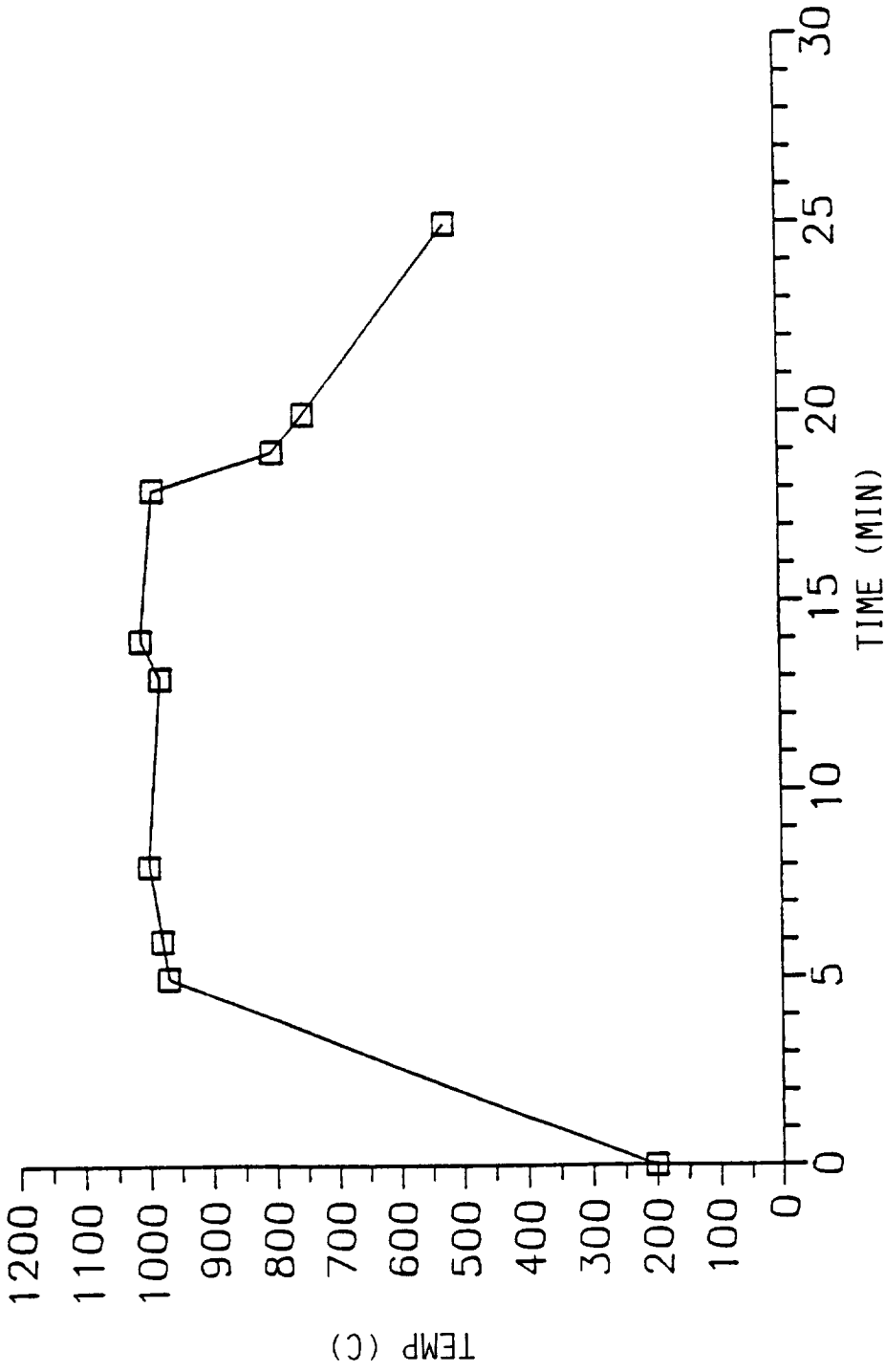

Figure 2.2. Time versus temperture for samples 9E-1 and 9E-2.

Initial work has been reported by Meek et al. (1988) on thermal shock properties of microwave sintered lunar simulant materials. The mechanical testing of these samples was carried out using conventional ASTM (American Society for Testing Materials) techniques. There is some question, however, about the procedure, so it was decided to look again at samples using a different technique, one which employs hardness data to determine the fracture toughness of a material and then relates this to thermal shock resistance. Some advantages of this technique are its low cost for analysis, a sample can be tested in many locations, and thermal shock resistance as a function of initial sample orientation in the microwave field can be determined.

Currently, we have prepared samples for testing at the Y-12 facility of Oak Ridge (operated by Martin Marietta) and are awaiting results. At the same time, other samples are currently being investigated using scanning electron microscopy to determine their microstructures.

An abstract for a paper on this work has been submitted for presentation at the 9th Princeton Conference on Space Manufacturing. The only uncertainty concerning this paper is whether we will receive data from the Y-12 facility in time to present it in this paper. If we do not, the paper will focus mainly on microstructural analysis of the samples as a function of processing technique.

For the next 16-month period, we propose to continue the work on lunar simulants, begin work on actual lunar sample material (Apollo 11, 15, 16), and begin work on carbonaceous chondrite material. Samples will be prepared in the same manner as the simulants. They will be thermally processed by conventional means and by using 2.45 GHz radiation. Their mechanical properties and thermal shock properties will be determined and then related to their observed microstructure.

The proposed budget for March 1, 1989 through June 31, 1990 is as follows:

I.	Salaries		
	A. Graduate Student	$15,872	
	B. Advisor	5,000	
	C. Shop	1,000	
	D. Secretarial	2,372	
	Benefits at 28%% of I.B-D	1,820	
	Subtotal	$24,192	
II.	Materials	1,000	
III.	Travel	800	
	Subtotal		25,992
IV.	Overhead at 38.5%% of I, II, and III		10,008
	TOTAL		$36,000

Reference

Meek, T. T., L. A. Fayerweather, M. J. Godbole, D. T. Vaniman, and R. B. E. Honnell, "Sintering Lunar Simulants Using 2.45 GHz Radiation," *Engineering Construction and Operations in Space, Proceedings of Space 88*, ASCE, 1988, p. 102-110.

N91-25210

Abundances of Volatile-Bearing Phases in Carbonaceous Chondrites and Cooling Rates of Meteorites Based on Cation Ordering of Orthopyroxenes

J. Ganguly
Department of Geosciences
The University of Arizona

The "deliverables" for the grant received during this period are (1) a comprehensive proposal for work during the period 3/1/89 to 2/28/90 and (2) results of preliminary calculations of volatile abundances in carbonaceous chondrites.

Both objectives have been met. The results of the calculations of the volatile abundances will be presented at the Ninth SSI Princeton Conference on Space Manufacturing, May 11, 1989. In addition, the method (Ganguly 1982) has been refined for the calculation of cooling rate on the basis of cation ordering in orthopyroxenes, and it has been applied to the derivation of cooling rates of some stony meteorites. Evaluation of cooling rate is important to the analysis of condensation, accretion, and post-accretionary metamorphic histories of meteorites. The method of "orthopyroxene speedometry" is widely applicable to meteorites and would be very useful in the understanding of the evolutionary histories of carbonaceous chondrites, especially since the conventional metallographic and fission track methods yield widely different results in many cases. The results will be presented at the Lunar and Planetary Science Conference XX, 1989. The following abstracts summarize the major conclusions of the volatile abundance and cooling rate calculations.

Theoretical Predictions of the Nature and Abundances of Volatile Bearing Phases in Carbonaceous Chondrites,
Jibamitra Ganguly, Department of Geosciences, University of Arizona, and Surendra K. Saxena, Department of Geology, Brooklyn College

The overwhelming majority of asteroidal bodies consist of carbonaceous chondrites. Thus, the study of carbonaceous chondrites is very important to the assessment of resource potentials of near-earth asteroids. The carbonaceous chondrites are important potential resources for volatiles which may be used for fuels and propellants. The volatiles are stored in the minerals as structurally bound components in the organics, and in the possible cometary cores. The hydrous minerals have been characterized as a mixture of phyllosilicates, but further characterizations by conventional methods have proved to be extremely difficult due to the extremely fine-grained nature of the material. However, these phases need to be properly characterized if we are to efficiently release their volatiles for practical uses.

In this work, we have calculated at several P-T conditions the nature and abundance of the volatile bearing phases by minimizing the Gibbs free energy (G) of the system Mg-Fe-Al-Si-C-H_2-O_2, constrained by the bulk composition of the Orgueil CI chondrite. The minimization was carried out using the method of Lagrangian multiplier and a thermochemical data base consisting of about 100 minerals and 70 vapor speices. Further, the effects of solid solutions (ideal and nonideal) have been taken into account. Due to the lack of adequate data, we have assumed that the phyllosilicates behave as ideal solutions.

The results show that a minimum pressure of about 1 bar at 500 K is needed to form the hydrous phases and that the primary hydrous minerals are antigorite and talc. Some amount of chlinochlore (~ 2 mol%) may also be present. The amount of water structurally bound in the minerals should be about 5-10 wt% of the condensed inorganics. The amount of crystalline graphite may be very small, within a few mol%. There is also abundant magnetite. The relatively high pressure required to form the hydrous phases could preclude their formation by direct condensation from solar gas.

The vapor phase in equilibrium with these crystalline phases consists primarily of H_2O (~ 70 mol%), CH_4 (~ 20 mol%), and CO_2 (~ 10 mol%). This may be an approximate composition of the possible cometary core if we assume that the core represents the trapped volatiles, the composition of which was controlled by reaction with the minerals and other condensed phases.

There are considerable uncertainties in the thermochemical data of the phyllosilicates, especially of the Fe-end members and in the thermodynamic mixing properties of their Fe-Mg joins. Thus, the above results must be treated with caution. Further studies on the refinement and systematization of the thermochemical properties are in progress. Also, we need to take into account sulfur and organics in free energy minimization calculations to develop a more reliable model of the mineralogical characteristics of carbonaceous chondrites. This work is to be published in the Proceedings of the May 1989 SSI Conference (Appendix E).

Acknowledgment: NASA Grant NAGW-1332.

Fe^{2+}-Mg Ordering in Orthopyroxenes and the Cooling Rates of Meteorites, Jibamitra Ganguly and Kunal Bose, Department of Geosciences, University of Arizona, and Subrata Ghose, Department of Geological Sciences, University of Washington

The cooling rates of meteorites have been a subject of central importance in the understanding of their origin and evolution. However, the commonly used methods for the determination of cooling rates of meteorites often yield conflicting results. A potentially powerful recorder of the cooling rates is the state of Fe-Mg ordering in

orthopyroxenes (OPx), which can be found in any stony and stony-iron meteorite, and as silicate inclusion in some iron meteorites. However, despite its many applications in terrestrial problems, this method has not yet been used to derive quantitative constraints on the cooling rates of meteorites.

The "cation-ordering speedometry" involves reconstruction of the ordering state of a sample at its peak temperature and numerical simulations of the change of site occupancies as a function of cooling rate (Ganguly 1982). A substantial amount of thermodynamic and kinetic data, which are required for these calculations, is available in the literature (Ganguly 1982, Anovitz, et al. 1988). An example of the simulated evolution of M2 site occupancy is shown in Figure 2.3, using an OPx from the Steinbach meteorite for which the measured XFe(M2) = 0.304 [XFe = $Fe^{2+}/(Fe^{2+} + Mg)$]. The cooling is assumed to follow the form $1/T = 1/T_0 + nt$, where T_0 is the peak temperature and n is a cooling time constant. The observed site occupancy is exactly reproduced as the quenched ordering state in a simulated evolution, which is characterized by T-t path with $n = 1.5(10^{-12})$ yr^{-1}. Similar calculations are carried out for orthopyroxenes from Shaw and Johnstown meteorites (Table 2.2). The cooling rates, given by nT^2, are strictly applicable around the closure temperatures (T_c) and are quite insensitive to errors in the estimation of T_0. Any other cooling law can also be used.

Figure 2.4 shows the effect of cooling rates on quenched M2 site occupancy for three bulk XFe values. For comparison, all XFe(M2) values are relative to those for a cooling rate of 150°C/my for the different bulk compositions. It is clear that the retrieved cooling rates are very sensitive to errors in the determination of site occupancies of natural samples, especially for Fe-poor compositions. A precision of 0.002 in the site occupancy determination is a difficult but attainable goal in single crystal X-ray analysis. This will limit the precision of the retrieved cooling rates of meteoritic orthopyroxenes to a factor of 5-10, depending on the composition and cooling rate.

The site occupancies of the meteoritic orthopyroxenes used in this work lack the high precisions required for reliable cooling rate calculations. Nonetheless, it is important to note that, despite their uncertainties, the inferred cooling rates for Shaw and Steinbach orthopyroxenes are in good agreement with those derived from metallographic properties of these meteorites (Taylor et al. 1979, Reid et al. 1974). In contrast, the ^{24}Pu track records were used to derive (Pellas and Storzer 1977, Pellas et al. 1978) a cooling rate for the Shaw meteorite below 350°C, which is three orders of magnitude slower than that shown in Table 2.2. Thus, either there was a drastic change of cooling rate of the Shaw meteorite between 400 and 350°C, or the ^{24}Pu result

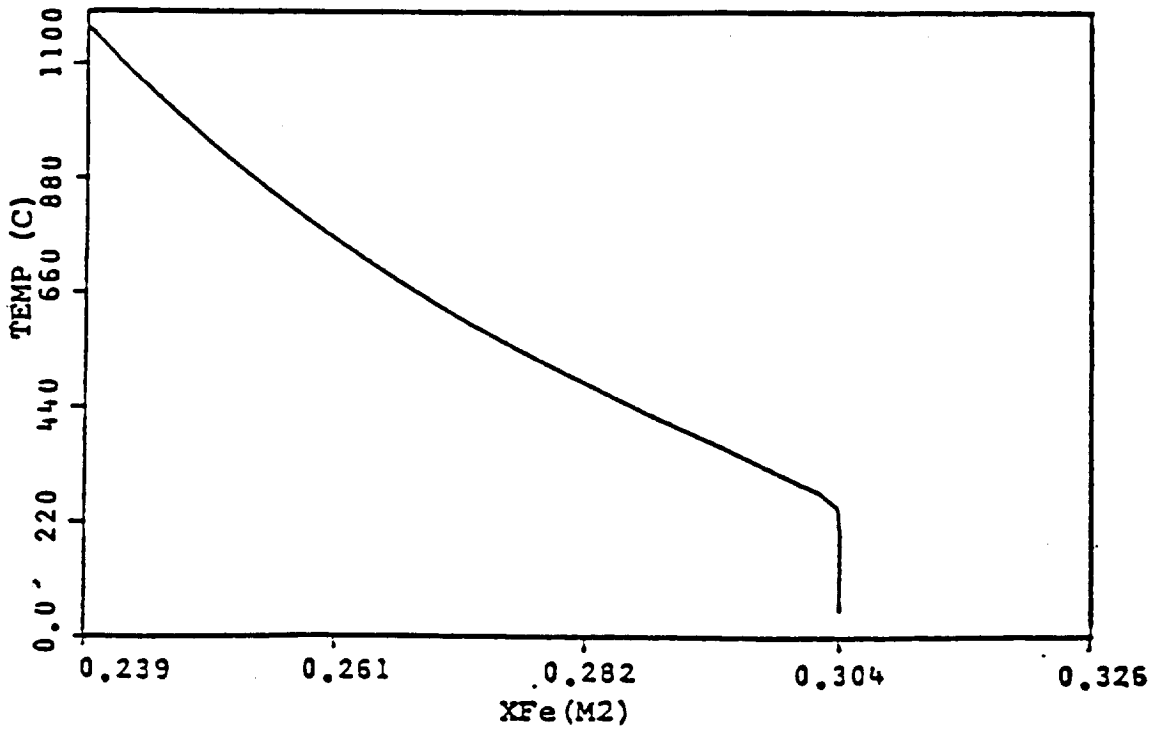

Figure 2.3

Table 2.2. Summary of cooling rate calculations of meteoritic orthopyroxenes.

Sample	$Fe^{2+}/(Fe^{2+}+Mg)$ Total	M2	T_c (°C)	n,yr^{-1}	$(dT/dt)_{T_c}$, °C/my	Site Occupancy Measurement
Johnstown	0.175	0.324	400	4E-9	1.8E3	X-ray (Dodd et al. 1975)
Steinbach	0.161	0.304	304	1.5E-12	0.5	X-ray (Reid et al. 74)
Johnstown	0.237	0.451	318	1.5E-12	0.5	X-ray[a]

[a] Preliminary results from this work.

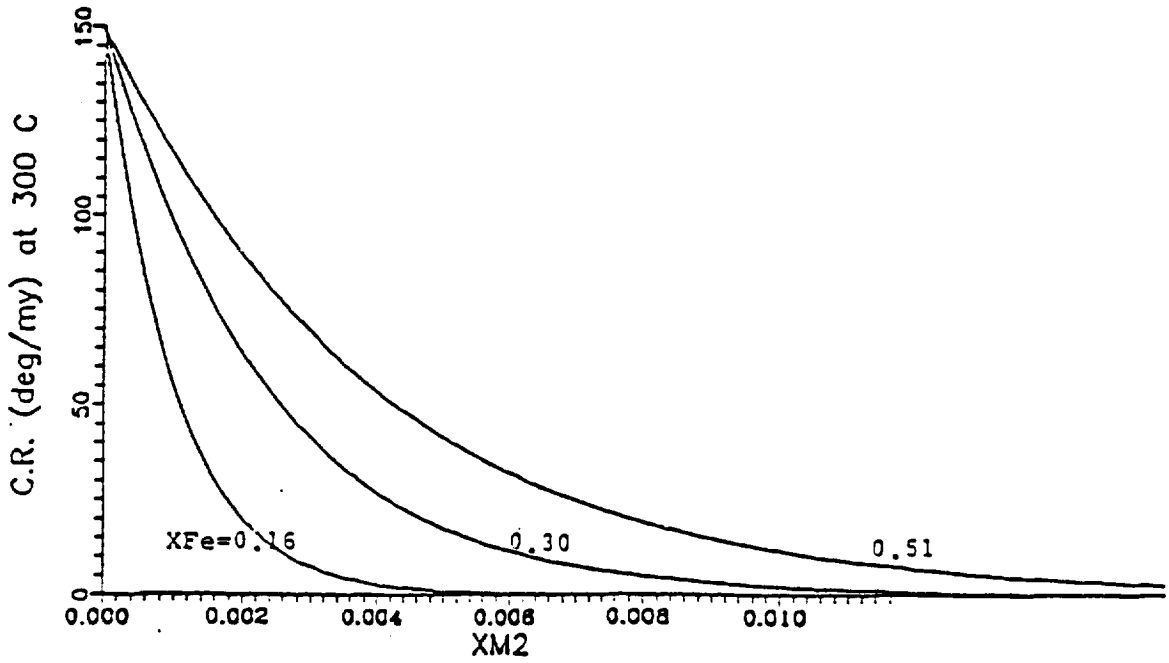

Figure 2.4

requires a careful reevaluation. Although the Johnstown meteorite is shocked (Mori and Takeda 1981), the high degree of Fe-Mg order in OPx suggests that the magnitude of shock was <450 Kb (Dundon and Hafner 1971). These results illustrate the potential applications and importance of the "cation ordering speedometry," which should be most widely applicable in the study of cooling rates and shock histories of meteorites owing to the widespread occurrence of orthopyroxenes.

Acknowledgments: NSF Grant EAR 8206656 and NASA Grant NAGW-1332.

References

Anovitz, L. M., et al., 1988, Amer. Min. 73, 1060-1071.

Dodd, R. T., et al., 1975, Geochim. Cosmochim. 39, 1585-94.

Dundon, R. W. and S. Hafner, 1971, Science, Nov.

Ganguly, J., 1982, Adv. Phys. Geochem. 2, 58-98.

Mori, H. and H. Takeda, 1981, EPSL 53, 266-274.

Pellas, P. and D. Storzer, 1977, Lunar and Planet. Sci. 8, 762-764.

Pellas, P., et al., 1978, Lunar and Planet. Sci. 9, 879-881.

Reid, A. W., et al., 1974, EPSL 22, 67-74.

Taylor, G. J., et al., 1979, Geochim. Cosmochim. 43, 323-337.

Beneficiation of Lunar Ilmenite Feedstock

J. Ruiz
Department of Geosciences
The University of Arizona

The first six months were devoted to (1) reviewing the chemical and physical characteristics of ilmenite in lunar material and (2) developing high-precision, low-abundance analyses for platinoids and other possibly important elements in space materials using an induced coupled plasma mass spectrometer.

Lunar Ilmenite

There is considerable literature on the chemistry of lunar ilmenite and the differences between lunar and terrestrial ilmenite. It is clear that terrestrial ilmenite is a poor analog to lunar ilmenite and should be avoided as a substitute material in any experiment since its physical and chemical properties will be different. If substitute material is needed for lunar ilmenite, it would be preferable to use synthetic ilmenite. A problem that was discovered during the literature review is that lunar regolith, which would be the starting material for ilmenite beneficiation, is not that well characterized. It is critical to know if ilmenite is free, the size of average ilmenite grain, and the size of average regolith material in order to be able to physically separate the ilmenite from the regolith. Consequently, we are in the process of asking NASA for lunar regolith so that we can characterize the material with ilmenite beneficiation in mind.

High-Precision Analyses of Platinoids

The techniques have been developed to analyze solutions which have a few parts per billion platinoids with reproducibility that is better than 7%. This will allow us to characterize any planetary material to determine if platinoids could be "mined" as a subproduct.

Future Work

In the next year we will characterize the physical characteristics of lunar regolith and continue developing the techniques to analyze small amounts of planetary material for economically viable elements.

Unconventional Propellant Performance

K. Ramohalli and M. Rascon
Department of Aerospace and Mechanical Engineering
The University of Arizona

This work involves the theoretical calculations of rocket performance of "exotic" fuels at various operating conditions such as chamber pressure, pressure ratios, and oxidizer-to-fuel ratios. By "exotic" fuels, we mean using materials that may not normally be used as fuels here on Earth due to low performance. The majority of the work is currently being done on a VAX using the CET 86 program by Gordon and McBride. The CET 86 program will be installed on our IBM PS/2 Model 80 to reduce computer costs. We have also received the JPL Solid Propellant Theoretical Performance program for the IBM, which handles solid fuels better than the CET 86 program. This program was developed by the Air Force and has been made available to us for restricted use. In addition, we also have received the AVCO version of the program. These enable easy comparison.

With the high cost of putting payloads into orbit, the ability to reduce the size and weight of the payload is highly beneficial. Since, in any space vehicle, the largest part of the vehicle consists of propellant, it is hoped that by finding space materials suitable for use as propellants, the overall size and weight of the vehicle can be reduced. To this end, this work is attempting to find propellants that will give acceptable performance, yet be producible or readily available in space scenarios. Another possibility is the use of materials, such kevlar and rubbers, that would be taken for other purposes. Also considered is the need for the propellant to be easily stored over long periods of time while ideally avoiding the use of heavy refrigeration systems.

Although extensive research has been done on Earth-transported propellants that have high performance characteristics, very little work has been done on propellants that give less than ideal performances. In additon to studying such overlooked propellants, we need to consider low chamber pressures, to help reduce weight, and high pressure ratios which can be achieved in atmospheres such as on Mars or the Moon. Some propellants considered unacceptable for use on Earth could be ideal for use elsewhere since trade-offs of performance for availability, storability, and cost are acceptable within the scope of this research.

We are approaching this problem by setting up the specific programs first on a VAX and on a PC. For the propellants I am presently considering, I am varying the chamber pressure and the oxidizer-to-fuel ratios for a variety of pressure ratios. Since just the present list of propellants will generate over 22,000 sets of data, we plan to present the data graphically, as well as in tabular form. After all the propellants have

been analyzed, we will be able to determine which ones (at which conditions) best meet our requirements.

We have set up the CET 86 program by Gordon and McBride on the VAX and have obtained results for a number of the propellant combinations being analyzed. A sample of these results is included (Appendix B). Several programs have been written to reduce the large amounts of data generated to include only the information needed, such as specific impulse, temperature, etc. We are currently working on a program to graphically display some of these data. Most of the initial runs were "verification" runs on conventional propellants. Nevertheless, one "exotic" extraterrestrial propellant is also shown in this appendix.

This work involves analyzing propellants at various operating conditions and determining which will give acceptable performance and yet be easily storable for long periods of time and be readily available in space missions. Work still to be done consists of completing the analysis of the remaining propellants and organizing the results into a more useful format. To assist in organizing the data, a commerical plotting program, such as the MathCAD program, would yield results in a more timely manner and make the development of a plotting program unnecessary. We will procure this and install it in 1989-90.

Jennifer Kares, an undergraduate student, has been assisting in the analysis of the fuels. Jeff Kahl, also an undergraduate student, has been assisting in the development of the various programs needed to process the data. These two are volunteering their time for academic credit, but at no cost to NASA at this time.

Development of Construction Materials Like Concrete From Lunar Soils Without Water

C. S. Desai, H. Saadatmanesh, and G. Frantziskonis
Department of Civil Engineering and Engineering Mechanics
The University of Arizona

Abstract

The development of construction materials such as concrete from lunar soils without the use of water requires a different methodology than that used for conventional terrestrial concrete. In this research project, a unique approach will be attempted that utilizes factors such as initial vacuum and then cyclic loading to enhance the mechanical properties of dry materials similar to those available on the moon. The application of such factors is expected to allow reorientation, and coming together, of particles of the materials toward the maximum theoretical density. If such a density can provide deformation and strength properties for even a limited type of construction, the approach can have significant application potential, although other factors such as heat and chemicals may be needed for specific construction objectives.

Introduction

Significant progress has been made in the area of space exploration in the past three decades. However, little has been done for development of construction materials for long-term shelters and work stations for man on other planets. For large-scale productivity on other planets, buildings and other structures are indispensable. Because of payload limitations on spacecrafts and the high cost of transportation, a prudent and efficient approach to construction on other planets requires that every effort be made to utilize the materials available on the planets themselves. The technique that is being developed in the Department of Civil Engineering and Engineering Mechanics is intended to utilize extraterrestrial "soils" to develop construction materials for building safe and serviceable structures.

Approach

Samples of lunar soil simulants of specimen size (3.0 × 6.0 inches) will be mixed in different proportions and will be tested under various levels of initial density and vacuum. Compacting the soil at different magnitudes of vacuum will give an indication of the effects of vacuum on lunar soil compactability. Then, cyclic loading, causing compression of the initial specimen, will be applied in a specially designed chamber using an MTS test frame. The experimental results will be plotted in terms of relations between initial density, initial vacuum, and number of loading cycles.

The material characteristics of the compacted samples (stress-strain response, angle of internal friction, and "apparent" cohesion) will be evaluated to assess the deformation and strength capabilities of the resulting compacted specimens.

Indeed, application of only compression cycles may not be able to provide the required deformation-strength characteristics for (all) construction objectives, and additional research to include other factors such as use of heat and chemicals would then be considered in subsequent research. This initial research would, however, provide the limit of compaction that can be achieved with cycles of compression without the use of water.

Results to Date

Samples of lunar soil simulant in grain sizes from 2 millimeters to less than 75 microns have been produced by crushing terrestrial basalt rocks. Approximately 0.25 cubic foot of lunar soil simulant, 30 percent of which is ultra-refined, is available for testing purposes.

A cylindrical vacuum chamber 15.0 inches high by 3 inches inside diameter has been machined from a single block of aluminum; design and fabrication of this device are supported by a grant from the Small Grants Program of the University of Arizona. The chamber is equipped with a ram-piston assembly to provide a means of loading the sample and is lined with Teflon to prevent cold-welding of the soil grains to the aluminum. Two ports in the chamber allow application of vacuum for both the top and bottom of the soil sample. Pressure is measured by a digital vacuum gauge with two Pirani PG-3 sensors attached to the chamber. The system is attached to a mechanical roughing pump and a diffusion-type vaccum pump capable of reducing the chamber pressure to 10 torr. Cyclic load is applied using an MTS hydraulic testing device which allows variation in load, cycle duration, and number of cycles and can automatically measure the displacement of the sample during loading.

Planned Research During the Next Year

A pilot series of tests will first be performed to establish the maximum compaction that can be achieved under different initial vacuums and density for a specimen of given initial height.

Then, a series of tests will be performed with three to four values of initial vacuum (V_0) and density (ρ_0). For each, the specimen will be subjected to cycles of compression loading. The results will be plotted in terms of variation of density with number of load cycles (N) for each V_0 and ρ_0. These results will be used to develop nondimensional relations between changing density as affected by V_0, ρ_o, and N.

A modified test device will be developed so that the compacted specimen can be tested with increasing axial stress, σ_1, (near) unconfined conditions, i.e., zero confining pressure σ_3 and different values of σ_3. The results will provide stress-strain relations in terms of $\sigma_1 - \sigma_3$ vs. ϵ_1 (axial stress). The deformation moduli and the strength parameters (angle of friction ϕ and cohesion C) can then be found from these stress-strain curves.

The above information will allow evaluation of the deformation-strength characteristics of the compacted specimens and the range of loading due to construction that such material is able to withstand.

It is felt that the above approach may not lead to materials with strengths required for (high) loads that may arise in common construction. Hence, the second phase of research would involve the use of factors such as heat and chemicals in addition to the cyclic compression loading. Acquisition of a furnace for this purpose is being considered at this time.

Acknowledgments

We would like to acknowledge the participation of Thomas Allen, Research Assistant, and Carl Peters, Technican, in this project.

III. SYSTEMS OPTIMIZATION

Interdependent Figure-of-Merit Software Development

K. Ramohalli and T. Kirsch
Department of Aerospace and Mechanical Engineering
The University of Arizona

This program was undertaken in order to understand the complex nature of interdependent performance in space missions. As the *first step* in a planned sequence of progress, a "spread sheet" program has been developed to evaluate different fuel/oxidizer combinations for a specific Martian mission. This program is to be linked with output attained using sophisticated software produced by Gordon and McBride. The data must be input by hand at this time. The programming to date makes use of 11 independent parameters. While the work is somewhat developed, some modifications such as the inclusion of aerobraking, in-situ propellant, output presentation, and automation of the data feed are still necessary. The program should prove to be quite valuable, even under its early stages of development.

Optimization is essential when faced with the incredible magnitude of costs, risks, and benefits involved with space exploration. We must decide not only what to use, but how to utilize it most effectively. Making the most of what we have and what we find is the essence of our NASA Center. A system of weights needs to be devised on which to measure our options. It is the goal of this work to devise a Figure of Merit (FoM) on which different choices can be presented and made (Fig. 3.1). The plan is to model typical missions to Mars, identify the parameters, and vary them until the best one is found. Initially, most of the focus is placed on propellant selection.

There has been some work done in the past and some currently under investigation which will prove crucial to our goals. Dr. Frisbee at JPL has been working on autonomous oxygen and carbon monoxide production from the Martian atmosphere for a number of years. He has provided his most current papers on the subject. They include the modeling information for power requirements, production rates, and system mass breakdown. There is a group willing to provide us with very reliable incremental velocity requirements for many different scenarios. There is a group in Austin, Texas, who have been doing feasibility studies for different lunar missions. They have neglected some important parameters regarding propellant selection, but their input still may prove useful. The tasks ahead are open for investigation.

The study utilizes current spread sheet technology and effectively demonstrates how changing a single parameter influences the feasibility of a mission. An IBM PC is currently being used to run LOTUS 123 Version 201. The plan is to keep the programming simple at first, building on the complexity with time. The first run of the program is for a specific mission, starting at LEO, making a landing on Mars, and from

- INDIVIDUAL FIGURES OF MERIT MISLEADING
  - Specific Impulse
  - Energy Density
  - Expansion Ratio
  - . . . . . .
- OVERALL MISSION IMPACT IMPORTANT
- MULTIVARIABLE PARAMETRIC PROBLEM
- EACH PARAMETER AFFECTS OTHERS
- COLOR-CODED QUANTITATIVE DISPLAY IS BEING DEVELOPED
  - I_{sp}, Transport, Energy Use (T, E), Storage, Refrigeration Needs, Products, ...

  (Recall Successful LP Program)

Figure 3.1. "Figure of merit" optimizations.

there placing a given payload into a Martian satellite orbit. The rocket staging was developed from the velocity requirements using Newton's laws and a minimum-energy transfer. This approach will utilize CET 86, Gordon and McBride's software for unconventional fuel performance. The current input parameters are made up of those placed on the fuel/oxidizer combination, the nozzle, the structural mass coefficient (tanks, pumps, refrigeration units, motors, etc.), and the payload itself. To date, they include the selection of the fuel and the oxidizer, whether the expansion is modeled as frozen or equilibrium flow, the mixture ratio, the chamber pressure, the ambient pressure, the expansion ratio, the nozzle's material density, its average thickness, the structural coefficient, and the payload mass. From this information, some useful quantities are found for each stage of the rocket and for the vehicle as a whole. They are made up of the following: exhaust velocities, mass flow rates, vehicular thrusts, throat areas, exit plane areas, nozzle coefficients, payload coefficients, initial masses, final masses, structural masses, fuel/oxidizer masses, and FoM. Currently, the FoM for each stage, as well as for the vehicle, is defined as the total initial mass divided by the mission payload. This will be modified to include risk, reliability, support hardware, etc. The real beauty of this approach to programming is the ease of immediate updating of the results.

To date, some runs have been accomplished. The last two months have been spent developing the basic logic for the program. A few additional parameters must be examined before the more visual aspects of the work can be effectively presented. The first is automating the data entry. All changes in the input have been entered by hand; a more efficient manner is under investigation. The LOTUS software is equipped with "macros" which allow complex, yet tedious tasks to be performed. The results should prove to be very powerful, especially when considering that over ten thousand points of propellant data have already been generated using CET 86. Having a subroutine to enter the data into the main program is not only feasible but also necessary for computer processing. The next step is to include an "aeroshell" in the model. The huge mass savings will prove to be a major factor in the minimization of the FoM. It will also make the mission profile much more realistic. Once these tasks have been accomplished, the real motivation for this initial spread sheet can be more effectively explored. In-situ propellant production will also start off simply, with the extraction of oxygen from the Martian atmosphere. These additions will make the data more presentable, both to those interested in finding an optimal solution and to others interested in viewing families of curves generated from other output data.

The research and complexity of the program are developing at a steady rate. The first major run of the spread sheet will come after the inclusion of "aerocapture" into

the model. The basic program will continue to evolve. The FoM must also contain a reliability factor. Leakage rates for all Earth-carried oxygen need to be included. The structural factor needs to be calculated using fuel density, chamber pressure, and cryogenic requirements. The different possibilities for in-situ propellant production must be examined. Oxygen can be produced from the atmosphere or from the polar ice cap. Other possibilities include hydrocarbons from water and CO_2. Further complexities will enhance the value of the work but will slow the computation speed. I have been in communication with the people at LOTUS regarding their Version 3; it is due to be released in the second quarter of 1989. Their newsletter claims that it meets their goals for speed and performance and, "123 Release 3 features significant power and performance enhancements including true three-dimensional spreadsheets, external database access, new recalculation techniques and graphics and printing improvements." We should be able to purchase an upgrade of the current version for about $200 and run the software on either of the SUN386i computers currently at the Center. The three-dimensional version would be a very useful means of storing both inputs and outputs.

Acknowledgments

The following people have been a tremendous help during the past two months; their efforts have not gone by unappreciated: Dr. K. Ramohalli, P.I.; Dr. R. Frisbee, JPL; Dr. J. Seutor, JPL; Dr. R. Beichel, Aerojet; Mario Rascon; and Jennifer Kares.

Quantitative Computer Simulations of Extraterrestrial Processing Operations

T. Vincent and P. Nikravesh
Department of Aerospace and Mechanical Engineering
The University of Arizona

Abstract

Three specific projects were initiated with late starting dates. The first and second projects, "Automatic Control of a Propellant Mixer" and "Computer Simulation of Engineering Processes," were started January 15, 1989, and the third project, "Control for Chaotic Mixing," was started February 1, 1989.

The first project is concerned with the automation of a small, solid-propellant mixer located on campus in the AME labs building. Temperature control is under investigation. A numerical simulation of the system is under development and will be tested using different control options. Control system hardware is currently being put into place.

The second project deals with the construction of mathematical models and simulation techniques for understanding various engineering processes. Computer graphic packages will be utilized for better visualization of the simulation results.

The third project is concerned with understanding and, hopefully, improving the mechanical mixing of propellants. Simulation of the mixing process is being done in conjunction with the second project. We will use this simulation capability to study how one can control for chaotic behavior to meet specified mixing requirements. An experimental mixing chamber is also being built. It will allow visual tracking of particles under mixing. The experimental unit will be used to test ideas from chaos theory, as well as to verify simulation results. This third project in the basic research category has clear applications to extraterrestrial propellant quality and reliability.

Introduction

In the production of solid propellants, components must first be mixed under specified conditions in order to produce a uniform product. To date, the batch processing of propellants is still largely a process with a human operator in the control loop. Not only is this unacceptable for space applications, but it makes it difficult to meet precise specified conditions.

Project I was initiated not only to automate processing, but to guarantee that the specified mixing conditions will be precisely met. Temperature control of the propellants is critical and was taken as the first automation task. During mixing, a specified temperature profile must be met.

Project II will be based upon some of the existing knowledge and capabilities of computational simulation of engineering processes. The algorithms and simulation software that will be compiled during the course of this project will be provided to any research participant in the NASA Center. At the start of this project, the main objective has been focused on the computer simulation of the entire mixing process.

Project III is concerned with the actual mechanical mixing of the propellants. Ultimately, one must be able to quantify the mixing process. Otherwise, how does one compare two mixtures? We must then seek out dynamical processes which yield "good" mixing in accordance with our definition.

Approach and Results--Project I

Two hot water tanks are currently in use with the University of Arizona mixer. One is set at 160°F and the other is set at 140°F. Currently, the operator draws water from one tank or the other to meet two temperature set points. This open-loop approach is undesirable, not only from the point of view that it requires an operator, but the temperature in the two tanks may vary considerably. Our approach is to continue to use the two tanks but with one set >160° and one set <140°. Two control valves will regulate the amount of water drawn from each tank, thereby maintaining a constant flow rate and allowing for control of the specified temperature set points.

A proportional plus integral controller has been investigated using a numerical simulation and has been shown to be satisfactory. Actual control for the mixing system will be by means of a small digital computer with A/D and D/A interfaces. Thermocouple readings will be read into the computer and the control algorithm will, in turn, send a signal out through the D/A channel to set the valves. The computer system and one thermocouple are already in place. The control valves are on order and some replumbing will be required.

Approach and Results--Project II

Until we acquire a workstation for computer graphics and simulations, we are using the Silicon Graphics Workstation at the Computer-Aided Engineering Laboratory (CAEL). Since this is a Unix-based system, transition to another Unix-based system, such as a SUN workstation, should be rather easy. The first problem that we have considered for computer simulation is the formation of the mixing process of Project III.

Approach and Results--Project III

There is a close relationship between chaos and mixing. Indeed, the "baker map" used to explain chaos is a mixing tool (stretch then fold). This presents us with an

inverse problem in controls. Rather than designing a controller to produce uniform stable motion, our objective is to introduce controls into a system to make the behavior as random as possible. How does one design a controller so that the controlled system map will be one which will guarantee mixing? As with most progress in chaos theory, a great deal of simulation is required. We are currently working with some maps which should produce good mixing. These will be tested against a mixing definition so that a comparison of maps can be made. We will then examine the control dynamics to produce the maps. These will be examined both numerically and with an experimental mixing chamber. The first chamber has already been built and will be tested shortly.

Acknowledgments

We wish to acknowledge the work of Richard Wilson (M.S. Candidate) on Project I, Michael Hicks (M.S. Candidate) on Project II, and Arthur Mazer (Ph.D. Candidate, Applied Math.) on Project III.

Energy Management Study for Lunar Oxygen Production

R. A. Fazzolare and B. G. Wong-Swanson
Department of Nuclear and Energy Engineering
The University of Arizona

Abstract

Energy management opportunities in the process of hydrogen reduction of ilmenite for lunar oxygen production are being investigated. An optimal energy system to supply the power requirements for the process will be determined.

Introduction

Oxygen is one of the most important materials necessary for space exploration and colonization. It provides life support on space stations and fuel for propulsion. The high cost of payload delivery from Earth and the high fuel requirement make any long-distance space journey unfeasible. Oxygen production in space, such as on the moon or asteroids, can provide "refueling stations" for life support, combustion, and propellant.

Different processes have been proposed for oxygen production in space. These processes will require high thermal and electrical power. This project examines the power requirements of one such process. Specifically, lunar oxygen production from ilmenite reaction with hydrogen will be studied to optimize its energy requirements.

Objective

The objective of the study is to determine an optimal energy system which would provide power for lunar oxygen production through hydrogen reduction of ilmenite. Ultimately, the goal is to develop an analytical model which would determine an appropriate optimal energy system for any given oxygen production process.

Background

The basic reactions for hydrogen reduction of ilmenite to produce oxygen are:

$$FeTiO_3 + H_2 \rightarrow\!\!\!\!\rightarrow Fe + TiO_2 + H_2O \quad (1)$$

$$H_2O \rightarrow\!\!\!\!\rightarrow H_2 + (1/2)O_2 \quad (2)$$

The first reaction occurs endothermically at temperatures ranging from 700°C to 1000°C. The per-pass conversion of H_2 to H_2O is about 5% at 900°C. The second reaction occurs through electrolysis, or thermal water splitting. As can be seen, there is a tremendous energy requirement, not just to meet the thermal and electrical

demands for the reactions to take place, but also for mining the ores, separating ilmenite from the ores, and pumping different materials through the system.

Figure 3.2 illustrates the process with a simplified block diagram. Mined regolith first passes through a beneficiator, where ilmenite is separated from non-ferrous ores. The ilmenite is then sent to the reactor, where hydrogen is introduced. The hydrogen removes oxygen from the FeO component in ilmenite to form water. Water is then separated into components of hydrogen and oxygen through electrolysis. The oxygen is then cooled, liquefied, and stored. The hydrogen is recycled through the system.

Approach

The energy management study for the ilmenite hydrogen reduction process will include the following:

1. Preparation of the ilmenite hydrogen reduction process flow diagram and determination of the appropriate temperatures and pressures for ilmenite feed, ilmenite/hydrogen reaction, water splitting, and the liquefied oxygen product. (This information will be developed with support from the Department of Chemical Engineering.)
2. Use of computer programs (presently available or newly developed) to perform mass, energy, and exergy balance of all the components in the ilmenite hydrogen reduction process. This analysis will show the irreversibilities of the various components, identify the ones which are high contributors to irreversibilities, and, as a result, determine energy management opportunities.
3. Application of the "Pinch Method" and use of commerically available computer programs to identify the various hot and cold streams in the process which could be used for process heat integration. Hot streams are those which need to be cooled; cold streams are those which need to be heated. The general approach of the Pinch Method is to combine all the hot streams in the process and plot them on an enthalpy-versus-temperature chart. All the cold streams are combined and put on the same chart. The point where the smallest ΔT occurs beteen the two curves is the pinch. The hot streams above the pinch should be utilized for preheating purposes. The cold streams below the pinch should be utilized for precooling. Thus, the Pinch Method shows how various flow streams may be integrated to reduce heating and cooling requirements. For example, since it is desirable to reject heat in the spent feeds at as close to ambient temperature as possible, the high-temperature slag exiting the reactor may be used to preheat recycled hydrogen.

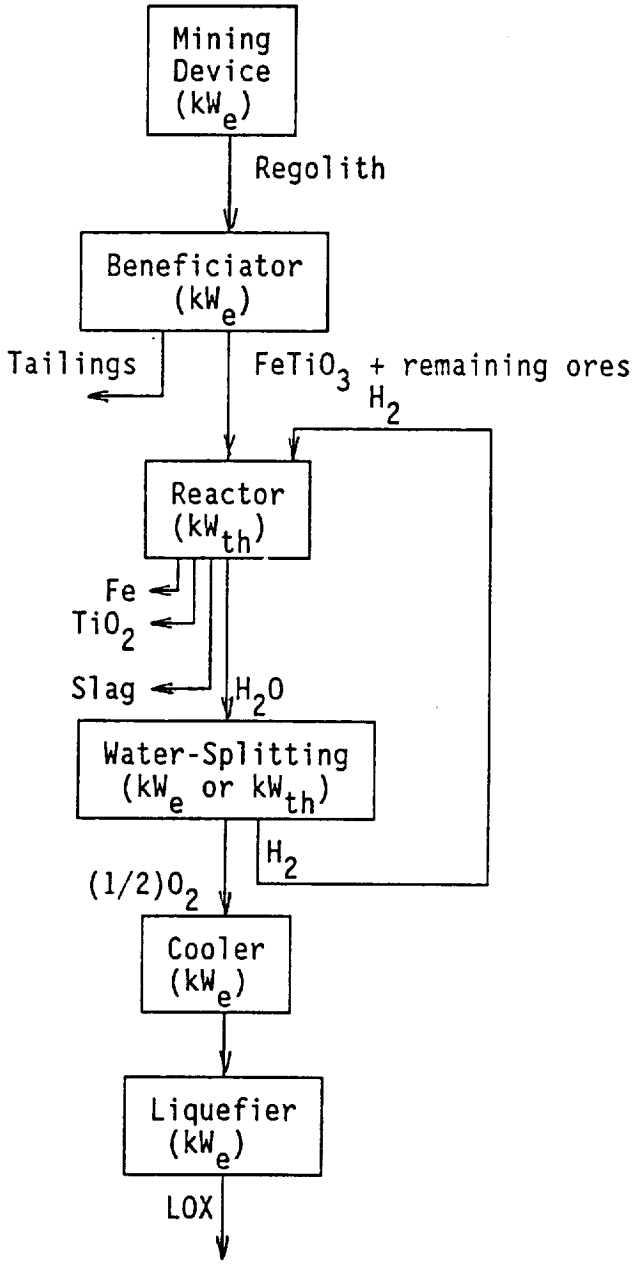

Figure 3.2. Block diagram for the process of hydrogen reduction of ilmenite to produce oxygen.

4. Exploration of opportunities to minimize the use of electrical energy. For example, investigate the current status of research in thermal water splitting to determine if the technology could be applied to replace the electrolysis portion of the ilmenite hydrogen reduction process.
5. Determination of the optimum source(s) of energy by setting the energy and capital (mass) targets.

Research Status and Results to Date

Due to problems with University registration, this project was not formally begun until January 1989 and, therefore, no analysis results have been obtained at this time.

The research effort thus far has been limited to reading references on related subjects:

1. W. W. Mendell (Ed.), *Lunar Bases and Space Activities of the 21st Century*, Lunar and Planetary Institute, Houston, 1985.
2. T. J. Kotas, *The Exergy Method of Thermal Plant Analysis*, Anchor Brendon Ltd., Essex, 1985.
3. T. Rosenqvist, *Principles of Extractive Metallurgy*, McGraw-Hill Ind., 1974.
4. Papers on the application of the Pinch Method to various industrial processes.

Future Work

Approach items (1) and (2) are expected to be completed during the next report period. The process flow diagram, as well as the process mass, energy, and exergy balance, will be presented in the next status report. The pinch analysis should also begin during this time.

IV. DATA BASE DEVELOPMENT

Development of the Data Base for Near-Earth Resources

D. R. Davis
Planetary Science Institute
Science Applications International Corporation

Development of the data base for near-Earth resources was begun in the period covered by this report.[1] Specific items accomplished were:

1. Definition of data base contents via discussions among the PSI staff and outside scientists such as Lucy McFadden and Mark Skyes.
2. Discussion/demonstration of dBase capabilities and possible organization of file(s) with L. Alvarez, Steward Observatory.
3. Data base entries for near-Earth asteroids consisting of data from the Russian ephemeris, a forthcoming review chapter for the Asteroids II book, and other literature sources.
4. Development of a list of asteroid observers worldwide to be contacted during the coordination phase of the project.

A copy of the data base as it now exists is included as Appendix C. It is currently set up in a spreadsheet format (which can easily be converted into an ASCII file), awaiting delivery of the dBase IV software from the University of Arizona as discussed with Dr. Lewis. We will transfer the data to dBase IV as soon as it arrives.

Bibliographic Search of the Literature on Lunar Processing

D. R. Criswell
California Space Institute
University of California, San Diego

The Lunar and Planetary Institute (LPI) search produced approximately 80 references. Most of these are available at the LPI. The product includes only the author, title, date, and reference. The earliest (Cooper et al, Certain ecological aspects of a closed lunar base, Rand Corp.) is dated 6 March 1958. The latest is a semi-popular article (Cole & Majdacic, Astronomy, vol. 16, 18-24) produced last year. The early references tend to be reports of government-sponsored engineering studies. The later are generally semi-popular and science press articles. These references will be obtained on disk from the LPI and can be converted into an ASCII file for access via IBM-compatible PCs.

At the Johnson Space Center (JSC) library a search was conducted of the major NASA data bases. The final print-out of references and short abstracts is 70 pages long. The document could not be obtained in electronic form through JSC. Most, likely all, of the useful references can be obtained through The University of Arizona library. Two days of travel and time to work at Tucson with the appropriate personnel will be allocated to obtain the desired references in computer-readable form.

Twenty-three sets of microfiche were received from NASA on the earliest references to use of lunar materials.

The Lunar and Planetary Receiving Lab (LPRL) at JSC has a small library with a very limited collection of materials on lunar utilization. However, an early study by Mr. A. Sanders (Extraterrestrial Consumables Production and Utilization, JSC, May 1972) was obtained and will be included. This report must be copied and the original returned to the JSC/Building 31 library. The University of Arizona library probably contains all the LPRL references of use to SERC. However, the group has produced "A Lunar Bibliography" (p. 50, March 1988) that should be of use.

Following completion of the code Z Lunar Enterprise Study, the above materials and the reports on lunar processing done under my direction at the LPI will be reviewed for references of greatest interest to SERC. Senior researchers who participated in the workshops supported by that study will also be contacted to request copies of any relevant works they have produced since 1980.

An Annotated Bibliography of Propellant Processing Methods

A. H. Cutler

Dr. Cutler has specialized in space resources research for many years, with special emphasis on oxygen reduction methods. He has been retained to write a comprehensive review of these methods, detailing advantages and disadvantages, listing byproducts, and presenting recommendations. As the first step, an extensive outline was prepared, and the portion of this outline covering product manufacture was selected as the initial goal. A working version of this section follows:

Products

I. Propellant
  A. Oxidizer
    1. Oxygen
      a. Production from lunar materials
        i. Slagging carbothermal
          - of ilmenite
          - of olivine
          - in integrated polyelement processes
        ii. Subsolidus reduction
          - ilmenite with H_2 or C
          - olinite with H_2 or C
        iii. Plasma processes
          - with $H^{\bullet}/H_2$ + $FeO{\cdot}XO_2$
          - with $Cl^{\bullet}/Cl_2$ + $FeO{\cdot}XO_2$
        iv. Slog electrolysis
          - bulk soil
          - mineral separates
          - with fluxes (Kesterk, EMEC)
      b. Production from asteroidal/Phobos/Deimos meet?
        i. Water splitting
          - electrolysis
          - photolysis
          - thermolysis
        ii. CO_2 processing
          - solid state electrolysis
          - carbonate? melt electrolysis
        iii. Oxide reductions, e.g., FeO + $(CH_2)_n$
      c. Production on Mars surface--variants of processes above

2. Peroxide
   a. H_2O_2 via Na_2O_2
   b. Direct $H_2 + O_2$
   c. Electrochemical means from O_2
   d. Water partial oxidation
3. Nitrogeneous oxidizers
   a. Organic N → NH_3
   b. Organic N → N_2
   c. N_2 → NH_3
   d. Organic N → NO
   e. NH_3 → $NO + H_2O$
   f. NO → NO_2
   g. $NO_2 + H_2O$ → HNO_3
   h. N_2O_4
   i. RFNA

B. Fuels
   a. Hydrogen
      i. From lunar soil
      ii. From asteroidal materials via hydrocarbons
      iii. Various routes from water (see above)
   b. Hydrocarbons
      i. Direct from asteroids phobos and demo
      ii. Reformed from initial pyrolyzate
      iii. Fischer-Tropsch synthesis from $CO + H_2O$
      iv. From CH_3OH
   c. Oxygenates--alcohols, ethers, etc.
      i. Methanol from $CO + H_2$
      ii. Higher alcohols from $CO + H_2$
      iii. Hydrocarbons → oxygenates
   d. Hydrocarbon--hydrogen mixtures
      (solubility of H_2 in various materials)
   e. Metals
      i. Al
      ii. Mg } see metal production below
      iii. Ca
   f. Metal/liquid mixtures

g. Nitrogeneous fuels
    i. Ammonia (see above)
    ii. Hydrazines from ammonia
        - Cl_2 process
        - O_2 process
        - organo substituted hydrazines

C. Thermal propellants
    1. Hydrogen (see above)
    2. Ammonia (see above)
    3. Hydrozine (see above)
    4. Others

D. Elecric propellants
    1. Calcium and potassium
    2. Compounds--Cl_2, SO_3, etc.

E. Mars propellants
    1. Hydrogen peroxide (see above)
    2. Hydrozine (see above)
    3. Fuel/oxidizer solutions
        a. Hydrocarbon--oxygen
        b. Peroxide/alcohol or peroxide/hydrocarbon
    4. Metal/sulfur propellants (MgS, CaS)

II. Structural Materials

A. Metallic
    1. Ferrous (Fe, Ni, Co)
        a. Fe--steel
            i. From magnetic collection
            ii. From subsolidus reduction
            iii. From slogging
        b. Iron alloys
            i. Imported alloying additions
            ii. Local source
        c. Forming and heat treating
            i. Forging
            ii. Casting
            iii. Machining
            iv. Carboxyl deposition

2. Non-ferrous metals
    a. Aluminum
        i. Winning
            - carbochlorination
            - plasma chlorination
            - fluorination
            - integrated processes
        ii. Forming
            - cast
            - roll
            - forge
            - machine
        iii. Alloying additions
            - local source--Mg, Mn
            - imported--Zn, Cu
    b. Magnesium
        i. Winning
            - carbothermal
            - salt electrolysis
            - plasma processing
        ii. Generation of MgO feed
        iii. Forming (as for aluminum)
        iv. Alloying additions
3. Vacuum refining
    a. Advantages and effects on properties
    b. Effect on local environment
4. Tool materials
    a. Tool steels--composition and properties
    b. Titanium carbide tool materials--cobalt bonded
        i. Cobalt source
        ii. Other binders
5. Brazes and solders
    a. Aluminum, magnesium, and calcium as vacuum brazes

B. Non-metallic
1. Bricks
    a. Morter bound
    b. Cut stone

c. Sintered

d. Slogged and cast

i. Glass

ii. Ceramic

2. Bogs

a. Wire

b. Glass

3. Beams and pillars

a. Fused soil

b. Sintered

c. Mortered

d. Packed form

4. Fibers--glass

5. Refractories

a. Graphite

b. Magnetite and CaO

c. CaS and MgS

d. Cr_2O_3

e. Titanium oxides

6. Cements

7. Inorganic Polymers

8. Sulfur

III. Explosives

A. Fuel/oxidizer explosives

1. Fuel/H_2O_2

a. Organic

b. Metallic

2. NH_4NO_3 + fuel

B. Nitrates from oxygenated organics and nitric acid

Preliminary Analysis of Surface Characteristics of Comet Tempel 2

H. Campins
Planetary Science Institute
Science Applications International Corporation

A preliminary analysis of the surface characteristics of Comet Tempel 2 has been completed and incorporated into the paper "The Nucleus of Comet Tempel 2" by M. F. A'Hearn, H. Campins, D. G. Schleicher, and R. L. Millis which was submitted to the *Astrophysical Journal*, March 1989 (Appendix D).

A detailed analysis of the surface characteristics of Comet Arend-Rigaux and Comet Tempel 2 is being carried out in collaboration with Dr. R. H. Brown (JPL).

---

[1] Although the period of performance for Year 1 is given as 9/1/88-12/31/89, please note that funding (and therefore work) did not begin on these projects until 12/17/88.

APPENDIX A

14654

Notes on Lunar Ilmenite

N91-25221

M. Hutson
Lunar and Planetary Laboratory
The University of Arizona

Opaques (mostly ilmenite) make up 0-5% of highland rocks, 1-11% of low-Ti mare basalts, and 10-34% of high-Ti mare basalts (Carter 1988). Apollos 11 and 17 sampled high-Ti basalts. Apollos 12 and 14 sampled low-Ti basalts. Apollo 15 sampled a complex mixture of mare and highland material. Apollo 16 sampled mainly highland material (Taylor 1975).

Mare Basalts (Rocks)

Ilmenite is the third most abundant mineral in Apollos 11 and 17 rocks. It is very conspicuous in Apollo 11 samples, with platy crystals occasionally reaching several millimeters in size (Levinson and Taylor 1971, Mason and Melson 1970). Ilmenite is found in a wide variety of shapes, ranging from euhedral to anhedral, blocky, tabular, platy, and skeletal forms (Frondel 1975, Levinson 1971). Ilmenite also occurs as rims surrounding armalcolite cores. These rimming ilmenites generally contain exsolved rutile and spinel (Frondel 1975). However, most ilmenite is homogeneous, and the ilmenites associated with armalcolite and exsolved rutile are "relatively rare and quantitatively minor" (Levinson and Taylor 1971).

Lunar ilmenite is almost pure $FeTiO_3$; a Mossbauer study of Apollo 11 ilmenite found no detectable ferric iron (Mason and Melson 1970). The following minor and trace elements have also been reported: Apollo 11--Al_2O_3, 0.1-0.3%; MnO, 0.3-0.6%; CaO, up to 0.3%; Cr_2O_3, 0.1-1.3%; V_2O_3, up to 0.2%; Zr_2O_3, up to 0.3%; and MgO, up to 6.0% (Mason and Melson 1970). Ilmenite appears to be the major host phase for Zr (Levinson and Taylor 1971). There does not appear to be any relationship between MgO content of ilmenite and its grain size or mineral association (Frondel 1975), although some researchers have suggested that high-magnesian ilmenite is associated with armalcolite (Frondel 1975). Levinson and Taylor (1971) state that high-magnesian ilmenite in Apollo 11 samples occurs as small tabular grains totally enclosed in pyroxene. Apollo 14 ilmenite contains 0.2-0.6 wt% ZrO_2 and up to 3.9 wt% MgO, which is noteworthy as the whole rock has lower MgO than that from other Apollo sites (approximately 8-8.5 wt%). In addition, ilmenite from one Apollo 14 sample contained Ti^{+3} (El Goresy et al. 1972). Apollo 17 sampled two types of basalts with different crystallization histories. Ilmenite is found as primary blocky crystals in both types of basalt and as rims around armalcolite in Type II basalts (El Goresy et al. 1974). Apollo

17 ilmenite contains 0.55-0.70 wt% MnO, 1.51-4.68 wt% MgO, and 0.48-1.05 wt% Cr_2O_3 (El Goresy et al. 1974).

Mare Soils

The lunar regolith contains material ranging from fines to blocks meters across. The material with grain size less than 1 mm is referred to as soil (Taylor 1975). This soil consists of mineral grains, rock fragments, glasses, and agglutinates, which are "glassy, rock and mineral fragments welded together by glass" (Taylor 1975). Agglutinates constitute up to half of the material in some size fractions (Levinson and Taylor 1971; Agosto 1988). As a result, the amount of ilmenite which is easily separated from lunar soils is considerably less than the normative ilmenite. This was shown by McKay and Williams (1979), who report modal abundances of 2.2% and 4.9% for Apollo 11 and 17 soils with normative abundances (calculated from TiO_2 contents) of 14.7% and 15.5%, respectively. They note that the available ilmenite in the average Apollo 17 mare soil is only one-third of the normative ilmenite. McKay and Williams (1979) also suggest that ilmenite abundance increases with decreasing grain size fraction. However, a study of Luna 24 soils does not support this correlation (Laul et al. 1987).

Frondel (1975) reports the results of x-ray studies; lunar and terrestrial ilmenite appear to have identical crystal structure parameters. She concludes: "It would appear that until we have many more x-ray and chemical analyses of both lunar and terrestrial ilmenites, the lunar ilmenite and its earthly counterpart can be assumed to be the same." However, it is known that reduction of lunar ilmenite is more difficult than for terrestrial ilmenite, due to the lack of ferric iron in the lunar ilmenite (Briggs 1988).

Finally, McKay and Williams (1979) note that hydrogen is implanted in lunar soils by the solar wind. Data on hydrogen content of lunar soils are sparse and not in good agreeement. Reported bulk soil hydrogen contents range from 30-145 ppm. McKay and Williams (1979) note that ilmenite is known to retain helium much more readily than other minerals. Although there are no data for hydrogen, they speculate that if hydrogen is retained similarly to helium, it could exist at the 1000 ppm level in lunar ilmenite.

Beneficiation

A discussion of possible techniques for mining and beneficiation of lunar ores is given by Williams et al. (1979). However, it appears that only William N. Agosto has actually attempted to separate ilmenite from lunar soils in the laboratory (Agosto 1984, 1985, 1988). Agosto has done electostatic separation experiments on simulant soils

(made with terrestrial ilmenites) and a 90-150 micron size fraction of an Apollo 11 soil. The experiments were run both in a vacuum and in a nitrogen atmosphere. Only 30% of the ilmenite was recovered in one pass in the vacuum (it is not clear whether he is referring to lunar or simulant ilmenites), while much better results were obtained using a nitrogen atmosphere, because of the density difference between ilmenite and other minerals in the soil (Agosto 1988). Ilmenite in the lunar simulant was concentrated from 10 wt% to 95 wt%, with 68% of the ilmenite recovered after one pass in nitrogen. Ilmenite in the Apollo 11 soil was concentrated from 10 vol% to 54 vol%, with 45% recovery after one pass (Agosto 1984). Perhaps some combination of magnetic and electrostatic separation is needed.

Bibliography*

Acton, C. F. (1988) Processing of metal and oxygen from lunar deposits. In untitled report of 1984 NASA LaJolla summer study on use of space resources (preprint).

Agosto, W. N. (1984) Electrostatic separation and sizing of ilmenite in lunar soil simulants and samples. *LPSC XV*, 1-2.

Agosto, W. N. (1985) Electrostatic concentration of lunar soil minerals. In *Lunar Bases and Space Activities of the 21st Century*, LPI.

Agosto, W. N. (1988) Lunar beneficiation. In untitled report of 1984 NASA LaJolla summer study on use of space resources (preprint).

Alexander, C. (1978) Extraterrestrial resources in the solar system. *The Foundation Report 2*, 1-6.

Allton, J. H., C. Galindo, Jr., and L. A. Watts. (1985) Guide to using lunar soil and simulants for experimentation. In *Lunar Bases and Space Activities of the 21st Century*, LPI.

Bence, A. E. (1988) Lunar resource evaluation and mine site selection. In untitled report of 1984 NASA LaJolla summer study on use of space resources (preprint).

Blank, H., A. El Goresy, J. Janicke, R. Nobiling, and K. Traxel. (1984) Partitioning of Zr and Nb between coexisting opaque phases in lunar rocks--determined by quantitative proton microprobe analysis. *EPSL 68*, 19-33.

BSVP (Basaltic Volcanism Project). Lunar highland basalts, Ch. 1.2.10, 268-281.

BSVP (Basaltic Volcanism Project). Lunar mare basalts, Ch. 1.2.9, 236-267.

Briggs, R. (1988) Oxidation/reduction of ilmenite and the design of an oxygen production facility for use on the moon. *SSI Update*, Vol. XIV, Issue 6, 1-5.

*References gathered so far. Question marks indicate that I don't have the information, I was looking at a photocopy, etc.

Carter, J. L. (1988) Lunar material resources: an overview. In untitled report of 1984 NASA LaJolla summer study on use of space resources (preprint).

Chyi, L. L. and W. D. Ehmann (1973) Zirconium and hafnium abundances in some lunar materials and implications of their ratios. *Proc. 4th Lun. Sci. Conf.*, 1219-1226.

Cutler, A. H. (1984) Lunar oxygen production by carbothermal processing. Grant proposal.

Cutler, A. H. (1985) A carbothermal scheme for lunar oxygen production. In *Lunar Bases and Space Activities of the 21st Century*, LPI.

Cutler, A. H. (????) Arc electrolysis of molten silicates (preprint).

Davis, P. A. (1980) Iron and titanium distribution on the moon from orbital gamma ray spectrometry with implications for crustal evolutionary models. *JGR 85*, 3209-3224.

Davis, P. A. and J. R. Arnold (????) Iron and titanium distribution on the lunar surface as determined by matrix inversion of gamma-ray orbital data. ???? (abstract).

Donnelly, R. P., L. J. Brennan, W. McMullan, and A. Rouillara (1970) Reduction of iron oxide in ilmenite beach sands. *Australian Mining*, March, 58-65.

Ehmann, W. D. and L. L. Chyi (1974) Abundances of the group IVB elements, Ti, Zr, and Hf and implications of their ratios in lunar materials. *Proc. 5th Lun. Conf.*, 1015-1024.

Ehmann, W. D., L. L. Chyi, A. N. Garg, and M. Z. Ali (????) The distribution of zirconium and hafnium in terrestrial rocks, meteorites and the moon. ????

El Goresy, A., L. A. Taylor, and P. Ramdohr (1972) Frau Mauro crystalline rocks: mineralogy, geochemistry and subsolidus reduction of the opaque minerals. *Proc. 3rd Lun. Sci. Conf.*, 333-349.

El Goresy, A., P. Ramdohr, O. Medenbach, and H. J. Bernhardt (1974) Taurus-Littrow TiO_2-rich basalts: opaque mineralogy and geochemistry. *Proc. 5th Lun. Conf.*, 627-652.

Engelhardt, W. V. (1979) Ilmenite in the crystallization sequence of lunar rocks. *Proc. Lun. Plan. Sci. Conf. 10th*, 677-694.

Frondel, J. W. (1975) *Lunar Mineralogy*, John Wiley and Sons.

Ganapathy, R., G. M. Papia, and L. Grossman (1976) The abundances of zirconium and hafnium in the solar system. *EPSL 29*, 302-308.

Garg, A. N. (????) Simultaneous determination of Zr and Hf by radiochemical neutron activation analysis and their distribution in lunar rocks and meteorites. ????

Gibson, M. A. and C. W. Knudsen (1985) Lunar oxygen production from ilmenite. In *Lunar Bases and Space Activities of the 21st Century*, LPI.

Grey, I. E., A. F. Reid, and D. G. Jones (1974) Reaction sequences in the reduction of ilmenite: 4—interpretation in terms of the Fe-Ti-O and Fe-Mn-Ti-O phase diagrams. *Trans. Inst. Min. Met. 83*, C105-C111.

Haskin, L. A. (1985) Toward a spartan scenario for use of lunar materials. In *Lunar Bases and Space Activities of the 21st Century*, LPI.

Hughes, S. S. and R. A. Schmitt (1985) Zr-Hf-Ta fractionation during lunar evolution. *Proc. 16th Lun. Plan. Sci. Conf.*, D31-D45.

Hussein, M. K., R. Kammel, and H. Winterhagen (1967) A study on the reduction mechanism of ilmenite ores. *Indian J. Technol. 5*, 369-377.

Hussein, M. K. and S. Z. El-Tawil (1967) Solid state reduction of Egyptian black sand ilmenite with hydrogen. *Indian J. Technol. 5*, 97-100.

Knudsen, C. W. and M. A. Gibson (1988) Processing lunar soils for oxygen and other materials. In untitled report of 1984 NASA LaJolla summer study on use of space resources (preprint).

Laul, J. C., O. D. Rode, S. B. Simon, and J. J. Papike (1987) The lunar regolith: chemistry and petrology of Luna 24 grain size fractions. *Geochim. Cosmochim. Acta. 51*, 661-673.

Levinson, A. P. and S. R. Taylor (1971) *Moon Rocks and Minerals*, Pergamon Press.

Lewis, J. S., T. D. Jones, and W. H. Farrand (????) Carbonyl extraction of lunar and asteroidal materials (unpublished).

Lewis, J. S. and R. A. Lewis (1987) *Space Resources: Breaking the Bonds of Earth*, Columbia Univ. Press.

Lindstrom, D. J. and R. H. Lewis (1984) Systematics of electrical conductivities in silicate melts and implications for melt structure. *EOS 65*, 290.

Lindstrom, D. J., R. H. Lewis, and L. A. Haskin (????) Electrical conductivity of lunar melts. ???? (abstract).

Mason, B. and W. G. Melson (1970) *The Lunar Rocks*, John Wiley and Sons.

McKay, G., J. Wagstaff, and S. R. Yang (1986) Zirconium, hafnium, and rare earth element partition coefficients for ilmenite and other minerals in high-Ti lunar mare basalts: an experimental study. ????

McKay, D. S., R. M. Fruland, and G. H. Heiken (1974) Grain size and the evolution of lunar soils. *Proc. 5th Lun. Conf.*, 887-906.

McKay, D. S. and R. J. Williams (1979) A geologic assessment of potential lunar ores. *Space Resources and Space Settlements*, NASA SP-428, 243-255.

Meek, T. T., D. T. Vaniman, F. H. Cocks, and R. A. Wright (1985) Microwave processing of lunar materials: potential applications. In *Lunar Bases and Space Activities of the 21st Century*, LPI.

Metzger, A. E. and R. E. Parker (1979) The distribution of titaniaum on the lunar surface. *EPSL 45*, 155-171.

Nakamura, Y., H. Fujimaki, N. Nakamura, and M. Tatsumoto (1986) Hf, Zr, and REE partition coefficients between ilmenite and liquid: implications for lunar petrogenesis. *Proc. 16th Lun. Plan. Sci. Conf.*, D239-D250.

Poggi, D., G. G. Charette, and M. Rigaud (????) Reduction of ilmenite and ilmenite ores. ????

Rao, D. Bhogeswara, U. V. Choudary, T. E. Erstfeld, R. J. Williams, and Y. A. Chang (1979) Extraction processes for the production of aluminum, titaniaum, iron, magnesium, and oxygen from nonterrestrial sources. *Space Resources and Space Settlements*, NASA SP-428, ??

Shima, M. (1979) The abundances of titanium, zirconium and hafnium in stony meteorites. *GCA 43*, 353-362.

Stanin, F. T. and L. A. Taylor (1979) Armalcolite/ilmenite: mineral chemistry, paragenesis, and origin of textures. *Proc. Lun. Plan. Sci. Conf. 10th*, 383-405.

Taylor, S. R. (1982) *Planetary Science: A Lunar Perspective*, Lunar and Planetary Institute.

Usselman, T. M. (1975) Ilmenite chemistry in mare basalts, and experimental study. *Abstract of Conf. on Origin of Mare Basalts and Their Implications for Lunar Evolution*, 164-168.

Visnapuu, A., B. C. Marek, and J. W. Jensen (1972) Conversion of ilmenite to rutile by a carbonyl process. U.S.D.I., Bureau of Mines Rept., Investigation 7719.

Volk, W. and H. H. Stotler (1970) Hydrogen reduction of ilmenite ores in a fluid bed. *J. of Metals*, January, 50-53.

Waldron, R. D. (1979) The role of chemical engineering in space manufacturing. *Chem. Eng.*, February 12, 80-94.

Walsh, R. H., H. W. Hockin, D. R. Brandt, P. L. Dietz, and P. R. Girardot (1960) The reduction of iron values of ilmenite to metallic iron at less than slagging temperatures. *Trans. of the Metall. Soc. of AIME 218*, 994-1003.

Webster, A. H. and N. F. H. Bright (1961) The system iron-titanium-oxygen at 1200 C and oxygen partial pressures between 1 atm and 2×10^{-4} atm. *J. Amer. Ceramic Soc. 44*, 110-116.

Williams, R. J. (1983) Enhanced production of water from ilmenite: an experimental test of a concept for producing lunar oxygen. *LPSC XIV Special Session Abstracts*, 34-35.

Williams, R. J. (1985) Oxygen extraction from lunar materials: an experimental test of an ilmenite reduction process. In *Lunar Bases and Space Activities of the 21st Century*, LPI.

Williams, R. J., D. S. McKay, D. Giles, and T. E. Bunch (1979) Mining and beneficiation of lunar ores. *Space Resources and Space Settlements*, NASA SP-428, 275-288.

OMIT
TO D-1
p. 29

APPENDIX B

```
THERMO
REACTANTS
C   5.9500  H   9.2500  O   0.3500  N   0.0500      0.0000    13.779000    -164000.00  S    298.150     F
AL  1.0000      0.0000      0.0000      0.0000      0.0000    18.000000          0.00  S    298.150     F
N   1.0000  H   4.0000  CL  1.0000  O   4.0000      0.0000    68.221001     -70690.00  S    298.150     O


NAMELISTS
$INPT2
KASE     =            20,
T        = 26*0.0000000E+00,
P        =   588.0000     , 25*0.0000000E+00,
PSIA     = T,
MMHG     = F,
NSQM     = F,
V        = 26*0.0000000E+00,
RHO      =   588.0000     , 25*0.0000000E+00,
ERATIO   = F,
OF       = F,
FPCT     = F,
FA       = F,
MIX      = 26*-1.000000     ,
TP       = F,
HP       = F,
SP       = F,
TV       = F,
UV       = F,
SV       = F,
RKT      = T,
SHOCK    = F,
DETN     = F,
TRACE    =  0.00000000000000000E+00,
SO       =  0.00000000000000000E+00,
SO       =  0.0000000E+00,
IONS     = F,
IDEBUG   =            0,
PHI      = F,
SIUNIT   = F,
INHG     = F,
TRNSPT   = F,
TRPACC   =  0.9999000000000000     ,
DIF      = F,
NODATA   = F,
U        =  1.00000000000000000E+30,
H        =  1.00000000000000000E+30
$END

NO INPT2 VALUE GIVEN FOR OF, EQRAT, FA, OR FPCT

SPECIES BEING CONSIDERED IN THIS SYSTEM
 J 6/79  AL                   J 6/63  ALC          J 9/79  ALCL          J 6/76  ALCL2         J 9/79  ALCL3
 J 6/63  ALH                  J12/79  ALN          J12/79  ALO           J 9/64  ALOCL         J12/67  ALOH
J12/79  ALO2                  J12/68  ALO2H        J 6/79  AL2           J 9/79  AL2CL6        J12/79  AL2O
J12/79  AL2O2                 J 3/78  C            J12/69  CCL           J12/68  CCL2          J 6/70  CCL3
P12/81  CCL4                  J12/67  CH           RUS 79  CHCL          P 6/81  CHCL3         J12/72  CH2
P12/81  CH2CL2                J 3/61  FORMALDEHYDE L 4/85  FORMIC ACID  J 6/69  CH3           P12/81  CH3CL
L 9/85  HYDROXYMETHYLENE      L 9/85  METHYLOXIDE  L 5/84  CH4           L 9/85  METHANOL      J 6/69  CN
J12/70  NCN RAD               J 6/66  CNN RAD      J 9/65  CO            J12/65  COCL          J 6/61  COCL2
J 9/65  CO2                   J12/69  C2           J12/68  C2CL2         L10/87  C2CL4         L10/87  C2CL6
```

```
J 3/67   C2H RAD          RUS 79   C2HCL           J 3/61   ACETYLENE       BUR 84   KETENE          BUR 84   C2H3 RAD
BUR 84   METHYL CYANIDE   BUR 84   CH3CO RAD       BUR 84   CH2CHO RAD      L 4/85   ETHYLENE        BUR 84   ACETALDEHYDE
L 4/85   ACETIC ACID      L 4/85   (FORMIC ACID)2  P10/83   ETHYL RAD       BUR 84   ETHYL OXIDE RAD L 5/84   ETHANE
BUR 84   AZOMETHANE       BUR 84   ETHANOL         BUR 84   DIMETHYL ETHER  J 3/67   CNC RAD         J 3/61   CYANOGEN
J 9/66   CCO RAD          J12/69   C3              DB6/61   C3H3 RAD        BUR 84   CYCLOPROPENE    BUR 84   PROPYNE
BUR 84   ALLENE           BUR 84   C3H5 RAD        BUR 84   CYCLOPROPANE    L 4/85   PROPYLENE       L 9/85   PROPYLENE OXIDE
L 9/85   I-PROPYL RAD     L 9/85   N-PROPYL RAD    L 4/85   PROPANE         L 1/84   1-PROPANOL      J 6/68   CARBON SUBOXIDE
J12/69   C4               BUR 84   BUTADIYNE       BUR 84   BUTAN-1EN-3YN   P10/85   CYCLOBUTADIENE  BUR 84   2-BUTYNE
P 4/84   1,3-BUTADIENE    BUR 84   2-BUTENE TRANS  BUR 84   2-BUTENE CIS    BUR 84   ISOBUTENE       BUR 84   1-BUTENE
L 4/85   (ACETIC ACID)2   L 9/85   S-BUTYL RAD     P10/83   N-BUTYL RAD     L 9/85   T-BUTYL RAD     L 4/85   ISOBUTANE
L 4/85   N-BUTANE         J 3/61   CARBON SUBNITRID J12/69  C5              P10/85   CYCLOPENTADIENE P12/52   CYCLOPENTANE
P12/52   1-PENTENE        P10/83   N-PENTYL RAD    L 5/87   T-PENTYL RAD    P10/85   CH3C(CH3)2CH3   P10/85   PENTANE
P10/85   ISOPENTANE       BUR 84   HEXATRIYNE      L12/84   PHENYL RAD      L12/84   PHENOXY RAD     L12/84   BENZENE
L12/84   PHENOL           BUR 84   CYCLOHEXENE     P10/83   N-HEXYL RAD     L 3/86   BENZALDEHYDE    P10/84   TOLUENE
L 6/87   CRESOL           P12/52   1-HEPTENE       P10/83   N-HEPTYL RAD    P 4/81   N-HEPTANE       P12/52   1-OCTENE
P10/83   N-OCTYL RAD      P 4/85   OCTANE          P 4/85   ISO-OCTANE      P10/83   N-NONYL RAD     BUR 84   NAPTHLENE
BUR 84   AZULENE          P10/83   N-DECYL RAD     L12/84   O-BIPHENYL RAD  L12/84   BIPHENYL        L 6/88   JET-A(G)
L 6/87   BIBENZYL         J 6/72   CL              J 6/66   CLCN            J 6/61   CLO             J 3/61   CLO2
J 9/65   CL2              J12/65   CL2O            J 3/77   H               J 3/64   HALO            L12/69   HCN
J12/70   HCO RAD          J 9/64   HCL             J12/70   HNCO            RUS 78   HNO             RUS 78   HNO2
RUS 78   HNO3             J 3/79   HOCL            J 9/78   HO2             J 3/77   H2              J12/65   H2N2
J 3/79   H2O              L 3/85   H2O2            J 3/77   N               J12/70   NCO             RUS 78   NH
RUS 78   NH2              J 6/77   NH3             RUS 78   NH2OH           RUS 78   NO              RUS 78   NOCL
RUS 78   NO2              RUS 78   NO2CL           J12/64   NO3             J 3/77   N2              RUS 78   N2H2
RUS 78   NH2NO2           RUS 78   N2H4            RUS 78   N2O             RUS 78   N2O3            RUS 78   N2O4
RUS 78   N2O5             RUS 78   N3              RUS 78   N3H             J 3/77   O               J 6/77   OH
J 3/77   O2               J 6/61   O3              J 6/79   AL(S)           J 6/79   AL(L)           J 9/79   ALCL3(S)
J 9/79   ALCL3(L)         J12/79   ALN(S)          J12/79   AL2O3(A)        J12/79   AL2O3(L)        J 3/78   C(GR)
P10/80   BENZENE(L)       P10/80   TOLUENE(L)      P10/80   OCTANE(L)       L 6/88   JET-A(L)        L 3/81   H2O(S)
J 3/79   H2O(L)           BAR73    NH4CL(A)        BAR73    NH4CL(B)
$RKTINP
EQL     = T,
FROZ    = T,
SUBAR   = 13*0.000000000000000E+00,
SUPAR   = 13*0.000000000000000E+00,
PCP     =   4.000000000000000     ,   10.00000000000000     ,
  50.00000000000000     ,   300.0000000000000     ,   700.0000000000000     ,
  1000.000000000000     , 16*0.000000000000000E+00,
TCEST   =   3800.000     ,
NFZ     =              1
$END

OF =   2.146732

                          EFFECTIVE FUEL          EFFECTIVE OXIDANT          MIXTURE
                              HPP(2)                  HPP(1)                  HSUBO
ENTHALPY
(KG-MOL)(DEG K)/KG        -0.41088475E+03         -0.30277596E+03         -0.33713185E+03

                              BOP(I,2)                BOP(I,1)                BO(I)
KG-FORM.WT./KG
C                         0.29623263E-01          0.00000000E+00          0.94139767E-02
H                         0.46052973E-01          0.34045770E-01          0.37861539E-01
O                         0.17425449E-02          0.34045770E-01          0.23780128E-01
N                         0.24893499E-03          0.85114424E-02          0.58857002E-02
AL                        0.20992566E-01          0.00000000E+00          0.66712276E-02
CL                        0.00000000E+00          0.85114424E-02          0.58065911E-02

POINT ITN   T       CO          H2          H2O         N2          ALO2H       ALCL3
  1   21 1992.24  -32.171     -17.065     -39.880     -25.739     -65.945     -83.014
ADD AL2O3(A)
  1    9 3226.01  -31.214     -18.522     -37.146     -27.433     -63.026     -77.834
PHASE CHANGE, REPLACE AL2O3(A)      WITH AL2O3(L)
```

```
  1    3 3105.89  -31.216          -18.349          -37.373          -27.279          -64.912          -78.939

POINT ITN    T       CO               H2               H2O              N2             AL2O3(L)          HCL
  2    4 2912.23  -31.806          -18.657          -38.232          -27.586          -95.488          -30.113
PC/PT= 1.735982    T =  2912.23
  2    2 2911.76  -31.808          -18.658          -38.234          -27.587          -95.496          -30.114
PC/PT= 1.738347    T =  2911.76
  3    4 2628.25  -32.753          -19.118          -39.651          -28.040         -100.956          -30.959
  4    4 2329.85  -33.886          -19.614          -41.425          -28.523         -108.469          -31.976
  5    4 1854.85  -36.186          -20.472          -45.256          -29.352         -126.427          -34.035
PHASE CHANGE, REPLACE AL2O3(L)        WITH AL2O3(A)
  5    2 1980.85  -35.946          -20.684          -44.528          -29.572         -121.613          -33.870

POINT ITN    T       CO               H2               H2O              N2             AL2O3(A)          HCL
  6    5 1476.72  -39.111          -21.555          -50.219          -30.418         -152.829          -36.649
  7    4 1279.91  -40.944          -21.977          -53.647          -30.839         -172.240          -38.236
  8    3 1204.78  -41.791          -22.158          -55.255          -31.023         -181.423          -38.964
```

THEORETICAL ROCKET PERFORMANCE ASSUMING EQUILIBRIUM COMPOSITION DURING EXPANSION

PC = 588.0 PSIA
CASE NO. 20

CHEMICAL FORMULA								WT FRACTION (SEE NOTE)	ENERGY CAL/MOL	STATE	TEMP DEG K
FUEL	C 5.95000	H 9.25000	O 0.35000	N 0.05000				0.433588	-164000.000	S	298.15
FUEL	AL 1.00000							0.566412	0.000	S	298.15
OXIDANT	N 1.00000	H 4.00000	CL 1.00000	O 4.00000				1.000000	-70690.000	S	298.15

O/F= 2.1467 PERCENT FUEL= 31.7790 EQUIVALENCE RATIO= 1.7901 PHI= 2.4523

	CHAMBER	THROAT	EXIT	EXIT	EXIT	EXIT	EXIT	EXIT
PC/P	1.0000	1.7383	4.0000	10.000	50.000	300.00	700.00	1000.00
P, ATM	40.011	23.017	10.003	4.0011	0.80022	0.13337	0.05716	0.04001
T, DEG K	3105.9	2911.8	2628.3	2329.9	1980.8	1476.7	1279.9	1204.8
RHO, G/CC	4.5182-3	2.7858-3	1.3486-3	6.1067-4	1.4390-4	3.2191-5	1.5917-5	1.1837-5
H, CAL/G	-669.95	-784.52	-942.64	-1097.51	-1339.84	-1549.15	-1628.37	-1658.47
U, CAL/G	-884.40	-984.60	-1122.27	-1256.18	-1474.52	-1649.48	-1715.33	-1740.33
G, CAL/G	-7599.94	-7281.36	-6806.92	-6295.98	-5759.60	-4844.06	-4484.16	-4346.63
S, CAL/(G)(K)	2.2312	2.2312	2.2312	2.2312	2.2312	2.2312	2.2312	2.2312
M, MOL WT	28.780	28.919	29.076	29.179	29.228	29.247	29.248	29.248
(DLV/DLP)T	-1.00815	-1.00572	-1.00299	-1.00120	-1.00033	-1.00001	-1.00000	-1.00000
(DLV/DLT)P	1.1546	1.1140	1.0642	1.0283	1.0091	1.0003	1.0000	1.0000
CP, CAL/(G)(K)	0.6955	0.6433	0.5726	0.5156	0.4341	0.4048	0.4009	0.4004
GAMMA (S)	1.1418	1.1453	1.1523	1.1607	1.1893	1.2018	1.2041	1.2044
SON VEL,M/SEC	1012.2	979.2	930.6	877.8	818.6	710.3	661.9	642.2
MACH NUMBER	0.000	1.000	1.623	2.155	2.892	3.819	4.279	4.478

PERFORMANCE PARAMETERS

AE/AT	1.0000	1.3390	2.3615	8.0066	31.241	60.513	80.124
CSTAR, FT/SEC	4876	4876	4876	4876	4876	4876	4876
CF	0.659	1.016	1.273	1.593	1.825	1.905	1.935
IVAC,LB-SEC/LB	187.0	204.8	228.7	265.7	292.4	301.9	305.4
ISP, LB-SEC/LB	99.8	154.0	192.9	241.4	276.6	288.8	293.3

MOLE FRACTIONS

AL	0.00002	0.00001	0.00000	0.00000	0.00000	0.00000	0.00000	0.00000
ALCL	0.00225	0.00118	0.00033	0.00005	0.00000	0.00000	0.00000	0.00000
ALCL2	0.00097	0.00055	0.00019	0.00004	0.00000	0.00000	0.00000	0.00000
ALCL3	0.00020	0.00015	0.00008	0.00003	0.00000	0.00000	0.00000	0.00000
ALO	0.00003	0.00001	0.00000	0.00000	0.00000	0.00000	0.00000	0.00000
ALOCL	0.00058	0.00032	0.00010	0.00002	0.00000	0.00000	0.00000	0.00000
ALOH	0.00013	0.00006	0.00002	0.00000	0.00000	0.00000	0.00000	0.00000
ALO2H	0.00014	0.00007	0.00002	0.00000	0.00000	0.00000	0.00000	0.00000
AL2O	0.00001	0.00000	0.00000	0.00000	0.00000	0.00000	0.00000	0.00000
CO	0.23679	0.23735	0.23761	0.23699	0.23467	0.22605	0.21883	0.21496
COCL	0.00001	0.00000	0.00000	0.00000	0.00000	0.00000	0.00000	0.00000
CO2	0.01092	0.01122	0.01200	0.01336	0.01604	0.02481	0.03203	0.03590
CL	0.00560	0.00422	0.00240	0.00103	0.00030	0.00001	0.00000	0.00000
CL2	0.00001	0.00001	0.00000	0.00000	0.00000	0.00000	0.00000	0.00000
H	0.01809	0.01325	0.00729	0.00304	0.00086	0.00002	0.00000	0.00000
HCN	0.00001	0.00000	0.00000	0.00000	0.00000	0.00000	0.00000	0.00000

HCO RAD	0.00001	0.00001	0.00000	0.00000	0.00000	0.00000	0.00000	0.00000
HCL	0.14182	0.14604	0.15050	0.15312	0.15432	0.15472	0.15473	0.15473
H2	0.31015	0.31407	0.31881	0.32265	0.32652	0.33573	0.34296	0.34683
H2O	0.10675	0.10537	0.10394	0.10260	0.10004	0.09136	0.08413	0.08027
NH3	0.00001	0.00001	0.00001	0.00000	0.00000	0.00000	0.00000	0.00000
NO	0.00012	0.00006	0.00002	0.00000	0.00000	0.00000	0.00000	0.00000
N2	0.07737	0.07767	0.07802	0.07825	0.07837	0.07842	0.07842	0.07842
O	0.00008	0.00004	0.00001	0.00000	0.00000	0.00000	0.00000	0.00000
OH	0.00230	0.00141	0.00058	0.00017	0.00003	0.00000	0.00000	0.00000
O2	0.00001	0.00000	0.00000	0.00000	0.00000	0.00000	0.00000	0.00000
AL2O3(A)	0.00000	0.00000	0.00000	0.00000	0.08883	0.08889	0.08889	0.08889
AL2O3(L)	0.08562	0.08690	0.08808	0.08863	0.00000	0.00000	0.00000	0.00000

ADDITIONAL PRODUCTS WHICH WERE CONSIDERED BUT WHOSE MOLE FRACTIONS WERE LESS THAN 0.50000E-05 FOR ALL ASSIGNED CONDITIONS

ALC	ALH	ALN	ALO2	AL2	AL2CL6	AL2O2
C	CCL	CCL2	CCL3	CCL4	CH	CHCL
CHCL3	CH2	CH2CL2	FORMALDEHYDE	FORMIC ACID	CH3	CH3CL
HYDROXYMETHYLENE	METHYLOXIDE	CH4	METHANOL	CN	NCN RAD	CNN RAD
COCL2	C2	C2CL2	C2CL4	C2CL6	C2H RAD	C2HCL
ACETYLENE	KETENE	C2H3 RAD	METHYL CYANIDE	CH3CO RAD	CH2CHO RAD	ETHYLENE
ACETALDEHYDE	ACETIC ACID	(FORMIC ACID)2	ETHYL RAD	ETHYL OXIDE RAD	ETHANE	AZOMETHANE
ETHANOL	DIMETHYL ETHER	CNC RAD	CYANOGEN	CCO RAD	C3	C3H3 RAD
CYCLOPROPENE	PROPYNE	ALLENE	C3H5 RAD	CYCLOPROPANE	PROPYLENE	PROPYLENE OXIDE
I-PROPYL RAD	N-PROPYL RAD	PROPANE	1-PROPANOL	CARBON SUBOXIDE	C4	BUTADIYNE
BUTAN-1EN-3YN	CYCLOBUTADIENE	2-BUTYNE	1,3-BUTADIENE	2-BUTENE TRANS	2-BUTENE CIS	ISOBUTENE
1-BUTENE	(ACETIC ACID)2	S-BUTYL RAD	N-BUTYL RAD	T-BUTYL RAD	ISOBUTANE	N-BUTANE
CARBON SUBNITRID	C5	CYCLOPENTADIENE	CYCLOPENTANE	1-PENTENE	N-PENTYL RAD	T-PENTYL RAD
CH3C(CH3)2CH3	PENTANE	ISOPENTANE	HEXATRIYNE	PHENYL RAD	PHENOXY RAD	BENZENE
PHENOL	CYCLOHEXENE	N-HEXYL RAD	BENZALDEHYDE	TOLUENE	CRESOL	1-HEPTENE
N-HEPTYL RAD	N-HEPTANE	1-OCTENE	N-OCTYL RAD	OCTANE	ISO-OCTANE	N-NONYL RAD
NAPTHLENE	AZULENE	N-DECYL RAD	O-BIPHENYL RAD	BIPHENYL	JET-A(G)	BIBENZYL
CLCN	CLO	CLO2	CL2O	HALO	HNCO	HNO
HNO2	HNO3	HOCL	HO2	H2N2	H2O2	N
NCO	NH	NH2	NH2OH	NOCL	NO2	NO2CL
NO3	N2H2	NH2NO2	N2H4	N2O	N2O3	N2O4
N2O5	N3	N3H	O3	AL(S)	AL(L)	ALCL3(S)
ALCL3(L)	ALN(S)	C(GR)	BENZENE(L)	TOLUENE(L)	OCTANE(L)	JET-A(L)
H2O(S)	H2O(L)	NH4CL(A)	NH4CL(B)			

NOTE. WEIGHT FRACTION OF FUEL IN TOTAL FUELS AND OF OXIDANT IN TOTAL OXIDANTS

THEORETICAL ROCKET PERFORMANCE ASSUMING FROZEN COMPOSITION DURING EXPANSION

PC = 588.0 PSIA
CASE NO. 20

	CHEMICAL FORMULA								WT FRACTION (SEE NOTE)	ENERGY CAL/MOL	STATE	TEMP DEG K
FUEL	C	5.95000	H	9.25000	O	0.35000	N	0.05000	0.433588	-164000.000	S	298.15
FUEL	AL	1.00000							0.566412	0.000	S	298.15
OXIDANT	N	1.00000	H	4.00000	CL	1.00000	O	4.00000	1.000000	-70690.000	S	298.15

O/F= 2.1467 PERCENT FUEL= 31.7790 EQUIVALENCE RATIO= 1.7901 PHI= 2.4523

	CHAMBER	THROAT	EXIT
PC/P	1.0000	1.7536	4.0000
P, ATM	40.011	22.816	10.003
T, DEG K	3105.9	2862.7	2537.0
RHO, G/CC	4.5182-3	2.7954-3	1.3828-3
H, CAL/G	-669.95	-785.63	-939.18
U, CAL/G	-884.40	-983.29	-1114.35
G, CAL/G	-7599.94	-7172.91	-6599.95
S, CAL/(G)(K)	2.2312	2.2312	2.2312
M, MOL WT	28.780	28.780	28.780
CP, CAL/(G)(K)	0.4771	0.4740	0.4690
GAMMA (S)	1.1692	1.1705	1.1726
SON VEL,M/SEC	1024.3	983.9	927.1
MACH NUMBER	0.000	1.000	1.619

PERFORMANCE PARAMETERS

AE/AT	1.0000	3.3128
CSTAR, FT/SEC	4836	4836
CF	0.667	1.018
IVAC,LB-SEC/LB	186.0	202.9
ISP, LB-SEC/LB	100.3	153.1

MOLE FRACTIONS

AL	0.00002	ALCL	0.00225	ALCL2	0.00097	ALCL3	0.00020
ALO	0.00003	ALOCL	0.00058	ALOH	0.00013	ALO2H	0.00014
AL2O	0.00001	CO	0.23679	COCL	0.00001	CO2	0.01092
CL	0.00560	CL2	0.00001	H	0.01809	HCN	0.00001
HCO RAD	0.00001	HCL	0.14182	H2	0.31015	H2O	0.10675
NH3	0.00001	NO	0.00012	N2	0.07737	O	0.00008
OH	0.00230	O2	0.00001	AL2O3(L)	0.08562		

ADDITIONAL PRODUCTS WHICH WERE CONSIDERED BUT WHOSE MOLE FRACTIONS WERE LESS THAN 0.50000E-05 FOR ALL ASSIGNED CONDITIONS

ALC	ALH	ALN	ALO2	AL2	AL2CL6	AL2O2
C	CCL	CCL2	CCL3	CCL4	CH	CHCL
CHCL3	CH2	CH2CL2	FORMALDEHYDE	FORMIC ACID	CH3	CH3CL
HYDROXYMETHYLENE	METHYLOXIDE	CH4	METHANOL	CN	NCN RAD	CNN RAD
COCL2	C2	C2CL2	C2CL4	C2CL6	C2H RAD	C2HCL
ACETYLENE	KETENE	C2H3 RAD	METHYL CYANIDE	CH3CO RAD	CH2CHO RAD	ETHYLENE
ACETALDEHYDE	ACETIC ACID	(FORMIC ACID)2	ETHYL RAD	ETHYL OXIDE RAD	ETHANE	AZOMETHANE
ETHANOL	DIMETHYL ETHER	CNC RAD	CYANOGEN	CCO RAD	C3	C3H3 RAD
CYCLOPROPENE	PROPYNE	ALLENE	C3H5 RAD	CYCLOPROPANE	PROPYLENE	PROPYLENE OXIDE

I-PROPYL RAD	N-PROPYL RAD	PROPANE	1-PROPANOL	CARBON SUBOXIDE	C4	BUTADIYNE
BUTAN-1EN-3YN	CYCLOBUTADIENE	2-BUTYNE	1,3-BUTADIENE	2-BUTENE TRANS	2-BUTENE CIS	ISOBUTENE
1-BUTENE	(ACETIC ACID)2	S-BUTYL RAD	N-BUTYL RAD	T-BUTYL RAD	ISOBUTANE	N-BUTANE
CARBON SUBNITRID	C5	CYCLOPENTADIENE	CYCLOPENTANE	1-PENTENE	N-PENTYL RAD	T-PENTYL RAD
CH3C(CH3)2CH3	PENTANE	ISOPENTANE	HEXATRIYNE	PHENYL RAD	PHENOXY RAD	BENZENE
PHENOL	CYCLOHEXENE	N-HEXYL RAD	BENZALDEHYDE	TOLUENE	CRESOL	1-HEPTENE
N-HEPTYL RAD	N-HEPTANE	1-OCTENE	N-OCTYL RAD	OCTANE	ISO-OCTANE	N-NONYL RAD
NAPTHLENE	AZULENE	N-DECYL RAD	O-BIPHENYL RAD	BIPHENYL	JET-A(G)	BIBENZYL
CLCN	CLO	CLO2	CL2O	HALO	HNCO	HNO
HNO2	HNO3	HOCL	HO2	H2N2	H2O2	N
NCO	NH	NH2	NH2OH	NOCL	NO2	NO2CL
NO3	N2H2	NH2NO2	N2H4	N2O	N2O3	N2O4
N2O5	N3	N3H	O3	AL(S)	AL(L)	ALCL3(S)
ALCL3(L)	ALN(S)	AL2O3(A)	C(GR)	BENZENE(L)	TOLUENE(L)	OCTANE(L)
JET-A(L)	H2O(S)	H2O(L)	NH4CL(A)	NH4CL(B)		

NOTE. WEIGHT FRACTION OF FUEL IN TOTAL FUELS AND OF OXIDANT IN TOTAL OXIDANTS

CALCULATIONS WERE STOPPED BECAUSE NEXT POINT IS MORE THAN 50 DEG BELOW TEMP RANGE OF A CONDENSED SPECIES

```
THERMO
REACTANTS
C   2.0000  H   6.0000      0.0000      0.0000      0.0000  100.000000     -30372.00  L    231.080     F
O   2.0000      0.0000      0.0000      0.0000      0.0000  100.000000      -3102.00  L     90.180     O


NAMELISTS
$INPT2
KASE     =            20,
T        = 26*0.0000000E+00,
P        =   100.0000    , 25*0.0000000E+00,
PSIA     = T,
MMHG     = F,
NSQM     = F,
V        = 26*0.0000000E+00,
RHO      =   100.0000    , 25*0.0000000E+00,
ERATIO   = F,
OF       = T,
FPCT     = F,
FA       = F,
MIX      =   2.000000    , 25*-1.000000    ,
TP       = F,
HP       = F,
SP       = F,
TV       = F,
UV       = F,
SV       = F,
RKT      = T,
SHOCK    = F,
DETN     = F,
TRACE    =  0.00000000000000000E+00,
SO       =  0.00000000000000000E+00,
SO       =  0.0000000E+00,
IONS     = F,
IDEBUG   =            0,
PHI      = F,
SIUNIT   = F,
INHG     = F,
TRNSPT   = F,
TRPACC   =  0.9999000000000000    ,
DIF      = F,
NODATA   = F,
U        =  1.00000000000000000E+30,
H        =  1.00000000000000000E+30
$END

SPECIES BEING CONSIDERED IN THIS SYSTEM
 J 3/78  C                 J12/67  CH                HYDROXYMETHYLENE  L 9/85  METHYLOXIDE       J 3/61  FORMALDEHYDE      L 4/85  FORMIC ACID
 J 6/69  CH3               L 9/85  HYDROXYMETHYLENE  L 9/85  METHYLOXIDE  L 5/84  CH4               L 9/85  METHANOL
 J 9/65  CO                J 9/65  CO2               J12/69  C2           J 3/67  C2H RAD           J 3/61  ACETYLENE
 BUR 84  KETENE            BUR 84  C2H3 RAD          BUR 84  CH3CO RAD    BUR 84  CH2CHO RAD        L 4/85  ETHYLENE
 BUR 84  ACETALDEHYDE      L 4/85  ACETIC ACID       L 4/85  (FORMIC ACID)2  P10/83  ETHYL RAD       BUR 84  ETHYL OXIDE RAD
 L 5/84  ETHANE            BUR 84  ETHANOL           BUR 84  DIMETHYL ETHER  J 9/66  CCO RAD          J12/69  C3
 DB6/61  C3H3 RAD          BUR 84  CYCLOPROPENE      BUR 84  PROPYNE       BUR 84  ALLENE            BUR 84  C3H5 RAD
 BUR 84  CYCLOPROPANE      L 4/85  PROPYLENE         L 9/85  PROPYLENE OXIDE  L 9/85  I-PROPYL RAD    L 9/85  N-PROPYL RAD
 L 4/85  PROPANE           L 1/84  1-PROPANOL        J 6/68  CARBON SUBOXIDE  J12/69  C4              BUR 84  BUTADIYNE
 BUR 84  BUTAN-1EN-3YN     P10/85  CYCLOBUTADIENE    BUR 84  2-BUTYNE     P 4/84  1,3-BUTADIENE     BUR 84  2-BUTENE TRANS
 BUR 84  2-BUTENE CIS      BUR 84  ISOBUTENE        BUR 84  1-BUTENE     L 4/85  (ACETIC ACID)2    L 9/85  S-BUTYL RAD
 P10/83  N-BUTYL RAD       L 9/85  T-BUTYL RAD       L 4/85  ISOBUTANE    L 4/85  N-BUTANE          J12/69  C5
```

```
 P10/85  CYCLOPENTADIENE   P12/52  CYCLOPENTANE      P12/52  1-PENTENE         P10/83  N-PENTYL RAD      L 5/87  T-PENTYL RAD
 P10/85  CH3C(CH3)2CH3     P10/85  PENTANE           P10/85  ISOPENTANE        BUR 84  HEXATRIYNE        L12/84  PHENYL RAD
 L12/84  PHENOXY RAD       L12/84  BENZENE           L12/84  PHENOL            BUR 84  CYCLOHEXENE       P10/83  N-HEXYL RAD
 L 3/86  BENZALDEHYDE      P10/84  TOLUENE           L 6/87  CRESOL            P12/52  1-HEPTENE         P10/83  N-HEPTYL RAD
 P 4/81  N-HEPTANE         P12/52  1-OCTENE          P10/83  N-OCTYL RAD       P 4/85  OCTANE            P 4/85  ISO-OCTANE
 P10/83  N-NONYL RAD       BUR 84  NAPTHLENE        BUR 84  AZULENE           P10/83  N-DECYL RAD       L12/84  O-BIPHENYL RAD
 L12/84  BIPHENYL          L 6/88  JET-A(G)          L 6/87  BIBENZYL          J 3/77  H                 J12/70  HCO RAD
 J 9/78  HO2               J 3/77  H2                J 3/79  H2O               L 3/85  H2O2              J 3/77  O
 J 6/77  OH                J 3/77  O2                J 6/61  O3                J 3/78  C(GR)             P10/80  BENZENE(L)
 P10/80  TOLUENE(L)        P10/80  OCTANE(L)         L 6/88  JET-A(L)          L 3/81  H2O(S)            J 3/79  H2O(L)
$RKTINP
EQL     = T,
FROZ    = T,
SUBAR   = 13*0.0000000000000000E+00,
SUPAR   = 13*0.0000000000000000E+00,
PCP     =   4.000000000000000    ,   10.00000000000000    ,
  50.00000000000000    ,   300.0000000000000    ,   700.0000000000000    ,
  1000.000000000000    , 16*0.0000000000000000E+00,
TCEST   =   3800.000    ,
NFZ     =            1
$END

OF =   2.000000

                                EFFECTIVE FUEL        EFFECTIVE OXIDANT          MIXTURE
ENTHALPY                           HPP(2)                HPP(1)                  HSUBO
(KG-MOL)(DEG K)/KG             -0.50828685E+03       -0.48782981E+02        -0.20195094E+03

KG-FORM.WT./KG                    BOP(I,2)              BOP(I,1)                BO(I)
C                              0.66512802E-01        0.00000000E+00         0.22170934E-01
H                              0.19953841E+00        0.00000000E+00         0.66512802E-01
O                              0.00000000E+00        0.62502343E-01         0.41668229E-01

POINT ITN    T       CO              H2O             CO2
  1   22 2789.94  -32.784         -38.746         -51.636

POINT ITN    T       CO              H2              CO2
  2    5 2557.97  -33.469         -20.139         -53.160
PC/PT= 1.763220   T =  2557.97

POINT ITN    T       CO              H2              H2O
  2    3 2555.57  -33.476         -20.141         -39.842
PC/PT= 1.773532   T =  2555.57
  2    1 2555.55  -33.476         -20.141         -39.842
PC/PT= 1.773642   T =  2555.55
  3    4 2223.64  -34.583         -20.458         -41.713
  4    4 1870.86  -36.065         -20.782         -44.368
  5    4 1360.67  -39.432         -21.346         -50.666
  6    5  965.08  -44.520         -22.063         -60.365

POINT ITN    T       CO2             H2              H2O
  7    5  830.97  -90.819         -22.469         -65.878
  8    3  783.58  -94.340         -22.661         -68.311
```

THEORETICAL ROCKET PERFORMANCE ASSUMING EQUILIBRIUM COMPOSITION DURING EXPANSION

PC = 100.0 PSIA
CASE NO. 20

	CHEMICAL FORMULA	WT FRACTION (SEE NOTE)	ENERGY CAL/MOL	STATE	TEMP DEG K
FUEL	C 2.00000 H 6.00000	1.000000	-30372.000	L	231.08
OXIDANT	O 2.00000	1.000000	-3102.000	L	90.18

O/F= 2.0000 PERCENT FUEL= 33.3333 EQUIVALENCE RATIO= 1.8623 PHI= 1.8623

	CHAMBER	THROAT	EXIT	EXIT	EXIT	EXIT	EXIT	EXIT
PC/P	1.0000	1.7736	4.0000	10.000	50.000	300.00	700.00	1000.00
P, ATM	6.8046	3.8365	1.7011	0.68046	0.13609	0.02268	0.00972	0.00680
T, DEG K	2789.9	2555.5	2223.6	1870.9	1360.7	965.1	831.0	783.6
RHO, G/CC	5.3053-4	3.2827-4	1.6794-4	7.9950-5	2.1991-5	5.1675-6	2.5726-6	1.9111-6
H, CAL/G	-401.32	-571.37	-786.06	-992.54	-1276.72	-1503.46	-1587.03	-1618.71
U, CAL/G	-711.93	-854.39	-1031.37	-1198.65	-1426.59	-1609.76	-1678.54	-1704.94
G, CAL/G	-9735.63	-9121.47	-8225.71	-7251.87	-5829.14	-4732.34	-4367.21	-4240.34
S, CAL/(G)(K)	3.3457	3.3457	3.3457	3.3457	3.3457	3.3457	3.3457	3.3457
M, MOL WT	17.849	17.943	18.014	18.037	18.042	18.042	18.046	18.058
(DLV/DLP)T	-1.00543	-1.00275	-1.00078	-1.00012	-1.00000	-1.00002	-1.00046	-1.00181
(DLV/DLT)P	1.1137	1.0620	1.0197	1.0034	1.0000	1.0003	1.0080	1.0330
CP, CAL/(G)(K)	0.8498	0.7323	0.6223	0.5685	0.5562	0.6037	0.6544	0.7187
GAMMA (S)	1.1863	1.2017	1.2248	1.2422	1.2470	1.2233	1.2056	1.1927
SON VEL,M/SEC	1241.7	1192.9	1121.2	1035.0	884.3	737.6	679.4	656.0
MACH NUMBER	0.000	1.000	1.600	2.149	3.061	4.117	4.636	4.866

PERFORMANCE PARAMETERS

AE/AT	1.0000	1.2995	2.2021	6.5794	24.953	48.323	64.200
CSTAR, FT/SEC	5776	5776	5776	5776	5776	5776	5776
CF	0.678	1.019	1.263	1.537	1.725	1.789	1.813
IVAC,LB-SEC/LB	222.9	241.3	266.3	299.6	324.6	333.6	337.0
ISP, LB-SEC/LB	121.6	183.0	226.8	276.0	309.7	321.2	325.5

MOLE FRACTIONS

CH4	0.00000	0.00000	0.00000	0.00000	0.00000	0.00001	0.00012	0.00046
CO	0.34501	0.34373	0.33901	0.32887	0.29596	0.23075	0.19170	0.17494
CO2	0.05072	0.05408	0.06037	0.07103	0.10404	0.16925	0.20828	0.22497
H	0.01623	0.00884	0.00272	0.00043	0.00000	0.00000	0.00000	0.00000
H2	0.29082	0.29759	0.30706	0.31901	0.35227	0.41747	0.45622	0.47207
H2O	0.29234	0.29373	0.29047	0.28062	0.24773	0.18252	0.14368	0.12757
O	0.00016	0.00004	0.00000	0.00000	0.00000	0.00000	0.00000	0.00000
OH	0.00465	0.00197	0.00038	0.00003	0.00000	0.00000	0.00000	0.00000
O2	0.00007	0.00002	0.00000	0.00000	0.00000	0.00000	0.00000	0.00000

ADDITIONAL PRODUCTS WHICH WERE CONSIDERED BUT WHOSE MOLE FRACTIONS WERE LESS THAN 0.50000E-05 FOR ALL ASSIGNED CONDITIONS

C	CH	CH2	FORMALDEHYDE	FORMIC ACID	CH3	HYDROXYMETHYLENE
METHYLOXIDE	METHANOL	C2	C2H RAD	ACETYLENE	KETENE	C2H3 RAD
CH3CO RAD	CH2CHO RAD	ETHYLENE	ACETALDEHYDE	ACETIC ACID	(FORMIC ACID)2	ETHYL RAD
ETHYL OXIDE RAD	ETHANE	ETHANOL	DIMETHYL ETHER	CCO RAD	C3	C3H3 RAD
CYCLOPROPENE	PROPYNE	ALLENE	C3H5 RAD	CYCLOPROPANE	PROPYLENE	PROPYLENE OXIDE

I-PROPYL RAD	N-PROPYL RAD	PROPANE	1-PROPANOL	CARBON SUBOXIDE	C4	BUTADIYNE
BUTAN-1EN-3YN	CYCLOBUTADIENE	2-BUTYNE	1,3-BUTADIENE	2-BUTENE TRANS	2-BUTENE CIS	ISOBUTENE
1-BUTENE	(ACETIC ACID)2	S-BUTYL RAD	N-BUTYL RAD	T-BUTYL RAD	ISOBUTANE	N-BUTANE
C5	CYCLOPENTADIENE	CYCLOPENTANE	1-PENTENE	N-PENTYL RAD	T-PENTYL RAD	CH3C(CH3)2CH3
PENTANE	ISOPENTANE	HEXATRIYNE	PHENYL RAD	PHENOXY RAD	BENZENE	PHENOL
CYCLOHEXENE	N-HEXYL RAD	BENZALDEHYDE	TOLUENE	CRESOL	1-HEPTENE	N-HEPTYL RAD
N-HEPTANE	1-OCTENE	N-OCTYL RAD	OCTANE	ISO-OCTANE	N-NONYL RAD	NAPTHLENE
AZULENE	N-DECYL RAD	O-BIPHENYL RAD	BIPHENYL	JET-A(G)	BIBENZYL	HCO RAD
HO2	H2O2	O3	C(GR)	BENZENE(L)	TOLUENE(L)	OCTANE(L)
JET-A(L)	H2O(S)	H2O(L)				

NOTE. WEIGHT FRACTION OF FUEL IN TOTAL FUELS AND OF OXIDANT IN TOTAL OXIDANTS

THEORETICAL ROCKET PERFORMANCE ASSUMING FROZEN COMPOSITION DURING EXPANSION

PC = 100.0 PSIA
CASE NO. 20

	CHEMICAL FORMULA	WT FRACTION (SEE NOTE)	ENERGY CAL/MOL	STATE	TEMP DEG K
FUEL	C 2.00000 H 6.00000	1.000000	-30372.000	L	231.08
OXIDANT	O 2.00000	1.000000	-3102.000	L	90.18

O/F= 2.0000 PERCENT FUEL= 33.3333 EQUIVALENCE RATIO= 1.8623 PHI= 1.8623

	CHAMBER	THROAT	EXIT	EXIT	EXIT	EXIT	EXIT	EXIT
PC/P	1.0000	1.7982	4.0000	10.000	50.000	300.00	700.00	1000.00
P, ATM	6.8046	3.7840	1.7011	0.68046	0.13609	0.02268	0.00972	0.00680
T, DEG K	2789.9	2489.7	2125.1	1762.6	1246.9	821.2	665.8	608.2
RHO, G/CC	5.3053-4	3.3061-4	1.7413-4	8.3974-5	2.3741-5	6.0083-6	3.1761-6	2.4337-6
H, CAL/G	-401.32	-573.62	-778.64	-976.46	-1243.98	-1447.91	-1517.83	-1543.11
U, CAL/G	-711.93	-850.80	-1015.22	-1172.70	-1382.80	-1539.34	-1591.95	-1610.82
G, CAL/G	-9735.63	-8903.50	-7888.50	-6873.69	-5415.72	-4195.30	-3745.25	-3577.94
S, CAL/(G)(K)	3.3457	3.3457	3.3457	3.3457	3.3457	3.3457	3.3457	3.3457
M, MOL WT	17.849	17.849	17.849	17.849	17.849	17.849	17.849	17.849
CP, CAL/(G)(K)	0.5784	0.5691	0.5547	0.5360	0.4991	0.4578	0.4420	0.4364
GAMMA (S)	1.2384	1.2432	1.2511	1.2621	1.2871	1.3213	1.3367	1.3425
SON VEL,M/SEC	1268.6	1200.8	1112.8	1018.0	864.6	710.9	643.8	616.7
MACH NUMBER	0.000	1.000	1.597	2.155	3.071	4.163	4.748	5.012

PERFORMANCE PARAMETERS

AE/AT	1.0000	1.2830	2.1549	6.2968	22.326	40.891	52.771
CSTAR, FT/SEC	5698	5698	5698	5698	5698	5698	5698
CF	0.691	1.023	1.263	1.529	1.704	1.760	1.780
IVAC,LB-SEC/LB	220.9	238.0	261.9	293.1	315.0	322.0	324.5
ISP, LB-SEC/LB	122.4	181.2	223.7	270.8	301.8	311.7	315.2

MOLE FRACTIONS

CO	0.34501	CO2	0.05072	H	0.01623	H2	0.29082
H2O	0.29234	O	0.00016	OH	0.00465	O2	0.00007

ADDITIONAL PRODUCTS WHICH WERE CONSIDERED BUT WHOSE MOLE FRACTIONS WERE LESS THAN 0.50000E-05 FOR ALL ASSIGNED CONDITIONS

C	CH	CH2	FORMALDEHYDE	FORMIC ACID	CH3	HYDROXYMETHYLENE
METHYLOXIDE	CH4	METHANOL	C2	C2H RAD	ACETYLENE	KETENE
C2H3 RAD	CH3CO RAD	CH2CHO RAD	ETHYLENE	ACETALDEHYDE	ACETIC ACID	(FORMIC ACID)2
ETHYL RAD	ETHYL OXIDE RAD	ETHANE	ETHANOL	DIMETHYL ETHER	CCO RAD	C3
C3H3 RAD	CYCLOPROPENE	PROPYNE	ALLENE	C3H5 RAD	CYCLOPROPANE	PROPYLENE
PROPYLENE OXIDE	I-PROPYL RAD	N-PROPYL RAD	PROPANE	1-PROPANOL	CARBON SUBOXIDE	C4
BUTADIYNE	BUTAN-1EN-3YN	CYCLOBUTADIENE	2-BUTYNE	1,3-BUTADIENE	2-BUTENE TRANS	2-BUTENE CIS
ISOBUTENE	1-BUTENE	(ACETIC ACID)2	S-BUTYL RAD	N-BUTYL RAD	T-BUTYL RAD	ISOBUTANE
N-BUTANE	C5	CYCLOPENTADIENE	CYCLOPENTANE	1-PENTENE	N-PENTYL RAD	T-PENTYL RAD
CH3C(CH3)2CH3	PENTANE	ISOPENTANE	HEXATRIYNE	PHENYL RAD	PHENOXY RAD	BENZENE
PHENOL	CYCLOHEXENE	N-HEXYL RAD	BENZALDEHYDE	TOLUENE	CRESOL	1-HEPTENE
N-HEPTYL RAD	N-HEPTANE	1-OCTENE	N-OCTYL RAD	OCTANE	ISO-OCTANE	N-NONYL RAD
NAPTHLENE	AZULENE	N-DECYL RAD	O-BIPHENYL RAD	BIPHENYL	JET-A(G)	BIBENZYL
HCO RAD	HO2	H2O2	O3	C(GR)	BENZENE(L)	TOLUENE(L)
OCTANE(L)	JET-A(L)	H2O(S)	H2O(L)			

NOTE. WEIGHT FRACTION OF FUEL IN TOTAL FUELS AND OF OXIDANT IN TOTAL OXIDANTS

```
2222222222222222222222222222222222222222222222222222222222222222222222222222222222222222222222222222222222222222222222222222222222
2222222222222222222222222     CCIT CCIT CCIT CCIT  University of Arizona  CCIT CCIT CCIT CCIT     22222222222222222222222222
2222222222222222222222222222222222222222222222222222222222222222222222222222222222222222222222222222222222222222222222222222222222
```

```
RRRRRRRR      AAAAAA      SSSSSSSS    CCCCCCCC    000000    NN      NN
RRRRRRRR      AAAAAA      SSSSSSSS    CCCCCCCC    000000    NN      NN
RR      RR   AA      AA  SS          CC          00    00  NN      NN
RR      RR   AA      AA  SS          CC          00    00  NN      NN
RR      RR   AA      AA  SS          CC          00    00  NNNN    NN
RR      RR   AA      AA  SS          CC          00    00  NNNN    NN
RRRRRRRR     AA      AA    SSSSSS    CC          00    00  NN  NN  NN
RRRRRRRR     AA      AA    SSSSSS    CC          00    00  NN  NN  NN
RR   RR      AAAAAAAAAA          SS  CC          00    00  NN    NNNN
RR   RR      AAAAAAAAAA          SS  CC          00    00  NN    NNNN
RR    RR     AA      AA          SS  CC          00    00  NN      NN
RR    RR     AA      AA          SS  CC          00    00  NN      NN
RR      RR   AA      AA  SSSSSSSS      CCCCCCCC    000000    NN      NN
RR      RR   AA      AA  SSSSSSSS      CCCCCCCC    000000    NN      NN
```

```
FFFFF   000   RRRR    000    000    999
F      0   0  R   R  0   0  0   0  9   9
F      0   0  R   R  0  00  0  00  9   9
FFFF   0   0  RRRR   0 0 0  0 0 0   9999
F      0   0  R R    00  0  00  0      9
F      0   0  R  R   0   0  0   0      9
F       000   R   R   000    000    999
```

KEVLAR

```
     J   000   BBBB          55555  7777    888
     J  0   0  B   B         5          7  8   8
     J  0   0  B   B         555        7  8   8
     J  0   0  BBBB             5      7    888
  J  J  0   0  B   B            5     7    8   8
  J  J  0   0  B   B         5   5   7     8   8
   JJJ    000   BBBB          555    7      888
```

Job FOR009 (578) queued to CCIT_IO_ROOM on 21-MAR-1989 15:55 by user RASCON, UIC [RASCON], under account NRS-2305 at priority 100, started on printer LTA1260 on 21-MAR-1989 15:55 from queue CCIT_WIDE.

```
2222222222222222222222222222222222222222222222222222222222222222222222222222222222222222222222222222222222222222222222222222222222
2222222222222222222222222222222222  Digital Equipment Corporation - VAX/VMS Version V4.7  22222222222222222222222222222222222222
2222222222222222222222222222222222222222222222222222222222222222222222222222222222222222222222222222222222222222222222222222222222
```

```
THERMO
REACTANTS
C   7.0000  H   5.0000  O   1.0000  N   1.0000      0.0000   30.000000     -50000.00  S    298.150     F
O   2.0000      0.0000      0.0000      0.0000      0.0000   70.000000      -3102.00  L     90.180     O


NAMELISTS
$INPT2
KASE    =           30,
T       = 26*0.0000000E+00,
P       =   100.0000    , 25*0.0000000E+00,
PSIA    = T,
MMHG    = F,
NSQM    = F,
V       = 26*0.0000000E+00,
RHO     =   100.0000    , 25*0.0000000E+00,
ERATIO  = F,
OF      = F,
FPCT    = F,
FA      = F,
MIX     = 26*-1.000000    ,
TP      = F,
HP      = F,
SP      = F,
TV      = F,
UV      = F,
SV      = F,
RKT     = T,
SHOCK   = F,
DETN    = F,
TRACE   =  0.00000000000000000E+00,
SO      =  0.00000000000000000E+00,
SO      =  0.0000000E+00,
IONS    = F,
IDEBUG  =           0,
PHI     = F,
SIUNIT  = F,
INHG    = F,
TRNSPT  = F,
TRPACC  =  0.9999000000000000    ,
DIF     = F,
NODATA  = F,
U       =  1.0000000000000000E+30,
H       =  1.0000000000000000E+30
$END

NO INPT2 VALUE GIVEN FOR OF, EQRAT, FA, OR FPCT

SPECIES BEING CONSIDERED IN THIS SYSTEM
 J 3/78  C                 J12/67  CH                  J12/72  CH2                 J 3/61  FORMALDEHYDE        L 4/85  FORMIC ACID
 J 6/69  CH3               L 9/85  HYDROXYMETHYLENE    L 9/85  METHYLOXIDE         L 5/84  CH4                 L 9/85  METHANOL
 J 6/69  CN                J12/70  NCN RAD             J 6/66  CNN RAD             J 9/65  CO                  J 9/65  CO2
J12/69  C2                 J 3/67  C2H RAD             J 3/61  ACETYLENE           BUR 84  KETENE              BUR 84  C2H3 RAD
 BUR 84  METHYL CYANIDE    BUR 84  CH3CO RAD           BUR 84  CH2CHO RAD          L 4/85  ETHYLENE            BUR 84  ACETALDEHYDE
 L 4/85  ACETIC ACID       L 4/85  (FORMIC ACID)2      P10/83  ETHYL RAD           BUR 84  ETHYL OXIDE RAD     L 5/84  ETHANE
 BUR 84  AZOMETHANE        BUR 84  ETHANOL            BUR 84  DIMETHYL ETHER      J 3/67  CNC RAD             J 3/61  CYANOGEN
 J 9/66  CCO RAD           J12/69  C3                  DB6/61  C3H3 RAD           BUR 84  CYCLOPROPENE        BUR 84  PROPYNE
 BUR 84  ALLENE            BUR 84  C3H5 RAD           BUR 84  CYCLOPROPANE      L 4/85  PROPYLENE           L 9/85  PROPYLENE OXIDE
 L 9/85  I-PROPYL RAD      L 9/85  N-PROPYL RAD        L 4/85  PROPANE           L 1/84  1-PROPANOL          J 6/68  CARBON SUBOXIDE
```

```
J12/69  C4                  BUR 84  BUTADIYNE            BUR 84  BUTAN-1EN-3YN       P10/85  CYCLOBUTADIENE      BUR 84  2-BUTYNE
P 4/84  1,3-BUTADIENE       BUR 84  2-BUTENE TRANS      BUR 84  2-BUTENE CIS        BUR 84  ISOBUTENE           BUR 84  1-BUTENE
L 4/85  (ACETIC ACID)2      L 9/85  S-BUTYL RAD         P10/83  N-BUTYL RAD         L 9/85  T-BUTYL RAD         L 4/85  ISOBUTANE
L 4/85  N-BUTANE            J 3/61  CARBON SUBNITRID     J12/69  C5                  P10/85  CYCLOPENTADIENE     P12/52  CYCLOPENTANE
P12/52  1-PENTENE           P10/83  N-PENTYL RAD        L 5/87  T-PENTYL RAD        P10/85  CH3C(CH3)2CH3       P10/85  PENTANE
P10/85  ISOPENTANE          BUR 84  HEXATRIYNE          L12/84  PHENYL RAD          L12/84  PHENOXY RAD         L12/84  BENZENE
L12/84  PHENOL              BUR 84  CYCLOHEXENE         P10/83  N-HEXYL RAD         L 3/86  BENZALDEHYDE        P10/84  TOLUENE
L 6/87  CRESOL              P12/52  1-HEPTENE           P10/83  N-HEPTYL RAD        P 4/81  N-HEPTANE           P12/52  1-OCTENE
P10/83  N-OCTYL RAD         P 4/85  OCTANE              P 4/85  ISO-OCTANE          P10/83  N-NONYL RAD         BUR 84  NAPTHLENE
BUR 84  AZULENE             P10/83  N-DECYL RAD         L12/84  O-BIPHENYL RAD      L12/84  BIPHENYL            L 6/88  JET-A(G)
L 6/87  BIBENZYL            J 3/77  H                   L12/69  HCN                 J12/70  HCO RAD             J12/70  HNCO
RUS 78  HNO                 RUS 78  HNO2                RUS 78  HNO3                J 9/78  HO2                 J 3/77  H2
J12/65  H2N2                J 3/79  H2O                 L 3/85  H2O2                J 3/77  N                   J12/70  NCO
RUS 78  NH                  RUS 78  NH2                 J 6/77  NH3                 RUS 78  NH2OH               RUS 78  NO
RUS 78  NO2                 J12/64  NO3                 J 3/77  N2                  RUS 78  N2H2                RUS 78  NH2NO2
RUS 78  N2H4                RUS 78  N2O                 RUS 78  N2O3                RUS 78  N2O4                RUS 78  N2O5
RUS 78  N3                  RUS 78  N3H                 J 3/77  O                   J 6/77  OH                  J 3/77  O2
J 6/61  O3                  J 3/78  C(GR)              P10/80  BENZENE(L)          P10/80  TOLUENE(L)          P10/80  OCTANE(L)
L 6/88  JET-A(L)            L 3/81  H2O(S)              J 3/79  H2O(L)
$RKTINP
EQL     = T,
FROZ    = T,
SUBAR   = 13*0.0000000000000000E+00,
SUPAR   = 13*0.0000000000000000E+00,
PCP     =   4.000000000000000     ,   10.00000000000000     ,
  50.00000000000000     ,   300.0000000000000     ,   700.0000000000000     ,
  1000.000000000000     , 16*0.0000000000000000E+00,
TCEST   =   3800.000      ,
NFZ     =              1
$END

OF =   2.333333

                          EFFECTIVE FUEL          EFFECTIVE OXIDANT          MIXTURE
                              HPP(2)                  HPP(1)                  HSUBO
ENTHALPY
(KG-MOL)(DEG K)/KG        -0.21122051E+03         -0.48782981E+02         -0.97514242E+02

                            BOP(I,2)                BOP(I,1)                BO(I)
KG-FORM.WT./KG
C                         0.58762991E-01          0.00000000E+00          0.17628898E-01
H                         0.41973565E-01          0.00000000E+00          0.12592070E-01
O                         0.83947130E-02          0.62502343E-01          0.46270054E-01
N                         0.83947130E-02          0.00000000E+00          0.25184140E-02

POINT ITN    T       CO2             H2O             CO              N2
  1   26 3306.25  -48.317         -38.781         -33.028         -30.270
  2    3 3173.58  -49.127         -39.425         -33.642         -30.619
PC/PT= 1.721214   T =  3173.58
  2    2 3173.97  -49.125         -39.423         -33.640         -30.618
PC/PT= 1.718340   T =  3173.97
  3    4 2985.96  -50.423         -40.457         -34.623         -31.180
  4    4 2803.16  -51.881         -41.619         -35.726         -31.813
  5    4 2522.53  -54.574         -43.760         -37.769         -32.966
  6    4 2250.87  -57.817         -46.312         -40.261         -34.292
  7    4 2130.35  -59.481         -47.601         -41.565         -34.925
  8    3 2079.98  -60.219         -48.166         -42.152         -35.191
```

THEORETICAL ROCKET PERFORMANCE ASSUMING EQUILIBRIUM COMPOSITION DURING EXPANSION

PC = 100.0 PSIA
CASE NO. 30

	CHEMICAL FORMULA						WT FRACTION (SEE NOTE)	ENERGY CAL/MOL	STATE	TEMP DEG K
FUEL	C	7.00000	H	5.00000	O	1.00000	1.000000	-50000.000	S	298.15
					N	1.00000	1.000000	-3102.000	L	90.18
OXIDANT	O	2.00000								

O/F= 2.3333 PERCENT FUEL= 30.0000 EQUIVALENCE RATIO= 0.8981 PHI= 0.8922

	CHAMBER	THROAT	EXIT	EXIT	EXIT	EXIT	EXIT	EXIT
PC/P	1.0000	1.7183	4.0000	10.000	50.000	300.00	700.00	1000.00
P, ATM	6.8046	3.9600	1.7011	0.68046	0.13609	0.02268	0.00972	0.00680
T, DEG K	3306.2	3174.0	2986.0	2803.2	2522.5	2250.9	2130.4	2080.0
RHO, G/CC	7.4645-4	4.5946-4	2.1469-4	9.3686-5	2.1651-5	4.2041-6	1.9351-6	1.3963-6
H, CAL/G	-193.78	-309.98	-479.07	-647.41	-910.79	-1163.61	-1270.46	-1313.20
U, CAL/G	-414.54	-518.71	-670.96	-823.31	-1063.01	-1294.26	-1392.11	-1431.21
G, CAL/G	-7924.62	-7731.54	-7461.00	-7201.91	-6809.10	-6426.70	-6251.76	-6176.71
S, CAL/(G)(K)	2.3383	2.3383	2.3383	2.3383	2.3383	2.3383	2.3383	2.3383
M, MOL WT	29.761	30.219	30.922	31.669	32.930	34.234	34.799	35.023
(DLV/DLP)T	-1.05882	-1.05590	-1.05111	-1.04562	-1.03536	-1.02334	-1.01761	-1.01523
(DLV/DLT)P	2.1377	2.1296	2.1025	2.0527	1.9127	1.6799	1.5437	1.4821
CP, CAL/(G)(K)	1.8589	1.8897	1.9152	1.9089	1.8022	1.5242	1.3301	1.2365
GAMMA (S)	1.1177	1.1135	1.1077	1.1024	1.0955	1.0919	1.0925	1.0936
SON VEL,M/SEC	1016.1	986.1	943.0	900.7	835.3	772.6	745.7	734.8
MACH NUMBER	0.000	1.000	1.638	2.163	2.933	3.687	4.025	4.165

PERFORMANCE PARAMETERS

AE/AT	1.0000	1.3658	2.4822	8.5432	37.830	78.003	106.02
CSTAR, FT/SEC	4993	4993	4993	4993	4993	4993	4993
CF	0.648	1.015	1.280	1.610	1.872	1.972	2.011
IVAC,LB-SEC/LB	190.9	210.5	237.2	276.3	310.1	323.4	328.5
ISP, LB-SEC/LB	100.6	157.6	198.7	249.8	290.5	306.1	312.1

MOLE FRACTIONS

CO	0.24329	0.22933	0.20668	0.18121	0.13526	0.08448	0.06163	0.05245
CO2	0.28136	0.30339	0.33845	0.37708	0.44526	0.51903	0.55184	0.56497
H	0.01709	0.01538	0.01295	0.01058	0.00702	0.00380	0.00256	0.00210
HO2	0.00016	0.00011	0.00007	0.00004	0.00001	0.00000	0.00000	0.00000
H2	0.01460	0.01384	0.01262	0.01127	0.00881	0.00597	0.00459	0.00401
H2O	0.13162	0.13882	0.14970	0.16098	0.17947	0.19796	0.20587	0.20901
N	0.00001	0.00000	0.00000	0.00000	0.00000	0.00000	0.00000	0.00000
NO	0.01167	0.01030	0.00841	0.00666	0.00427	0.00243	0.00180	0.00157
NO2	0.00001	0.00001	0.00001	0.00000	0.00000	0.00000	0.00000	0.00000
N2	0.03163	0.03289	0.03473	0.03655	0.03933	0.04189	0.04292	0.04332
O	0.04465	0.03939	0.03212	0.02537	0.01593	0.00836	0.00568	0.00471
OH	0.06506	0.05970	0.05172	0.04365	0.03107	0.01941	0.01470	0.01286
O2	0.15885	0.15682	0.15255	0.14660	0.13357	0.11665	0.10840	0.10499

ADDITIONAL PRODUCTS WHICH WERE CONSIDERED BUT WHOSE MOLE FRACTIONS WERE LESS THAN 0.50000E-05 FOR ALL ASSIGNED CONDITIONS

C CH CH2 FORMALDEHYDE FORMIC ACID CH3 HYDROXYMETHYLENE

METHYLOXIDE	CH4	METHANOL	CN	NCN RAD	CNN RAD	C2
C2H RAD	ACETYLENE	KETENE	C2H3 RAD	METHYL CYANIDE	CH3CO RAD	CH2CHO RAD
ETHYLENE	ACETALDEHYDE	ACETIC ACID	(FORMIC ACID)2	ETHYL RAD	ETHYL OXIDE RAD	ETHANE
AZOMETHANE	ETHANOL	DIMETHYL ETHER	CNC RAD	CYANOGEN	CCO RAD	C3
C3H3 RAD	CYCLOPROPENE	PROPYNE	ALLENE	C3H5 RAD	CYCLOPROPANE	PROPYLENE
PROPYLENE OXIDE	I-PROPYL RAD	N-PROPYL RAD	PROPANE	1-PROPANOL	CARBON SUBOXIDE	C4
BUTADIYNE	BUTAN-1EN-3YN	CYCLOBUTADIENE	2-BUTYNE	1,3-BUTADIENE	2-BUTENE TRANS	2-BUTENE CIS
ISOBUTENE	1-BUTENE	(ACETIC ACID)2	S-BUTYL RAD	N-BUTYL RAD	T-BUTYL RAD	ISOBUTANE
N-BUTANE	CARBON SUBNITRID	C5	CYCLOPENTADIENE	CYCLOPENTANE	1-PENTENE	N-PENTYL RAD
T-PENTYL RAD	CH3C(CH3)2CH3	PENTANE	ISOPENTANE	HEXATRIYNE	PHENYL RAD	PHENOXY RAD
BENZENE	PHENOL	CYCLOHEXENE	N-HEXYL RAD	BENZALDEHYDE	TOLUENE	CRESOL
1-HEPTENE	N-HEPTYL RAD	N-HEPTANE	1-OCTENE	N-OCTYL RAD	OCTANE	ISO-OCTANE
N-NONYL RAD	NAPTHLENE	AZULENE	N-DECYL RAD	O-BIPHENYL RAD	BIPHENYL	JET-A(G)
BIBENZYL	HCN	HCO RAD	HNCO	HNO	HNO2	HNO3
H2N2	H2O2	NCO	NH	NH2	NH3	NH2OH
NO3	N2H2	NH2NO2	N2H4	N2O	N2O3	N2O4
N2O5	N3	N3H	O3	C(GR)	BENZENE(L)	TOLUENE(L)
OCTANE(L)	JET-A(L)	H2O(S)	H2O(L)			

NOTE. WEIGHT FRACTION OF FUEL IN TOTAL FUELS AND OF OXIDANT IN TOTAL OXIDANTS

THEORETICAL ROCKET PERFORMANCE ASSUMING FROZEN COMPOSITION DURING EXPANSION

PC = 100.0 PSIA
CASE NO. 30

	CHEMICAL FORMULA								WT FRACTION (SEE NOTE)	ENERGY CAL/MOL	STATE	TEMP DEG K
FUEL	C	7.00000	H	5.00000	O	1.00000	N	1.00000	1.000000	-50000.000	S	298.15
OXIDANT	O	2.00000							1.000000	-3102.000	L	90.18

O/F= 2.3333 PERCENT FUEL= 30.0000 EQUIVALENCE RATIO= 0.8981 PHI= 0.8922

	CHAMBER	THROAT	EXIT	EXIT	EXIT	EXIT	EXIT	EXIT
PC/P	1.0000	1.7841	4.0000	10.000	50.000	300.00	700.00	1000.00
P, ATM	6.8046	3.8140	1.7011	0.68046	0.13609	0.02268	0.00972	0.00680
T, DEG K	3306.2	2979.4	2572.9	2172.6	1600.3	1118.3	936.2	867.1
RHO, G/CC	7.4645-4	4.6428-4	2.3980-4	1.1359-4	3.0844-5	7.3562-6	3.7657-6	2.8461-6
H, CAL/G	-193.78	-315.17	-464.58	-609.44	-810.82	-972.02	-1030.01	-1051.48
U, CAL/G	-414.54	-514.11	-636.38	-754.51	-917.67	-1046.69	-1092.52	-1109.37
G, CAL/G	-7924.62	-7281.84	-6480.63	-5689.64	-4552.66	-3586.89	-3219.18	-3079.02
S, CAL/(G)(K)	2.3383	2.3383	2.3383	2.3383	2.3383	2.3383	2.3383	2.3383
M, MOL WT	29.761	29.761	29.761	29.761	29.761	29.761	29.761	29.761
CP, CAL/(G)(K)	0.3730	0.3698	0.3650	0.3585	0.3438	0.3236	0.3129	0.3081
GAMMA (S)	1.2181	1.2203	1.2239	1.2289	1.2410	1.2600	1.2712	1.2766
SON VEL,M/SEC	1060.7	1007.9	937.9	863.7	744.9	627.4	576.6	556.1
MACH NUMBER	0.000	1.000	1.605	2.159	3.051	4.067	4.587	4.817

PERFORMANCE PARAMETERS

AE/AT	1.0000	1.2962	2.2087	6.6763	24.926	46.973	61.368
CSTAR, FT/SEC	4834	4834	4834	4834	4834	4834	4834
CF	0.684	1.022	1.266	1.542	1.732	1.795	1.818
IVAC,LB-SEC/LB	187.0	202.2	223.4	251.8	272.7	279.8	282.4
ISP, LB-SEC/LB	102.8	153.5	190.2	231.7	260.2	269.7	273.2

MOLE FRACTIONS

CO	0.24329	CO2	0.28136	H	0.01709	HO2	0.00016
H2	0.01460	H2O	0.13162	N	0.00001	NO	0.01167
NO2	0.00001	N2	0.03163	O	0.04465	OH	0.06506
O2	0.15885						

ADDITIONAL PRODUCTS WHICH WERE CONSIDERED BUT WHOSE MOLE FRACTIONS WERE LESS THAN 0.50000E-05 FOR ALL ASSIGNED CONDITIONS

C	CH	CH2	FORMALDEHYDE	FORMIC ACID	CH3	HYDROXYMETHYLENE
METHYLOXIDE	CH4	METHANOL	CN	NCN RAD	CNN RAD	C2
C2H RAD	ACETYLENE	KETENE	C2H3 RAD	METHYL CYANIDE	CH3CO RAD	CH2CHO RAD
ETHYLENE	ACETALDEHYDE	ACETIC ACID	(FORMIC ACID)2	ETHYL RAD	ETHYL OXIDE RAD	ETHANE
AZOMETHANE	ETHANOL	DIMETHYL ETHER	CNC RAD	CYANOGEN	CCO RAD	C3
C3H3 RAD	CYCLOPROPENE	PROPYNE	ALLENE	C3H5 RAD	CYCLOPROPANE	PROPYLENE
PROPYLENE OXIDE	I-PROPYL RAD	N-PROPYL RAD	PROPANE	1-PROPANOL	CARBON SUBOXIDE	C4
BUTADIYNE	BUTAN-1EN-3YN	CYCLOBUTADIENE	2-BUTYNE	1,3-BUTADIENE	2-BUTENE TRANS	2-BUTENE CIS
ISOBUTENE	1-BUTENE	(ACETIC ACID)2	S-BUTYL RAD	N-BUTYL RAD	T-BUTYL RAD	ISOBUTANE
N-BUTANE	CARBON SUBNITRID	C5	CYCLOPENTADIENE	CYCLOPENTANE	1-PENTENE	N-PENTYL RAD
T-PENTYL RAD	CH3C(CH3)2CH3	PENTANE	ISOPENTANE	HEXATRIYNE	PHENYL RAD	PHENOXY RAD
BENZENE	PHENOL	CYCLOHEXENE	N-HEXYL RAD	BENZALDEHYDE	TOLUENE	CRESOL
1-HEPTENE	N-HEPTYL RAD	N-HEPTANE	1-OCTENE	N-OCTYL RAD	OCTANE	ISO-OCTANE

N-NONYL RAD	NAPTHLENE	AZULENE	N-DECYL RAD	O-BIPHENYL RAD	BIPHENYL	JET-A(G)
BIBENZYL	HCN	HCO RAD	HNCO	HNO	HNO2	HNO3
H2N2	H2O2	NCO	NH	NH2	NH3	NH2OH
NO3	N2H2	NH2NO2	N2H4	N2O	N2O3	N2O4
N2O5	N3	N3H	O3	C(GR)	BENZENE(L)	TOLUENE(L)
OCTANE(L)	JET-A(L)	H2O(S)	H2O(L)			

NOTE. WEIGHT FRACTION OF FUEL IN TOTAL FUELS AND OF OXIDANT IN TOTAL OXIDANTS

```
                                EEEEE  N    N  DDDD            000   FFFFF                J   000   BBBB
                                E      N    N  D   D         0   0  F                    J  0   0  B   B
2222222222222222222222222222222 E      NN   N  D   D         0   0  F                    J  0   0  B   B  2222222222222222222222222222222
2222222222222222222222222222222 EEEE   N N  N  D   D         0   0  FFFF               J  0   0  BBBB   2222222222222222222222222222222
2222222222222222222222222222222 E      N  NN  D   D         0   0  F                 J  J  0   0  B   B  2222222222222222222222222222222
                                E      N   N  D   D         0   0  F                 J  J  0   0  B   B
                                EEEEE  N   N  DDDD            000   F                  JJJ    000   BBBB

                                RRRR     AAA     SSSS   CCCC   000   N   N
                                R   R   A   A   S      C      0   0  N   N
                                R   R   A   A   S      C      0   0  NN  N
                                RRRR    A   A    SSS   C      0   0  N N N
                                R R     AAAAA       S  C      0   0  N  NN
                                R  R    A   A       S  C      0   0  N   N
                                R   R   A   A   SSSS    CCCC   000   N   N

                                FFFFF   000   RRRR    000    000    999
                                F      0   0  R   R  0   0  0   0  9   9
                                F      0   0  R   R  0  00  0  00  9   9
                                FFFF   0   0  RRRR   0 0 0  0 0 0   9999
                                F      0   0  R R    00  0  00  0      9
                                F      0   0  R  R   0   0  0   0      9
                                F       000   R   R   000    000    999

                                   J   000   BBBB          55555  7777    888
                                   J  0   0  B   B         5         7  8   8
                                   J  0   0  B   B         555       7  8   8
                                   J  0   0  BBBB             5     7    888
                                J  J  0   0  B   B            5    7    8   8
                                J  J  0   0  B   B         5  5    7    8   8
                                 JJJ    000   BBBB          555    7     888
```



```
+-----------------------------------------+
|                                         |
| Received: ..............................|
|                                         |
| Date    : ..............................|
|                                         |
| Operator: ..............................|
+-----------------------------------------+
```

```
Job FOR009 (578) queued to CCIT_IO_ROOM on 21-MAR-1989 15:55 by user RASCON, UIC [RASCON], under account NRS-2305 at priority 100,
completed on printer LTA1260 on 21-MAR-1989 15:55 from queue CCIT_WIDE.

22222222222222222222222222222222222222222222222222222222222222222222222222222222222222222222222222222222222222222222222222222222222
22222222222222222222222222222222  Digital Equipment Corporation - VAX/VMS Version V4.7  22222222222222222222222222222222222222222222
22222222222222222222222222222222222222222222222222222222222222222222222222222222222222222222222222222222222222222222222222222222222

         1         2         3         4         5         6         7         8         9         0         1         2         3
12345678901234567890123456789012345678901234567890123456789012345678901234567890123456789012345678901234567890123456789012345678901234
```

APPENDIX C

Number	Name	a	e	i	omega	w	M	q	Diameter	Period	V(1,0)	Amplitudes	Class	Pv	References
	1937UB Hermes							0.62							
	1950DA							0.84							
	1951XA							0.51							
	1959LM							0.72							
	1973NA							0.88							
	1974MA							0.12							
	1978CA							0.88	1.9	3.748			S(10)	0.06	8
	1979VA							1		3.6			CF(2)		
	1979XB							0.65							
	1981VA								1.8					0.07	4
	1982DB							0.82							
	1982TA							0.52	1.7(S) 1.8(R)		15.7			0.33(S) 0.28(R)	4,
	1983LC							0.76							
	1983TF2							0.66							
	1983VA							0.81							
	1983VB							0.96							
	1984KB							0.52	0.7				S(11)	0.1	9
	1986JK							0.9					C(12)		
	1986PA							0.59							
	1987KF							0.59							
	1987OA							0.61							
	1987QA							0.88							
	1987SB							0.75							
	1987SY							0.6							
	1988EG							0.64							
	1988TA							0.79					C(13)		
	5025P-L							0.15							
	6311P-L							0.97							
	6713P-L							0.8							
	1988VP1							0.79							
	1988XB							0.76							
	1989AC							0.9							
	1989AZ							0.86							
133	Eros	1.1583663(2)	0.2228556	10.82623	303.74013	178.56784	122.06938	1.13	22	5.27			S(2)	0.18	10
719	Albert							1.13							
887	Alinda	2.1917002(2)	0.559008	9.25599	110.22682	349.66782	355.5391	1.1	1.2(S) 5.9(R)	73.97	14.09		S(2)	0.23(R) 0.12(R)	4
1036	Ganymed	2.6645933(2)	0.5365783	26.44737	215.62463	131.60167	313.73721	1.23	38.5(S) 87.5(R)		9.6		S(2)	0.17(S) 0.03(R)	4
1221	Amor	1.9192081	0.4354754	11.89801	170.86736	26.26689	208.11179	1.08							
1566	Icarus	1.0779852	0.8267816	22.89332	87.49949	31.17593	48.92903	0.19	0.9(S) 0.9(R)	2.273	16.75			0.12 0.39(R)	4
1580	Betulia	2.1918191(14)	0.4901462	52.11302	61.70256	159.31107	43.23522	1.12	7.4	6.13			C(14)	0.03	11
1620	Geographos	1.2118109(2)	0.3354856	13.31906	336.7	276.61221	212.33876	0.83	2.0(S) 2.7(R)		15.91		S(2)	0.19(S) .11(R)	4
1627	Ivar	1.8626727(2)	0.3971427	8.44759	132.63002	167.37779	236.71615	1.12	8.1(S) 10.2(R)	4.798	13.36		S(2)	0.12(S) .08(R)	4
1685	Toro	1.3670701(5)	0.4358521	9.37478	273.75616	126.87895	225.10126		5.2(R) 3.1(S)	10.196	14.22			0.14(R) 0.31(S)	4
1862	Apollo	1.4712113(2)	0.5598442	6.34958	35.36775	285.16336	19.67018	0.65	1.4	3.065			Q(2)	0.21	6
1863	Antinous	2.2590375(2)	0.5598442	6.34958	35.36775	285.16336	19.67018	0.89	1.8	4.02			SU(2)	0.18	
1864	Daedalus	1.1609952(6)	0.6147112	22.1563	6.11702	325.36883	90.22275	0.56		8.57			SQ(6)		
1865	Cerberus	1.0802064(2)	0.1669061	16.0916	212.38757	325.10211	218.88903	0.58	1.0(S) 13.2(R)	6.8	17.1		S(2)	0.26(S) 0.17(R)	4
1866	Sisyphus	1.8933658	0.592675	41.15075	63.008061	292.9162	187.6533	0.87	8.2(S) 13.2(R)		12.9			0.18(S) 0.07(R)	4
1915	Quetzalcoatl	2.5370817(2)	0.5740106	20.45079	162.38676	347.84106	49.77921	1.08	0.3(S) 0.05(R)	4.9	19.27		SMU(2)	0.29(S) 0.16(R)	4
1916	Boreas	2.2716716(3)	0.4504199	12.85017	310.23013	335.32166	198.80937	1.25					S(3)		

1	1917	Cuyo	2.149398	0.5048552	23.98337	187.83588	194.19571	353.61636	1.06						
1	1943	Anteros	1.430298(2)	0.255899	8.70519	245.76398	338.15616	214.90784	1.06	1.8(S)		16	S(2)	0.22(S)	4
										2.6(R)				0.10(R)	
1	1951	Lick	1.3905249(15)	0.0616467	39.0961	130.13399	140.40717	209.94965	1.3				A(15)		
1	1980	Tezcatlipoca	1.7094184(3)	0.3652399	26.84838	246.0916	115.23865	151.37994	1.09	4.3(S)		14.15	SU(3)	0.21(S)	4
										6.8(R)				0.08(R)	
1	1981	Midas	1.7762983	0.6501989	39.83437	356.51595	267.68185	329.10117	0.62						
2	2059	Baboquivari	2.6506663	0.5260623	10.9953	200.46254	191.28668	4.8118	1.26						
2	2061	Anza(1960UA)	2.2639019(16)	0.5372786	3.74081	207.34161	155.8308	183.58042	1.05		11.5		TCG(16)		
2	2062	Aten	0.9664191(1)	0.825996	18.93686	108.02875	147.89163	24.49963	0.79	0.9			S(1)	0.2	3
2	2063	Bacchus	1.0775353	0.3494244	9.41957	32.6831	55.01283	130.54814	0.7						
2	2100	Ra-Shalom	0.832089(2)	0.4363715	15.76003	170.27494	355.92296	27.17462	0.47	2.4(R)	19.79	16.43	C(2)	0.08(R)	4
										1.7(S)				0.16(S)	
2	2101	Adonis	1.8747862	0.7639414	1.35996	350.57656	41.69714	355.02197	0.44						
2	2102	Tantalus	1.2900732	0.298486	64.01166	93.71879	61.61973	107.94471	0.9						
2	2135	Aristaeus	1.5999357	0.5032714	23.03911	190.77791	290.59957	86.95645	0.8						
2	2201	Oljato	2.1757492	0.7105624	2.51479	76.39765	95.72617	0.18775	0.63	1.2(S)	>21.	15.86		0.12(R)	4
										1.4(R)				0.52(S)	
2	2202	Pele	2.907682	0.5122192	8.78271	169.72619	217.25943	317.82989	1.12						
2	2212	Hephaistos	2.1672116(7)	0.8338571	11.80419	27.88999	208.27302	181.70232	0.36				SG(7)		
2	2329	Orthos	2.1024614	0.6587443	24.40612	168.86636	115.78333	182.99007	0.82						
2	2340	Hathor	0.8139709(3)	0.4499333	5.85547	210.99391	39.78085		0.16				CSU(3)		
2	2368	Beltrovata	2.1051823(3)	0.4127799	5.25709	287.17567	41.94518	318.56612	1.21	2.3(S)	5.9	16	SQ(3)	0.13(S)	4
										3.8(R)				0.05(R)	
2	2608	Seneca	2.1912138(10)	0.5809893	15.33761	168.92256	33.86941	336.81179	1.01	0.9	5.9		S(10)	0.16	8
3	3102	1981QA	2.1507685(2)	0.4490919	8.11519	171.7379	154.24488	20468523	1.19		148		QRS(2)		
3	3103	1982BB	1.1065476(8)	0.3545792	20.94209	129.26354	253.7046	289.15166	0.91	1.1(S)	5.71	15.16	E(8)	0.63(S)	4
										1.5(R)				0.53(R)	
3	3122	1981ET3	1.7687102	0.4223896	22.18105	335.57423	27.18659	37.49196	1.02						
3	3199	Nefertiti	1.5715552(2)	0.2836854	32.97132	339.43884	53.28995	173.15009	1.13	2.2(R)	3	15.32	S(2)	0.26(R)	4
										1.8(S)				0.11(R)	
3	3200	Phaethon	1.2712503(9)	0.8901732	22.08857	264.91071	321.80756	87.96383	0.11	6.9			F(9)	0.08	7
3	3271	1982RB	2.1029508	0.3947563	24.99761	158.3915	158.66861	121.88125	1.27						
3	3288	Seleucus	2.0320703(2)	0.157597	5.9352	218.152	349.20613	207.90714	1.1	2.8(R)	75	15.3	S(2)	0.17(R)	
										1.9(S)				0.35(S)	
3	3352	McAuliffe	1.8790539	0.3692907	4.77731	106.90168	15.56136	129.98022	1.19						
3	3360	1981VA	2.4604328	0.7438949	22.00617	215.9381	59.18132	31.17154	0.63	1.8(S)		16.85		0.10(S)	
										2.9(R)				.04(R)	
3	3361	Orpheus	1.209454	0.3226401	2.68776	189.17012	301.60438	261.12066	0.82						
3	3362	Khufu	0.9894954	0.1685915	9.92035	152.00408	51.85454	142.76245	0.53	0.7(S)		18.45		0.16(S)	4
										1.0(R)				0.07(R)	
3	3551	1983RC	2.0918948(17)	0.4869563	9.51494	173.37374	193.03196	355.75832	1.07	0.8(S)	4.93	17.11	V(17)	.40(S)	4
										0.9(R)				0.28(R)	
3	3552	1983SA	4.2363740(18)	0.7130884	30.74613	350.07178	316.57347	255.68374	1.21	18.7(S)		13.65	D(18)	0.02(S)	4
										29.6(R)				0.01(R)	
3	3553	Mera	1.6447099	0.3203805	36.76134	231.97605	288.83803	67.77769	1.12						
3	3554	Amun	0.9737222(4)	0.2804185	23.35615	358.0276	359.3114	56.90161	0.7	2			M(4)	0.17	5
3	3671	Dionysius	2.1956644	0.5426289	13.62787	81.80421	203.60973	219.01058	1.01						
3	3691	1982FT	1.7743435	0.2840253	20.37319	348.26442	234.6422	17.50107	1.27						
3	3752	1985PA							0.99						
3	3753	1986TO							0.18						
3	3757	1982XB							1.02	0.5(S)	9.012	18.99	S(2)	0.15(S)	12
										0.7(R)				0.09(R)	
3	3838	1986WA							0.45						
3	3908	1980PA							1.04				V(17)		
		1972RB							1.1						

1977VA	1.13			XC(3)	
1979QB	1.3				
1980AA	1.05		2.7		
1980WF	1.08	0.6		QU(2)	0.18
1980YS	1.23				
1981QB	1.08				
1982YA	1.12				
1983LB	1.19				
1983RB	1.09				
1985DO2	1.23			V(17)	
1985TB	1.11				
1985WA	1.13				
1986DA	1.17	2.3	3.58	M(4)	0.12
1986LA	1.06				
1986NA	1.17				
1986RA	1.23			C(12)	
1987FA	1.21				
1987QB	1.14				
1987SL	1.15				
1987SF3	1.05				
1987UA	1.22				
1987WC	1.01				
1988NE	1.21				
1988PA	1.28				
1988SM	1.09				
1988TJ1	1.14				
1788P-L	1.18				
1988TJ1	1.14				
1988VN4	1.23				

REFERENCES: DIAMETERS AND pV

1. "standard" non-rotating thermal model.
2. "non-standard" fast-rotating thermal model.
3. Morrison et al., 1976, Cruikshank and Jones, 1977.
4. Veeder et al., 1987, 1988.
5. Tedesco & Gradie, 1987.
6. Lebofsky et al., 1981.
7. Veeder et al., 1984.
8. Lebofsky et al., 1979.
9. Bell et al., 1988.
10. Lebofsky & Rieke, 1979.
11. Lebofsky et al., 1978.
12. Helin et al., 1983.

REFERENCES: PERIOD

1. Ostro et al, 1984.
2. Veverka & Liller 1969, Miner & Young, 1969.
3. Dunlap, 1974.
4. Dunlap et al., 1973.
5. Hahn, 1983.
6. Binzel, 1987.
7. Gehrels et al., 1971.
8. Harris p.c., Harris & Young in prep.
9. Hahn & Harris personal communication.
10. Harris & Young, 1983.
11. Wisniewski, 1987.
12. Degewij, 1987.
13. Taylor, 1985.
14. Dunlap & Taylor, 1979.
15. Harris & Young, 1985.
16. Tedesco et al., 1978.
17. Lupishko et al., 1986.
18. Binzel and Tholen, 1983.
19. Rakos, 1960.
20. Bowell, 1977.
21. Harris, p.c., Harris, Young & Gibson in prep.
22. Debehogne et al., 1983.

RENCES: SEMI-MAJOR AXIS AND CLASS

Gradie, 1976.
Tholen, 1984a.
data from Degewij et al., 1978 classified by Tholen, 1988.
Tedesco & Gradie, 1987.
data from Dunlap et al., 1973 classified by Tholen, 1988.
data from Zellner et al., 1975 classified by Tholen, 1988.
data from Bowell et al., 1978 classified by Tholen, 1988.
Taxonomy inferred by Veeder et al., 1989 from high albedo and neutral colors of Wisniewski, 198
Tholen, 1987.
Degewij, 1978.
Bell et al., 1988.
Wisniewski, 1987.
Tholen, 1988.
Tedesco et al., 1978.
Wisniewski, personal communication.
data from Rakos, 1960 classified by Tholen, 1988.
Tholen et al., 1988.
Tholen, 1984b, Tholen, 1988.

APPENDIX D

The Nucleus of Comet P/Tempel 2

Michael F. A'Hearn[1,2]

Astronomy Program, University of Maryland

Humberto Campins[1]

Planetary Science Institute

David G. Schleicher[2] and Robert L. Millis

Lowell Observatory

Submitted to *Astrophysical Journal*, February 1989
Received:

1. Visiting Astronomer at the Infrared Telescope Facility which is operated by the University of Hawaii under contract from the National Aeronautics and Space Administration.
2. Visiting Astronomer at the 88–inch telescope of the University of Hawaii.

Manuscript correspondence
Michael F. A'Hearn
Astronomy Program
University of Maryland
College Park, Md. 20742

ABSTRACT

We present the results of simultaneous optical photometry and infrared radiometry of comet P/Tempel 2. Periodic variations of brightness, previously detected in the optical by others, are present at all wavelengths in our data. Because the optical and thermal lightcurves are in phase, we conclude that the variations are caused by the changing apparent cross-section of an elongated nucleus rotating with a period near 8.9 hours. The variation of flux with aperture allows us to separate the contributions of the nucleus and the coma. In the apertures with which we monitored the lightcurve, the contribution by the coma is roughly 25% at maximum light in the optical and undetectable at the level of 10% at all times in the thermal infrared. By applying a standard thermal model, we have determined the following nuclear properties: effective radius at maximum light, 5.9 km; visual geometric albedo, 0.022; and projected axial ratio near 2. The nucleus is very red. Based on the observed rate of outgassing, roughly 1% of the surface is active. Properties common to all nuclei of periodic comets appear to include the very low albedo and the high axial ratio. The active fraction of the surface and the spectral reflectivity appear to vary significantly among nuclei.

I. INTRODUCTION

Over the last ten years or so, a resurgence of interest in measuring the properties of cometary nuclei has occurred. This resurgence is motivated by a desire to better understand the relationship between the nucleus and the more readily observed phenomena in the coma and to explore the relationship between cometary nuclei and Amor-Apollo (AA) asteroids. The comae of comets have been conceptualized for many years as the product of outgassing from a dirty snowball (Whipple, 1950) but the detailed nature of that snowball has remained elusive. Even the dramatic results from the Vega and Giotto spacecraft have left many questions unanswered concerning the nature of cometary nuclei, not the least of which is the degree to which P/Halley is typical of all comets. The possible relationship of comets to asteroids is based on the long-standing idea, originally suggested by Öpik (1963), that a significant fraction of the AA asteroids are extinct cometary nuclei. Current estimates from dynamical arguments suggest, with very large error bars, that roughly half the AA asteroids are derived from comets (Wetherill, 1988).

Unfortunately, it is very difficult to observe cometary nuclei. The only totally unambiguous observations are those from spacecraft, but ground-based observations have been made which, with varying degrees of certainty, appear to refer to a cometary nucleus rather than to material of the coma. These results have been reviewed recently (A'Hearn, 1988; Weissman et al., 1989) and will not be discussed in detail here. In general there are two possible approaches to the problem of studying cometary nuclei from Earth. Jewitt and Meech (1988) have concentrated on observing comets optically at large heliocentric distances when the activity of the comet is expected to be small. We, on the other hand, have concentrated on observing comets which are relatively inactive even at small heliocentric distances. This approach permits one to study the nuclei in the thermal infrared as well as in the optical (Campins *et al.*, 1987; hereafter CAM87; Millis *et al.*, 1983; hereafter MAC88). With both approaches there is always some uncertainty about the contamination of the measurements by coma although observers universally argue that their own measurements are relatively free from this problem.

Comet P/Tempel 2 is a particularly interesting object. It has been considered repeatedly as a potential target for a cometary mission, but none of these has yet come to fruition. Nevertheless, because of this possibility, the comet has been

the object of ground-based study by numerous astronomers. It is known from the orbital lightcurve (Sekanina, 1979)[1] that for much of the preperihelion arc the brightness of the coma is negligible. Similarly, the non-gravitational force is very small (Marsden, 1985) suggesting low activity per unit mass of the nucleus (although a fortuitous geometry could also lead to a small non-gravitational effect even with significant outgassing). P/Tempel 2 is, therefore, one of the few comets, the nuclei of which might be observable near perihelion. Accordingly, we planned an observational program of simultaneous optical and infrared photometry similar to those we carried out earlier on comets P/Neujmin 1 (CAM87) and P/Arend-Rigaux (MAC88). Other groups also observed P/Tempel 2 at this apparition. Jewitt and Luu (1988a) determined a rotational period from ccd photometry obtained well before perihelion, while Wisniewski (1988) confirmed the period and determined the rotational lightcurve from conventional broadband photometry in May 1988. Wisniewski's rapidly distributed lightcurve was invaluable in the planning of our observing strategy. In particular, after the first few observations we were able to predict the times of subsequent maxima and minima in order to optimize the observations.

II. OBSERVATIONS

The observations were scheduled for June 1988 near the time of the comet's closest approach to Earth. Although this time was somewhat after the predicted onset of activity, the lightcurve of Sekanina (1979) implied that activity would still be weak and the advantage to be gained by observing at minimum geocentric distance was significant. The infrared observations were carried out at the NASA Infrared Telescope Facility (*IRTF*) to measure the thermal emission from the comet on 1988 June 10 and 11 UT. The optical measurements were made with the University of Hawaii 88–inch telescope during the same two nights and during a small portion of the night of June 9 UT. Subsequent nights were cloudy. The observing circumstances at the midpoint of the two full nights are given in Table 1.

[1] An updated version of the orbital lightcurve, including data from the apparition of 1983, was widely distributed by the *International Halley Watch* and is the version actually used.

Table 1
Observational Circumstances June 10.9

r_H = 1.72 AU	phase = 20°
Δ = 0.79 AU	$\dot{r}_H$ = −9.9 km/s

In the infrared, the standard N filter (reference wavelength = 10.1 μm; Tokunaga, 1986) and *IRTF* bolometer were used most frequently to define the lightcurve. The temporal variations were monitored using the 4–mm aperture. A few N observations were made near maximum and minimum light (phases chosen to minimize the temporal variations) in 4 apertures, 3, 4, 5, and 6.5 mm, for which drift scans on stars yielded effective angular diameters of 5.3, 7.0, 7.8 and 8.7 arcsec, respectively. The chopper throw was 30 arcsec north-south. Based on the photometry with different apertures, we estimate that the coma contribution to the reference beam was less than 0.5% of the comet's peak brightness. Measurements with the standard M (4.8 μm) and Q (20.0 μm) filters were also made to determine color temperatures. The star α Boötis was used as a primary standard; the adopted magnitudes were M = −2.12, N = −3.17 and Q = −3.13 (Tokunaga 1986). Two stars near the comet in the sky, α Serpentis and 110 Virginis, were observed frequently and used as local standards to monitor extinction and check for any instrumental variations. Neither of the local standards showed intrinsic variability although some changes in extinction were detected and corrected for. The observations were reduced and calibrated using the procedure and absolute fluxes discussed by Tokunaga (1986).

The optical observations were made with a photometer and pulse-counting electronics from Lowell Observatory and the standard *International Halley Watch (IHW)* filters which isolate various emission bands and portions of the reflected continuum. These filters are described in detail in an appendix to the *IHW Archive of Observations of P/Giacobini-Zinner* (in press). On June 9 an *EMI* 6256S phototube was used completing the identical system to that which was used previously for comet P/Arend-Rigaux (MAC88). On June 10 and 11, we used an RCA 31034A phototube which allowed use of filters at longer wavelengths than were used in the previous study. Since most of June 9 was devoted to another project, only about 1 1/2 hours were spent observing P/Tempel 2. Consequently, the data from that night were not well calibrated. The temporal variations were monitored using the two filters for the continuum at 4845 Å and 6840 Å and

an aperture of 10.1 arcsec. Sky was observed far from the comet (usually several tens of arcmin) after each set of observations of the comet (usually 3 thirty-second integrations in each of the two continuum filters). The stars HD149363 and HD120086 were used for absolute calibration via the standard magnitudes defined by the *IHW* while observations of two nearby comparison stars were interspersed between every set of cometary observations to monitor any variations in transparency and/or instrumental sensitivity. There was no indication of intrinsic variability in the brightness of the nearby comparison stars or in the extinction coefficients. Mean extinction coefficients for the two nights were used in reducing the data. Two or three times each night — usually near the times of maximum and minimum light when the brightness of the comet was changing most slowly — observations were made in apertures of 14.2, 20.0, and 28.5 arcsec in order to determine the radial brightness profile of the coma. An accurate measurement of this profile is required if the contributions of the nucleus and the coma to the observed signal are to be disentangled. The comet was also observed a few times through other filters of the *IHW* set in order to estimate production rates of various gasses, gas-to-dust ratio, *etc.*

A. Brightness Variations

The 6840–Å observations taken through the 10.1–arcsec aperture and the N magnitudes measured through a 7–arcsec aperture are listed in Tables 2 and 3 and are plotted as a function of time in Figures 1 and 2 for the nights of 10 and 11 June, respectively. It is evident that both the reflected optical and the thermal infrared brightnesses of the comet were varying in a seemingly periodic way. The existence of this variation was, in fact, no surprise. Jewitt and Luu (1988a) had reported cyclic variations in April with an approximately 9–hour period and a peak-to-peak amplitude of 0.7 mag. in the R passband, in good agreement with the amplitude we observed at N, while Wisniewski (1988), from V-filter observations in late May, had produced a convincing light curve for Tempel 2 having a period of 8 hr. 58 min. and an amplitude of 0.5 mag. Wisniewski's observations were made through photometer apertures of 17 and 12 arc sec diameter; Jewitt and Luu observed with a CCD. The difference in optical amplitude reported by these investigators and the yet smaller amplitude of approximately 0.4 mag which we observed in June at 6840Å, very probably can be attributed to greater dilution by the coma of the signal from the nucleus as the comet became more active because, based on Sekanina's (1987) determination of the polar orientation, we

T2-FIG1

(T2FIG1.M60)

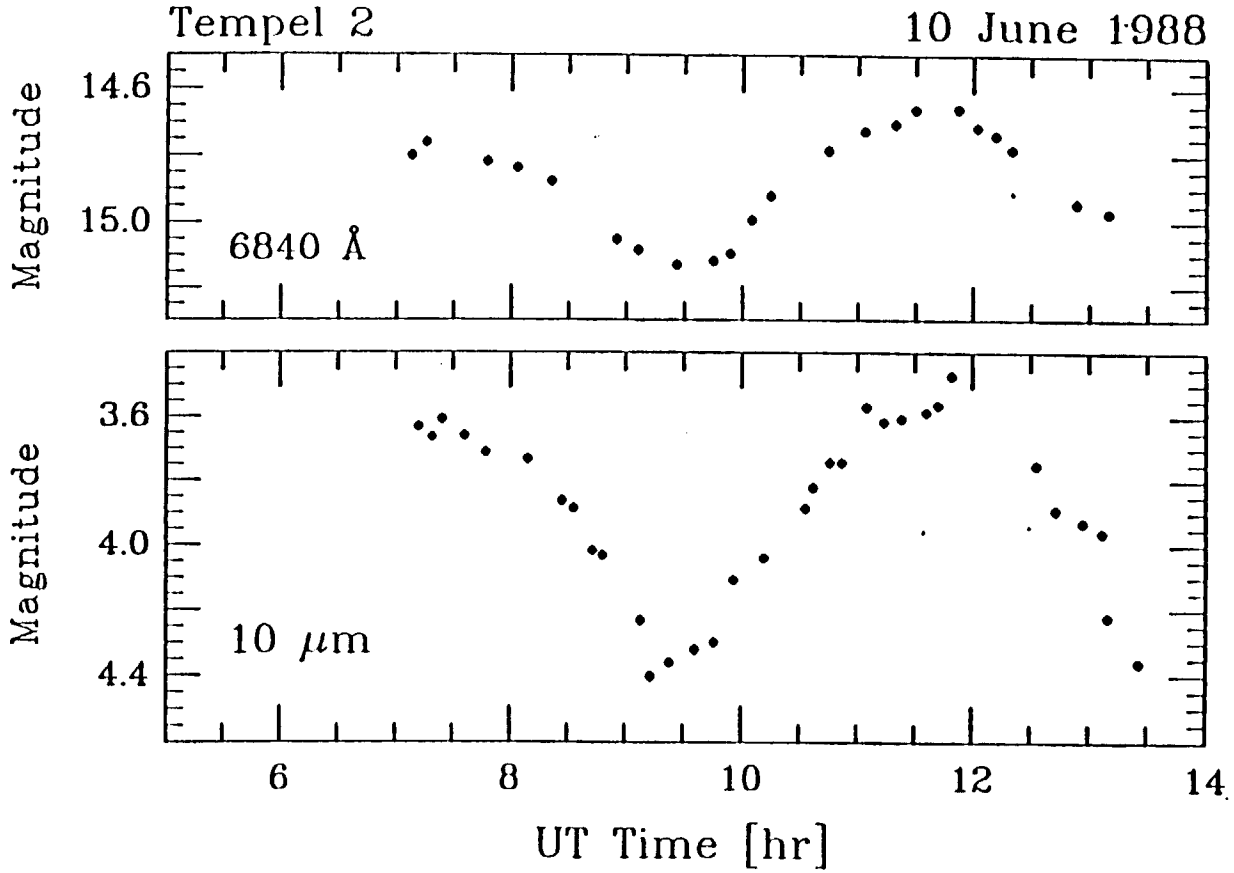

T2 - FIG 2

(T2FIG2.MAC)

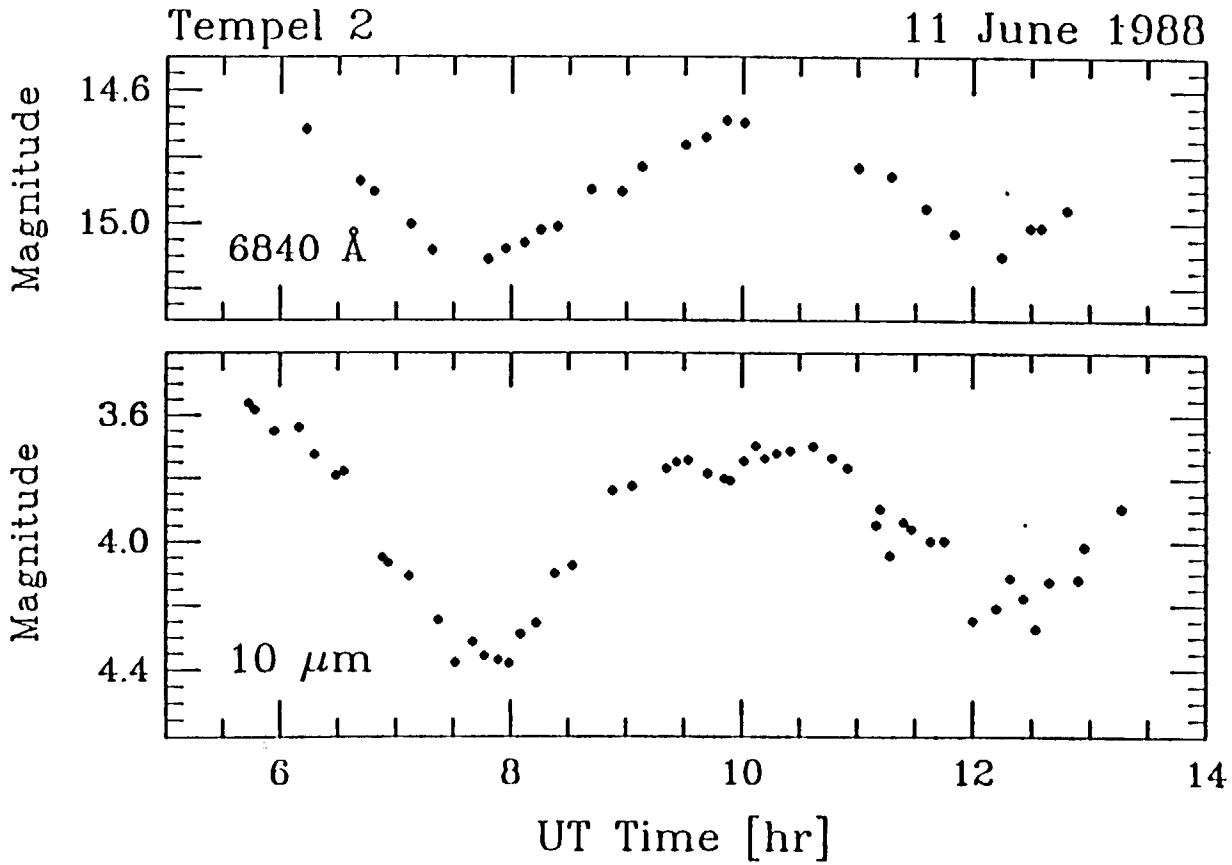

all observed the comet at nearly identical projections. On the other hand, the observations of P/Tempel 2 in 1987 by Jewitt and Meech (1988), which exhibited a much smaller amplitude (<0.3 mag given our present knowledge of the period), were obtained when the sub-Earth and sub-solar points were at cometographic latitudes corresponding to a projection factor approximately half that for the later observations. Consequently, the smaller optical amplitude in 1987 is likely due to the different aspect.

Table 2

Table 3

Although our observations do not extend over a sufficient time interval to permit a precise period determination, we have estimated the period using the method of phase dispersion minimization (Stellingwerf 1978). This technique was previously applied to comet P/Arend-Rigaux by MAC88 and the reader is referred to that paper for details of the method. We performed separate period searches on the 4845–Å, 6840–Å, and 10–μm data for P/Tempel 2 from 10 and 11 June. The statistic θ (see MAC88) for each of these data sets is shown plotted against period in Figure 3. Possible periods in the data are those for which there is a local minimum in this plot. The increase in depth of the minima towards shorter periods is, to some degree, an artifact of the method. In computing θ, the data are divided into phase bins and the dispersion of the data points within each bin computed. The shorter the period, the narrower is each bin in time, and the less the intrinsic brightness variation of the comet will contribute to the dispersion within a bin. Note that the plots for all 3 data sets show a sharp minimum at a period of 4.45 days. This period corresponds to a light curve having one maximum and one minimum per cycle. We believe, however, based on evidence which will be presented later in this paper, that the light curve must have 2 maxima and 2 minima per cycle. Consequently, the true period is twice the value quoted above, in good agreement with the results of Jewitt and Luu (1988a, 1989) and Wisniewski (1988). Indeed, a broad minimum is present in Figure 3 at a period near 9 hours. We note that this is the shortest photometrically determined rotational period for a cometary nucleus except for the very first period

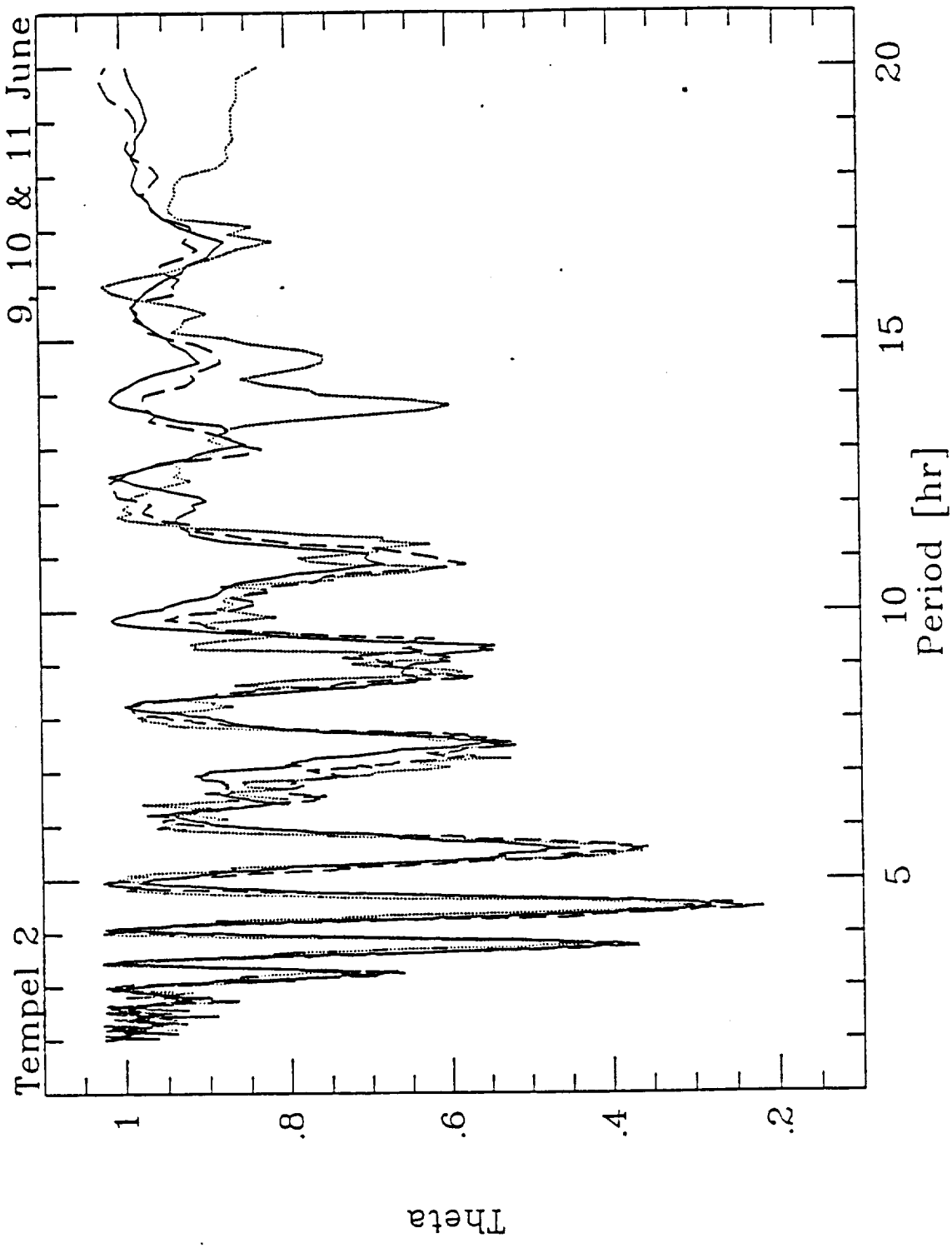

T2 - Fig. 3

(T2FIG3.M60)

so determined. Fay and Wisniewski (1978) determined a period of 5.2 hours for P/d'Arrest although the rather small amplitude of the variation yielded poor signal-to-noise ratio in the resultant power spectrum. All other rotational periods recently determined seem to be substantially longer.

Figure 4 shows the observations from 10 and 11 June phased according to a period of 8.9 hours and plotted as open circles and filled circles, respectively. In addition, the observations from 9 June have been included (as filled triangles) in the plot of the 4845–Å data. Zero phase arbitrarily has been set at 7.75 hrs. U.T. on 9 June. Since the observations from 9 June are poorly calibrated, we have simply shifted those data arbitrarily to the same mean brightness as the data at the same phase from the other nights. Note that the apparent peak in the abbreviated light curve from 9 June at phase 0.1 is coincident with a maximum in the light curve from the other two nights.

It is apparent in Figures 1, 2, and 4 that the reflected optical and thermal infrared light curves are closely in phase as was also the case for P/Arend–Rigaux (MAC88). Now, as in the earlier paper, we interpret the alignment of the visible and infrared light curves to mean that the brightness variations result from the changing apparent cross section of an elongated, rotating nucleus. If the brightness variations were due to albedo features on the nucleus, the visible and IR light curves should be 180° out of phase. The large difference in amplitude between the visible and infrared light curves results at least in part from greater dilution of the optical observations by the signal from the coma. In order to derive the size, shape, and albedo of P/Tempel 2's nucleus, it is necessary to first remove this contamination by the coma.

B. Removal of Coma

As noted above, observations were made of the aperture-dependence of the flux several times at the three monitoring wavelengths — 4845 Å, 6840 Å, and 10.1 μm. These observations were usually made near maximum or minimum light in order to minimize the temporal variation of the comet's brightness during the interval required to make measurements through all apertures. The sequence of these measurements was such that an observation with the monitoring aperture (10.1 arcsec and 7.0 arcsec in the optical and infrared, respectively) was interpolated between each of the observations with the other apertures. This procedure took up to an hour so it was necessary to use smooth curves through

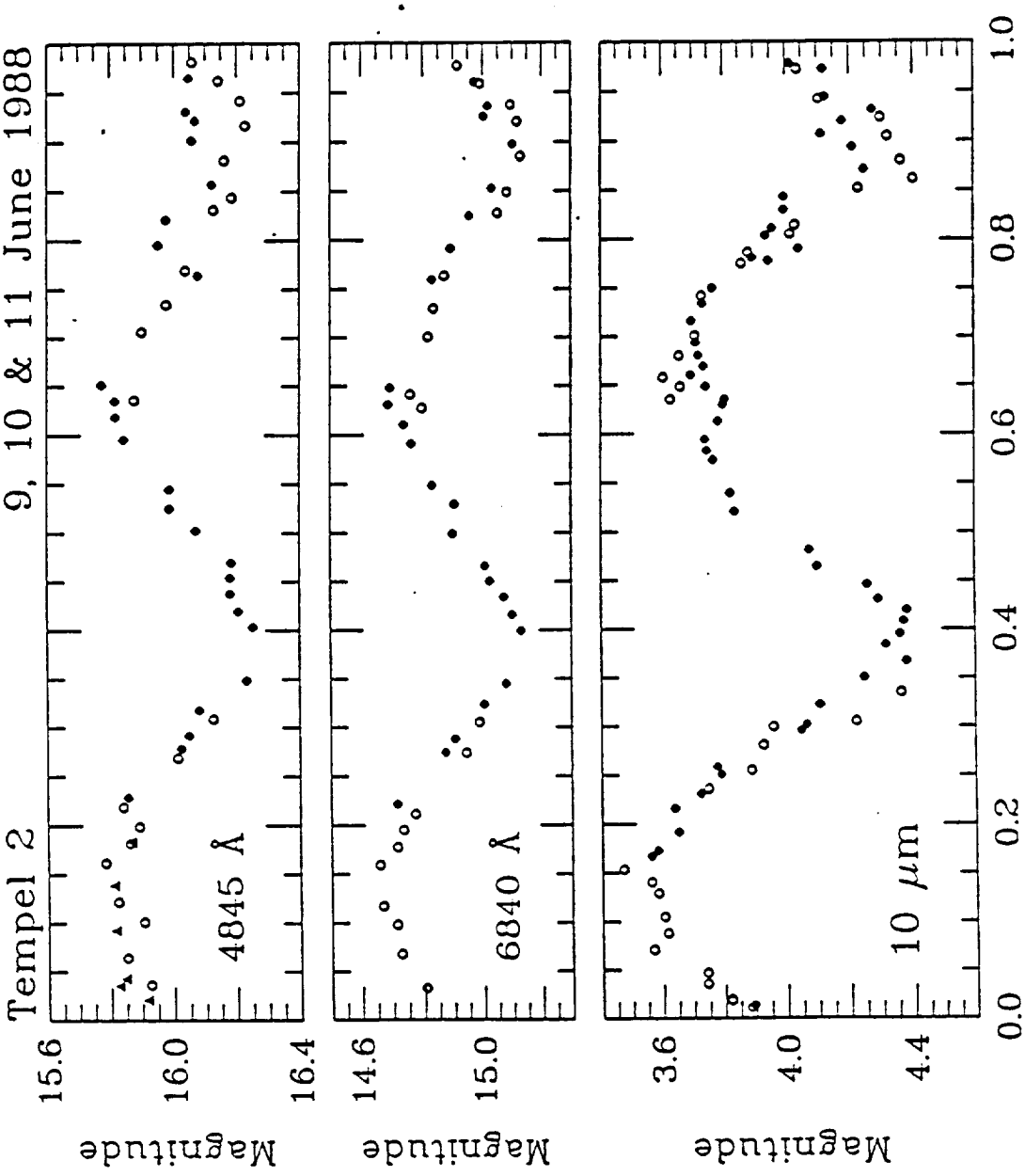

T2 - Fig. 4

(T2FIG4.MSD)

the data in Figures 1 and 2 to correct the observations to a common time assuming that the variation in flux was the same in all apertures, an assumption justified *a posteriori*. These corrections were as large as 6%.

A simple radial outflow model for the dust predicts a surface brightness which varies as ρ^{-1}, where ρ is the projected distance from the nucleus, which in turn implies that the flux in a centered aperture varies linearly with the diameter. Although this is clearly an oversimplification since the coma may be varying, it provides a convenient reference point. In Figures 5 and 6 we have plotted the flux as a function of diameter of the aperture. An examination of the variation with aperture size at 10.1 μm shows that a horizontal straight line adequately describes the data. Fitting straight lines by least squares and comparing the value of those lines at 7.0 arcsec and 0 arcsec shows that the contribution by the coma to the monitoring aperture is 10% $\pm$ 10% at maximum light. Thus, there is not a statistically significant detection of the coma at this wavelength and we assume that the contribution is nil for our reductions. There was not enough signal to even attempt to measure the variation with aperture size with the M and Q filters and therefore we have assumed that the contribution by the coma at those wavelengths is also negligible. At least for Q, this assumption is supported *a posteriori* by the modelling discussed below.

At optical wavelengths, however, there is clearly a contribution by the coma. In Figure 6, the straight lines have been fitted by least squares to observations through the 10.1, 14.2, 20.0, and 28.5–arcsec apertures. The standard deviations of the slopes are roughly 10% and the variation in slope from one set of observations to the next is not statistically significant. Based on the average slopes from Figure 6, the contribution by the coma to the flux in the 10.1-arcsec aperture at maximum light is 25% of the total flux at 4845 Å and 20% of the total flux at 6840 Å. At minimum light, the contributions are 35% and 28%, respectively.

The lack of variation in the optical brightness profiles, it should be noted, argues strongly that the coma is not contributing significantly to the observed brightness variations. For one thing, the amplitude of the observed variations is markedly greater than the variation in the coma contribution to the signal in the 10.1–arcsec aperture. Secondly, since the crossing time for dust in our apertures is comparable to the rotational period, any substantial variation in coma production would produce readily apparent distortions of the coma brightness profiles.

The coma contribution to the observations of the comet in the 10.1–arcsec

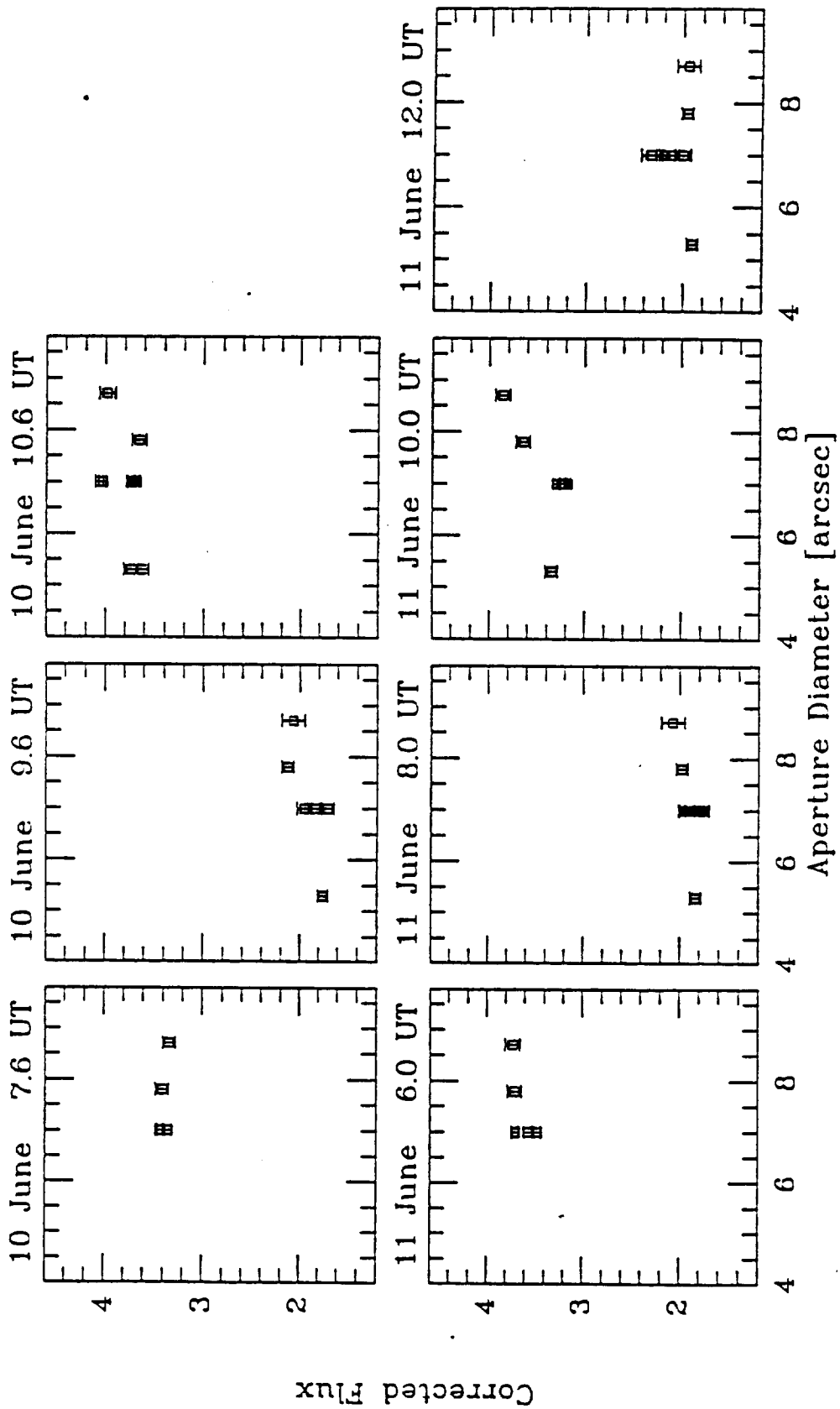
10 June 7.6 UT
10 June 9.6 UT
10 June 10.6 UT
11 June 6.0 UT
11 June 8.0 UT
11 June 10.0 UT
11 June 12.0 UT
Corrected Flux
Aperture Diameter [arcsec]

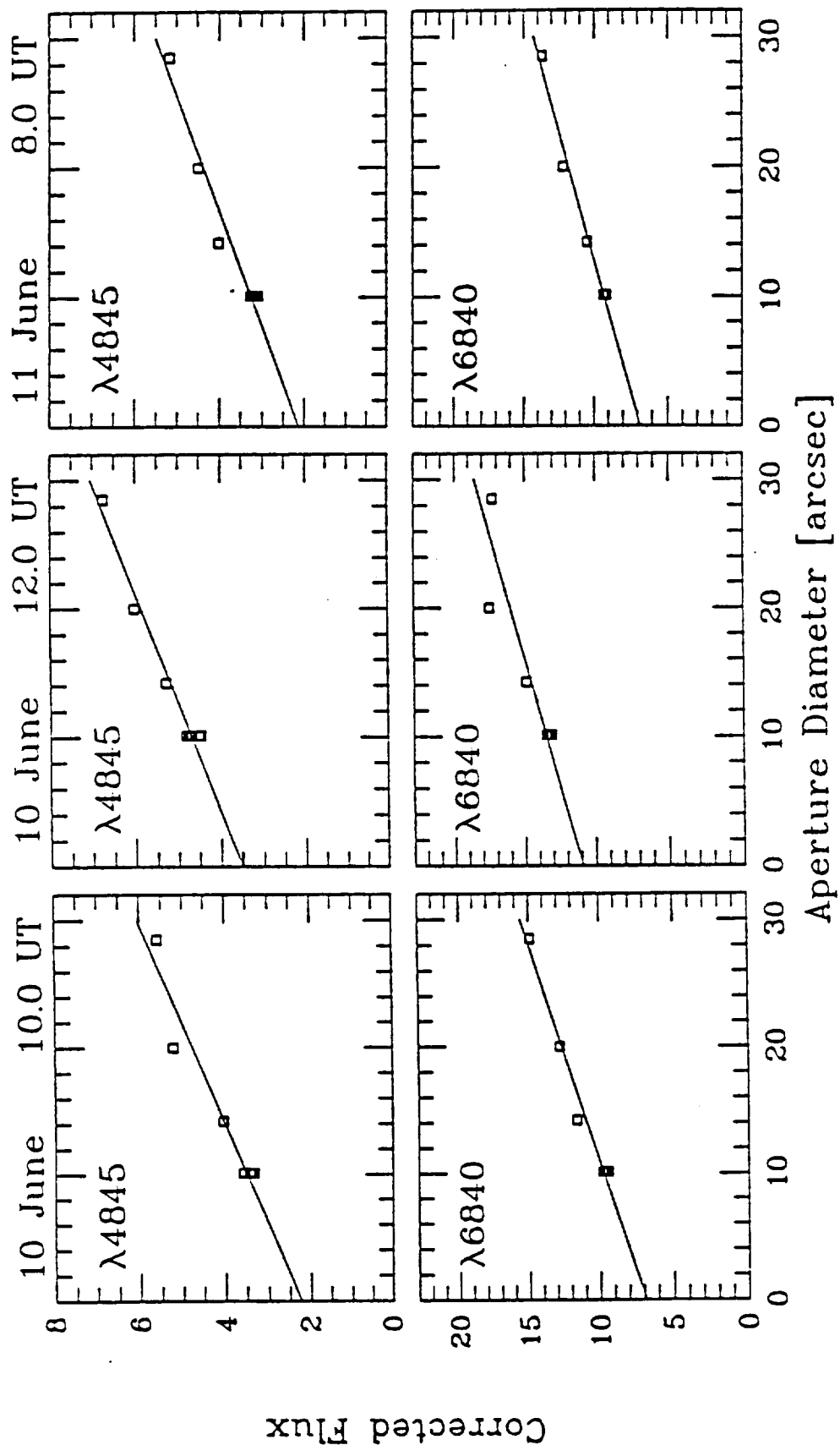
10 June 10.0 UT
λ4845
10 June 12.0 UT
λ4845
11 June 8.0 UT
λ4845
λ6840
λ6840
Corrected Flux
Aperture Diameter [arcsec]

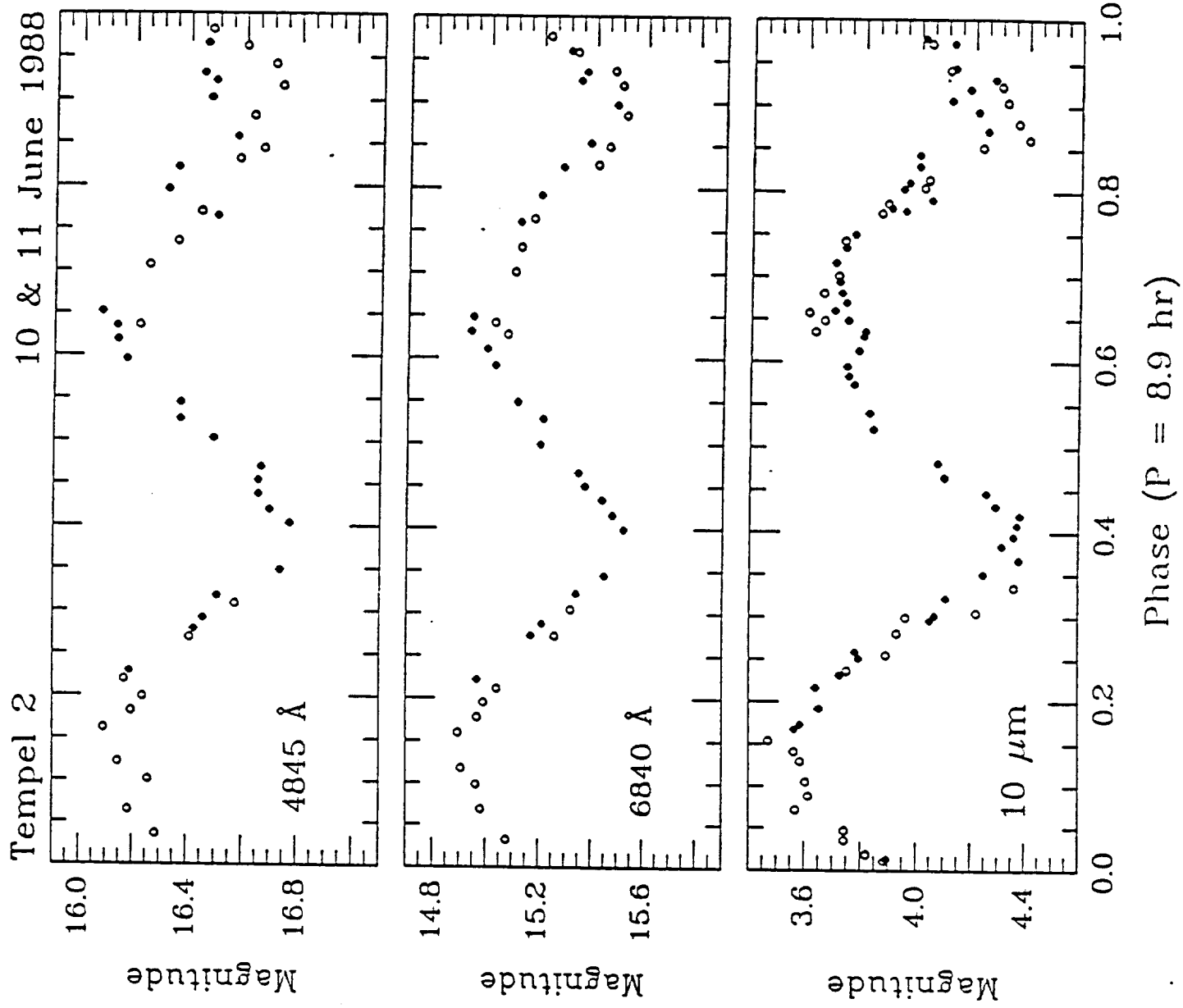

T2 · Fig. 7

(T2F167.M60)

aperture has been calculated on the basis of these values of the slope and subtracted from the observed signal to give the brightness of the nucleus alone. Columns 3 and 7 of Table 2 contain these nuclear magnitudes on the standard system defined by the *IHW*. These values are plotted as a function of lightcurve phase in Figure 7. The observed magnitudes at N, given in Table 3, are also plotted in Figure 7. We have already argued that these 10.1–μm observations directly refer to the nucleus and do not require correction for coma.

A careful comparison of the panels in Figure 7 shows that the amplitude of the optical lightcurves is about 0.55 mag while that in the infrared is near 0.80 mag. There are two possible explanations of this difference. One is that we have underestimated the amount of coma contamination of the optical measurements. In fact examination of Figure 6 does suggest a tendency for the observed variation with aperture to deviate from linearity in the sense of being convex upwards. Curvature of this type has been seen in some other comets and has been attributed to the effects of radiation pressure (Jewitt and Meech, 1987) or evaporation of grains (Baum and Kreidl, 1986). To explore the impact of possible curvature in the brightness profile of the coma, quadratic fits to the data in Figure 6 were performed. These fits yielded nuclear fluxes at maximum light 10 to 50% smaller than deduced from the linear fits and, therefore, gave lightcurve amplitudes closer to that observed in the infrared. However, a reduced chi–squared analysis indicates that the quality of the quadratic fits is not significantly improved over that of the linear fits. Accordingly, we see no compelling justification for adopting the quadratic fits in computing the contribution by the coma. This is particularly true in the absence of any physical understanding of why the brightness profile should follow a quadratic function.

An alternative explanation of the difference in amplitude between the optical and IR lightcurves comes from the work of Brown (1985). Brown has shown that for elongated bodies, the amplitude of the thermal signal will be a function of wavelength as well as aspect. Because we have only the 10.1–μm lightcurve for P/Tempel 2, we are unable to confirm whether this effect is actually present in this comet. If it is, then it is by no means clear that the optical and IR lightcurves should have the same amplitude. In any case, it is important to emphasize that if the coma contribution has been underestimated, the result will be an overestimate of the albedo of the nucleus but, because the albedo turns out to be so low anyway, the determination of the nuclear size will be unaffected.

C. Emission by the Coma

The observations of the coma, aimed at deriving rates of outgassing of the various molecular species, were also interspersed with the monitoring observations. These observations were, therefore, much less complete than if determination of the outgassing were our primary goal. The only species measured with large fields of view were OH and CN, the former because it is the best measure of the total gaseous outflow and the latter because it is usually the easiest species to measure in comets. C_2 and C_3 were measured only in the 10.1 arcsec aperture used for monitoring the variability. Of these, C_2 was measured numerous times because, if strong, it could contaminate the measurements of the continuum at 4845 Å. Fortunately, the emission was weak enough that the contamination of the 4845–Å flux in the 10.1–arcsec aperture was negligible although still strong enough that we were able to detect it reliably with the filter centered on the emission band (5140 Å).

The observations of OH required special treatment because of the nonlinearity of atmospheric attenuation with airmass in the filter used to isolate this band. The *IHW* has modelled the atmospheric attenuation in this filter (Carsenty, private communication) using the actual transmission curve of this filter and atmospheric parameters suitable for Mauna Kea. The extinction can be linearized for these specific conditions by using an effective airmass:

$$X_{eff} = X - 0.07257 \times X^2; (B - stars)$$
$$X_{eff} = X - 0.0348 \times X^2; (comets)$$
$$k_{comet} = 0.9234 \times k_B$$

Conversion to fluxes, both for OH and for the other species, was carried out using the transformations provided by the *IHW* (*cf.* appendices to the Giacobini-Zinner archive, in press). These formulae require continuum measurements which are used to remove the continuum that underlies the emission bands. In all cases the measurements of the continuum were sufficiently close in time that no correction was needed for the rotational variation. The resultant fluxes in the emission bands are given in Table 5 below.

The dust in the coma was measured as a byproduct of the removal of the brightness of the coma from the nuclear brightness as described above. This process is subject to all the uncertainties discussed in the previous section to an even higher degree since the desired component is now the smaller of the two

components being separated. A single measurement at 4845 Å in an aperture of 56.8 arcsec is less susceptible to these problems (only 28% of the light was due to the nucleus) but even in this case the result is somewhat uncertain.

III. MODELLING AND INTERPRETATION

A. Coma

We interpret the observed emission-band fluxes in the coma in terms of molecular production rates as is common in cometary studies. The fluorescence efficiencies (g-factors) used to convert fluxes to column densities are given in Table 4. The column densities are then converted to production rates using a Haser model with the parameters given in Table 4. From the abundances of OH, we also calculate the production rate of H_2O using a vectorial model (Festou, 1981) with the parameters given in Table 4. For the species for which we have multiple measurements, there is no statistically significant variation with time so we have averaged all measurements to give an average production rate for June 10–11 for a given aperture. These results are given in Table 5. An examination of the relative abundances of the various gaseous species shows that the ratio of other species to H_2O is somewhat lower than typical of active comets but not by a large factor.

Table 4
Haser Model Parameters
(at r=1.72AU)

Species	L/N [erg-s^{-1}]	Parent Scale [km]	Daughter Scale [km]
OH	8.23×10^{-16}	1.20×10^{5}	3.41×10^{5}
CN	1.16×10^{-13}	3.60×10^{4}	8.83×10^{5}
C_2	1.53×10^{-13}	4.71×10^{4}	3.24×10^{5}
C_3	3.39×10^{-13}	2.94×10^{3}	1.77×10^{5}

Vectorial Model Parameters
(at r=1 AU)

$\tau(H_2O)$ = 82400 s	τ(OH) = 200,000 s
v(OH) = 1.15 km/s	fraction H_2O to OH = 0.93

The production of dust is given by the quantity $Af\rho$ (A'Hearn *et al.*, 1983), a directly observable (*i.e.*, model independent) quantity which, for pure radial outflow at constant velocity and for constant scattering, is proportional to the production of those grains dominating the optical scattering. Since it was shown above that the coma was constant to within our precision, we quote only a single value for each aperture. A few measurements were made with a filter at 3650 Å (see Table 7 below) through the 10.1–arcsec aperture but, as with M and Q, there was not sufficient signal-to-noise ratio to separate the coma from the nucleus directly. On the other hand, these data clearly show that the amplitude of the lightcurve at this wavelength is roughly 0.7 magnitudes, noticeably greater than that found at longer optical wavelengths. These data will be discussed in more detail below but, since all evidence points to a constant coma, the amplitude suggests that the contribution by the coma is less than 20%, thereby allowing us to set an upper limit on the brightness of the coma at this wavelength.

We note that all our modelling is based on models that assume spherical symmetry whereas it is well know that the coma of P/Tempel 2 is not circularly symmetric (*e.g.* Sekanina, 1987). In many cases the lack of spherical symmetry will not materially affect the conclusions since, *e.g.*, a set of jets in the plane of

the sky can be modelled as simple fractions of the spherically symmetric case. Deviations from spherical symmetry become systematically less important as the field of view increases and in the limiting case in which one observes the entire comet the discrepancies vanish. For this reason we place much heavier weight on the observations with the large (56.8–arcsec) aperture. Temporal variability is not included in any of our models and one must remember that any 'production rates' represent an average rate over some appropriate interval depending on the transit time of material in the field of view and the lifetimes of the relevant species and their parents.

Table 5
Production of the Coma

Species	Aperture Diam. [arcsec]	Radius [10^4 km]	Flux [erg-cm^{-2}-s^{-1}]	$\bar{N}$ [cm^{-2}]	Q [s^{-1}]
Gas					
OH	56.8	1.62	3.3×10^{-12}	8.4×10^{11}	2.1×10^{27}
	10.1	0.29	1.5×10^{-13}	1.17×10^{12}	1.9×10^{27}
H_2O	56.8	1.62	-	-	3.2×10^{27}
	10.1	0.29	-	-	3.8×10^{27}
CN	56.8	1.62	1.6×10^{-12}	4×10^{9}	3×10^{24}
C_2	10.1	0.29	5×10^{-14}	8×10^{8}	2×10^{24}
C_3	10.1	0.29	3×10^{-14}	8×10^{8}	6×10^{22}
Dust					
Wavelength [Å]	Aperture Diam. [arcsec]	Radius [10^4 km]	Flux [erg-cm^{-2}-s^{-1}-Å^{-1}]		Afρ [cm]
3650	10.1	0.29	$<3\times10^{-16}$		<18
4845	56.8	1.62	3.0×10^{-15}		15
	10.1	0.29	6.1×10^{-16}		18
6840	10.1	0.29	4.4×10^{-16}		17

The ratio of gas to dust is conveniently parameterized by the ratio $Q(H_2O)/Af\rho$. This ratio is independent of the effects due to the finite field of view of the instruments although it differs from the true ratio of gas to dust both by a conversion of units ($Af\rho$ has the units of cm) and by parameters of the dust and the gas which may vary from time to time and from comet to comet. In particular, it varies with the wavelength of the light used to determine $Af\rho$ due to the variation of reflectivity with wavelength. Nevertheless, we believe that this is the most observationally reasonable parameter for monitoring the ratio of gas to dust. Feldman and A'Hearn (1985) showed that the parameter did exhibit a correlation with heliocentric distance, which might indicate a variation of modelling parameters but might also indicate real physical differences with heliocentric distance. At a given distance, the comets considered there showed rather little scatter. Comet P/Halley exhibited significant variation with heliocentric distance and closer than 1 AU did deviate noticeably from the usual relationship with distance (Feldman *et al.*, 1987). Typical values of this ratio in P/Halley are in the range 10^{25} to 10^{26} $(cm\text{-}s)^{-1}$ using ultraviolet light and these numbers would be very roughly 2/3 that value if the continuum were measured at 4845Å. Comets generally considered to be dust-poor like P/Encke and Bradfield 1979 X have values near 2×10^{26} using the continuum at 4845Å. The value for P/Tempel 2 is roughly 1×10^{26} $[cm\text{-}s]^{-1}$, a very typical value for comets at this heliocentric distance. The only comet of which we are aware that exhibits a substantially higher value of this parameter is P/Neujmin 1 (CAM87) for which the dust was undetectable and for which we estimate a lower limit of 1×10^{27} $[cm\text{-}s]^{-1}$.

B. Nucleus

The nucleus was modeled using the "standard" thermal modeling program described by Lebofsky *et al.*(1986) as in the previous modeling of comets P/Neujmin 1 (CAM 87) and P/Arend-Rigaux (MAC 88). The input parameters used were the following: thermal phase coefficient 0.01 mag/degree, visible phase coefficient 0.035 mag/degree, thermal emissivity 0.9, and thermal beaming factor 0.9. The visible phase coefficient is consistent with but not strongly constrained by the data at phases < 30° presented by Sekanina (1987, Figure 11). None of the other coefficients are known for this or for any comet but are taken from the standard model for asteroids. Because the observations were made at a relatively small phase angle (Table 1), the results of the model are not very sensitive to assumptions about phase coefficients. This type of thermal modeling is appropriate

for comets that are relatively inactive, such as P/Tempel 2, because the amount of energy that goes into sublimation is negligible compared to the total incident radiation (CAM 87). The calculated effective radius at maximum light, which depends only on the infrared measurements as long as the optical albedo is low, is 5.90 +0.24/-0.68 km. In this calculation a 10.1–μm magnitude at maximum light of 3.532 was used. This value includes the monochromatic correction of −0.043 magnitudes for 270K, given by Tokunaga (1986). The larger uncertainty towards smaller radii is due to the possibility that the coma contributes as much as 20% of the 10.1–μm flux at maximum light (see section 2).

The axial ratios obtained from the corrected visible lightcurve amplitude (0.55 mag) and the 10.1μm lightcurve amplitude (0.80 mag) were averaged to determine a minimum axial ratio for the nucleus of 1.9 +0.6/-0.2; the larger uncertainty towards a more elongated nucleus is again due to the possibility of a larger contribution by the coma. At the time of our observations, Earth was nearly in the equatorial plane of the comet according to the model of Sekanina (1987); if so, and assuming that the nucleus of this comet can be approximated by a prolate spheroid rotating about a minor axis, the observed lightcurve amplitude and effective radius are consistent with overall nuclear dimensions of 16.3 x 8.6 x 8.6 km. The geometric albedo is 0.022 with an estimated uncertainty of +.004/-.006. The effects of departures from sphericity on the results of the standard thermal model have been discussed by Brown (1985). We estimate the error in the calculated effective radius introduced by ignoring sphericity to be +/- 5%. Brown's non-spherical thermal model predicts that the amplitude of the rotational lightcurve will be larger in the thermal infrared than in the visible. This effect could explain the different amplitudes observed in the visible and at 10.1 μm; on the other hand, this difference could also be due to an incomplete removal of the coma contribution in the visible (*cf.* section II.). A more refined analysis of our observations and those of MAC 88 aimed at improving our knowledge of the shape of the nuclei of comets P/Tempel 2 and P/Arend-Rigaux is in progress (Brown et al., in preparation).

The observations at M (4.8 μm) and Q (20 μm), presented in Table 6, provide a check on the thermal modeling. Several measurements at Q were made at different points in the lightcurve in search of possible temperature variations predicted by the non-spherical thermal model. We detected only statistically marginal N−Q color variations, a mean N−Q = 1.85 was observed, consistent with the brightness temperatures of 270 K at N and 256 K at Q, predicted by the standard thermal

model. The comet was considerably fainter at M, hence the fluxes in this bandpass were not as well determined as those for Q. Only single values for M were obtained for each day near a maximum in the lightcurve; these are slightly higher than predicted by the standard thermal model. This excess in the M flux is qualitatively similar to that observed in comet P/Arend-Rigaux (MAC 88), where a significant contribution (approx. 33% of the flux) from the dust was observed in the M bandpass. In the case of comet P/Tempel 2, however, we could not obtain aperture photometry in the M filter to quantify the contribution by the dust coma at this wavelength.

Table 6
Additional Thermal Data

UT [hr]	M [mag]	UT [hr]	Q [mag]
June 10		June 10	
12.48	8.56	13.05	1.98
June 11		June 11	
10.25	8.28	07.60	2.34
		08.98	1.99
		09.63	1.73
		10.72	1.94
		11.58	2.13

The albedo of the nucleus derived here is an effective visual albedo but some additional information is available on the variation of albedo with wavelength. The narrowband magnitudes given in Table 2 yield directly the color of the nucleus (averaging values near maximum light), $CI\,(48-68) = m\,(4845) - m\,(6840) = 1.18$ whereas the solar color in this system is 0.87 based on observations of solar analogs. The nucleus of comet P/Tempel 2 is therefore rather red, with a reflectivity gradient, (ds/dλ)/s = 14% per kÅ. This result is in excellent agreement with the spectrophotometry of Tempel 2 at large heliocentric distance obtained by Spinrad *et al.* (1979) and in reasonably good agreement with the results contemporaneous with ours by Jewitt and Luu (1989). The three sets of data are

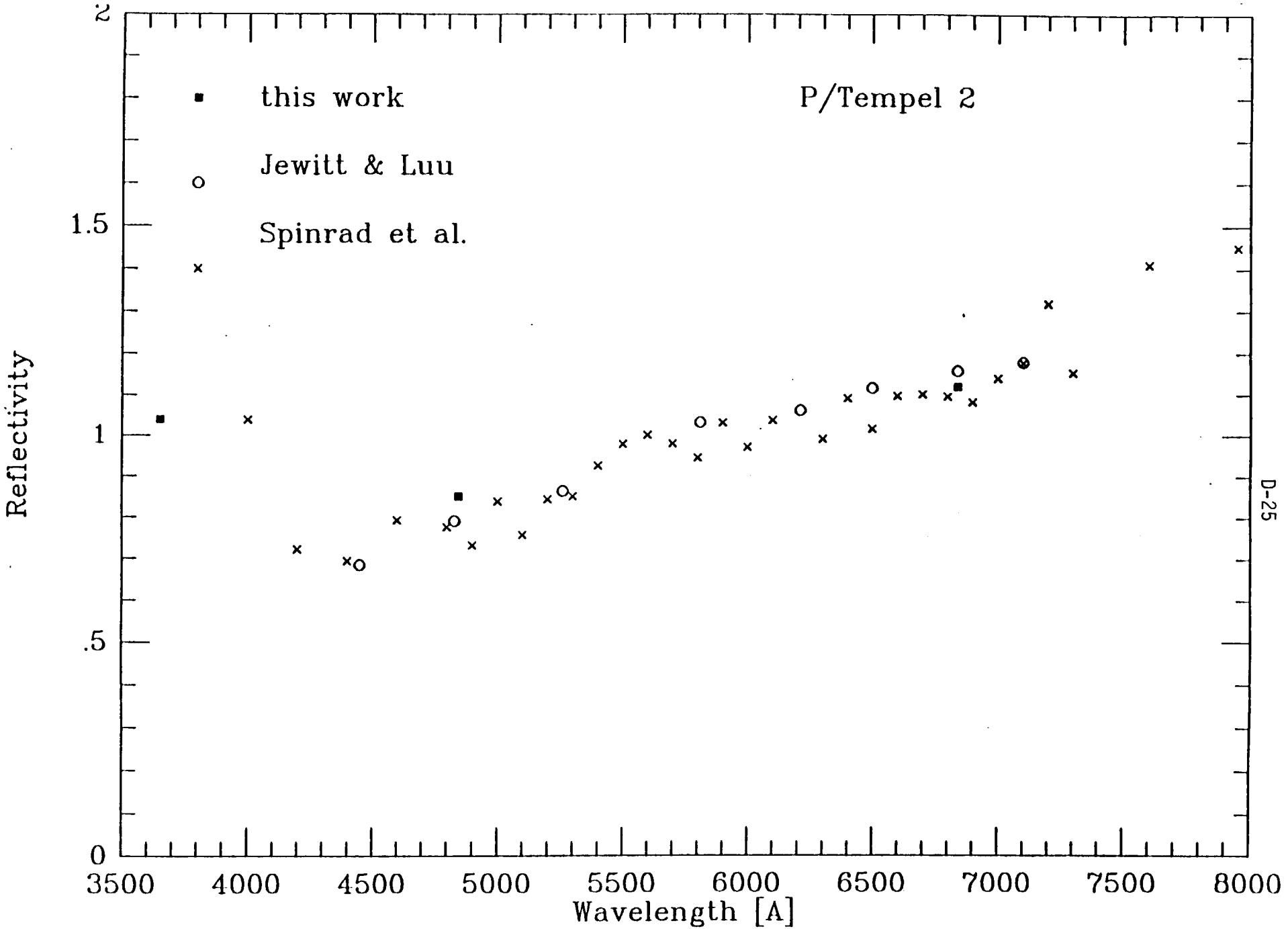
this work
Jewitt & Luu
Spinrad et al.
P/Tempel 2
Reflectivity
Wavelength [A]
0
.5
1
1.5
2
3500
4000
4500
5000
5500
6000
6500
7000
7500
8000
D-25

shown in Figure 8. Since the value of the albedo-area product by Spinrad *et al.* is also in good agreement with our value near minimum light, we infer that no coma was present at the time of the measurements by Spinrad *et al.*. Those data suggest that the reflectivity increases at the shortest wavelengths.

Although we have data at 3650 Å, we can not reliably remove the coma from those data because the signal-to-noise ratio is inadequate. Our data for the combined nucleus and coma at four different times are given in Table 7. Uncertainties are roughly 0.02 mag at the two longer wavelengths and rather larger but not well determined at 3650 Å. The table shows quite clearly the redness of P/Tempel 2 between 4845 Å and 6840 Å with only marginally significant variations between maximum and minimum. The color index between 3650 Å and 4845 Å, however, varies from bluer than the sun at maximum light to slightly redder at minimum light. Since all data at longer wavelengths imply that the coma is constant, and since the amplitude at 3650 Å is 0.7 mag (averaging the two maxima and comparing with the single minimum), significantly greater than at longer optical wavelengths, we conclude that the contribution by the coma at maximum light is less than 20%. We can therefore set a lower limit to the nuclear brightness: $m_{nuc}(3650) < 17.1$ at maximum light yielding a color $CI(36-48) = m(3650) - m(4845) < 1.0$ compared to the corresponding solar color of 1.17. This corresponds to a slope of the reflectivity of $-13\%/\text{kÅ}$. The agreement among the three sets of data in Figure 8 is excellent and the behavior at short wavelengths, although based on only two points with limited precision, is remarkable. The two points at the shortest wavelengths in Figure 8, one of ours and one from Spinrad *et al.*, are individually no more than three standard deviations above an extrapolation of the data at longer wavelengths but the agreement between the two totally independent results is striking. Given the uncertainties in the data, we do not want to overinterpret this result but believe that the effect is real. The repeatability of the spectrum over many different aspects and, at least for the filter photometry, with rotational phase indicates that the surface is rather homogeneous in color.

Table 7
Color of P/Tempel 2
(10.1 arcsec aperture)

Date UT	m(3650) [mag]	m(4845) [mag]	CI(36-48) [mag]	CI(48-68) [mag]
Jun 10.475	16.97	15.90	1.08	1.20
Jun 11.333	17.56	16.23	1.34	1.16
Jun 11.404	16.73	15.82	0.91	1.08
Jun 11.471	17.36	15.97	1.40	1.12
solar color	—	—	1.17	0.87

It is also significant that the color of the nucleus is quite different from the color of the grains in the coma. Examination of Table 5 shows that the grains in the coma have a very neutral color whereas the nucleus is distinctly red except at the shortest wavelengths. Jewitt and Luu (1989) have reached a similar conclusion based on their long-slit spectra of the comet. There is no way of determining, from either our data or those of Jewitt and Luu, whether the difference is due to selective ejection of grains or to differences in scattering properties between the grains on the surface and grains in the optically thin coma.

We can combine the outgassing rate observed in the coma and the size of the nucleus to estimate the fraction of active area on the nucleus. Determination of that fraction depends, of course, on where the active area is on the nucleus since that determines the effective insolation. We have used the methods described by Cowan and A'Hearn (1979) to estimate the outgassing of water molecules per unit area for an isothermal nucleus (rapid rotation and high thermal conductivity), for a model which is everywhere in local equilibrium (low thermal inertia) and for a model in which parallels of latitude are isotherms (rapid rotation). The range of rates of outgassing is from 2×10^{16} to 5×10^{17} cm^{-2} s^{-1}. According to the nuclear model of Sekanina (1987), the vent is at a high cometographic latitude. For this latitude and obliquity 90° and each latitude line being an isotherm, a typical rate of outgassing would be of order 3×10^{16} cm^{-2} s^{-1}. This is a lower limit to the outgassing per unit area since concentration of the heating to the daytime side non-linearly increases the outassing so that the average over the day is higher. Thus if the outgassing is from a single active vent vaporizing in equilibrium, its

maximum area is 11 km^2 or 3% of the total surface. Much smaller areas are likely since the outgassing per unit area increases if the active area is more nearly normal to the direction to the sun or if a latitude line is much hotter on the dayside than on the nightside as we would expect. It is clear from this discussion that comet P/Tempel 2, like comets P/Arend-Rigaux and P/Neujmin 1, has an almost totally inactive nucleus. The fraction of the surface which can be active in all three comets is at least an order of magnitude less than the fraction for P/Halley which itself has activity from no more than 30% of the surface (based on 15% in the sunlit hemisphere and an assumed comparable area on the dark hemisphere).

We also note that the geometry of Sekanina's model predicts that the vent should be alternating between daylight and darkness at the time of our observations so that some variability might be expected (Sekanina, 1988). Because the lifetimes of H_2O and OH are both longer than the rotational period of the nucleus, the observed variation will be much less than the true variation in outgassing. A variation of the outgassing from one day to the next has been reported (A'Hearn *et al.*, 1988) and will be discussed in more detail elsewhere. On the other hand, the constancy of the coma contributed by the dust argues against significant fluctuations in the outgassing unless the velocity of the dust leads to a transit time in our aperture much longer than the rotational period. If the velocity of the dust was < 0.1 km/s this would be the case and we should not see significant fluctuations.

Table 8
Summary of Nuclear Properties

R_{eff} = 5.9 km	p_v = 0.022	Axial Ratio > 1.9
P = 8.9 hr	T_B = 270 K	Active fraction < 3%
prolate spheroid: 16.3×8.6×8.6 km		

The combination of the red slope of the reflectivity at long optical wavelengths with a possible increase in the ultraviolet is unusual. The only similar curve of spectral reflectivity for a small body of which we are aware is that of comet P/Schwassmann-Wachmann 1 (S-W1). Although we can not be sure that the quiescent phase of this comet is a bare nucleus, that point is often advocated and not unreasonable. Cochran *et al.* (1982) measured the reflectivity of S-W1 in its quiescent phase and found a reflectivity similar to that of P/Tempel 2. Also as for

P/Tempel 2, they found that the coma of S-W1 (measured during a subsequent outburst) was of a different color. The two comets are not, however, identical since the albedo of S-W1 was found by Cruikshank and Brown (1983) to be 0.13, very much higher than found here for P/Tempel 2

The reflectivities of these two comets appear unlike those of any standard types of asteroids. They are also significantly different from the reflectivities of other recently measured cometary nuclei: P/Neujmin 1 (CAM87) was very red even at the shortest wavelengths; P/Arend-Rigaux (MAC88) was almost neutral in color; P/Halley (Thomas and Keller, 1989) was significantly less red at optical wavelengths. These other comets are similar in visual albedo and axial ratio and show a range of active surface fractions spanning the fraction found above for P/Tempel 2. The present results for P/Tempel 2 thus support the contention that cometary nuclei form a diverse group with no clear-cut match among the AA asteroids.

We note finally that the results found here bear on models of cometary nuclei. The results discussed here are generally consistent with the model of Sekanina (1987) in regard to the polar orientation and the general geometric description of the outgassing as being from a vent at high cometographic latitude. The combination of these results with similar results on the fraction of the surface which is active on other cometary nuclei qualitatively supports the widely discussed picture involving a mantle which gradually builds up on the surface of the nucleus, thereby choking off the vaporization.

IV. SUMMARY

Simultaneous photometry at infrared and optical wavelengths has allowed us to determine the albedo, size, and projected shape of the nucleus of comet P/Tempel 2. In gross size and shape it appears to be nearly identical to the nucleus of P/Halley, a prolate spheroid with axes 16 x 8 1/2 x 8 1/2 km. It differs from that of P/Halley in that the active portion of the surface is much less, of order 1% as opposed to an estimated 15–30% for P/Halley. The rotational period of the nucleus is near 9 hours, the second shortest of the photometrically determined rotational periods for comets. The outgassing and the changes in the observed amplitude of the rotational modulation appear to be consistent with the nuclear model for this comet by Sekanina (1987) although other aspects of the model (such as the assumption that the nucleus is oblate) appear to need revision. The spectral

reflectivity of the nucleus is red in the optical, but there is a suggestion that the reflectivity increases in the ultraviolet. In the optical the redness is significantly greater than for P/Halley and comparable to the redness of some but not all other cometary nuclei and D asteroids. The increase at ultraviolet wavelengths, if real, is similar only to that seen for P/S-W1.

Observations of the nuclei of several periodic comets in recent years have made it clear that they are all dark and usually very aspherical. Furthermore, most of the surface is inactive on the nuclei of all periodic comets for which the relevant data exist. There is a selection effect in this conclusion because nuclei active over their entire surface are much harder to detect inside the coma. Nevertheless, a picture of gradual development of a mantle culminating in extinction of activity qualitatively fits all the available data on cometary nuclei. It is still premature to make statements regarding the distribution of sizes or rotational periods because the sample of objects is too small and, at least as far as sizes are concerned, subject to very strong selection effects. Finally, it seems clear that nuclei differ significantly from one another in their spectral reflectivity. Although there are many similarities to D and C asteroids, there also appear to be significant differences. For this reason, there is as yet no physical connection that can be directly established between cometary nuclei and Amor-Apollo asteroids.

V. ACKNOWLEDGEMENTS

We particularly thank Wieslaw Wisniewski for providing his lightcurve to us in the short interval between his and our observing runs and Uri Carsenty for carrying out the calculations for the extinction in the OH filter. We thank Larry Lebofsky and Mike Feierberg for providing the programs for the thermal models. We also thank Dave Jewitt for providing his results prior to publication and Bob Hawaii Brown for informative discussions of the effects of asphericity on the thermal models. MFA'H was supported by NASA grant NSG 7322, HC was supported by NSF grant ~~xxxx~~ and University of Arizona contract ~~zzzz~~ to PSI, and DGS and RLM were supported by NASA contract NGR-03–003–001. This is PSI contribution yyy.

1 1 3 4 3 3

AST 87 18071

REFERENCES

[1] A'Hearn, M. F. (1988). Observations of cometary nuclei. *Ann. Rev. Earth Planet. Sci.* **16**, 273–293.

[2] A'Hearn, M. F., Feldman, P. D., Roettger, E., and Schleicher, D. (1988). Periodic comet Tempel 2 (1987g). IAU Circular 4622.

[3] A'Hearn, M. F., Schleicher, D. G., Feldman, P. D., Millis, R. L., and Thompson, D. T. (1984). Comet Bowell 1980b. *Astron. J.* **89**, 579–591.

[4] Baum, W. A., and Kreidl, T. J. (1986). Volatiles in cometary grains. In *Asteroids, Comets, Meteors II*. (C.-I. Lagerkvist, B. A. Lindblad, H. Lundstedt, and H. Rickman, Eds.). Uppsala Universitet, Uppsala, pp. 397–402.

[5] Brown, R. H. (1985). Ellipsoidal geometry in asteroid thermal models: The standard radiometric model. *Icarus* **64**, 53–63.

[6] Campins, H., A'Hearn, M. F., and McFadden, L.-A. (1987). The bare nucleus of comet Neujmin 1. *Astrophys. J.* **316**, 847–857.

[7] Cochran, A. L., Cochran, W. D., and Barker, E. S. (1982). Spectrophotometry of comet Schwassmann-Wachmann 1. II. It's color and CO+ emission. *Astrophys. J.* **254**, 816–822.

[8] Cowan, J. J., and A'Hearn, M. F. (1979). Vaporization of comet nuclei: Light curves and lifetimes. *The Moon and the Planets* **21**, 155–171.

[9] Cruikshank, D. P., and Brown, R. H. (1983). The nucleus of comet p/Schwassmann-Wachmann 1. *Icarus* **56**, 377–380.

[10] Fay, T. D., J., and Wisniewski, W. (1978). The light curve of the nucleus of comet d'Arrest. *Icarus* **34**, 1–9.

[11] Feldman, P. D., and A'Hearn, M. F. (1985). Ultraviolet albedo of cometary grains. In *Ices in the Solar System*. (J. Klinger, D. Benest, A. Dollfus, and R. Smoluchowski, Eds.). D. Reidel, Dordrecht, pp. 453–461.

[12] Festou, M. C. (1981). The density distribution of neutral compounds in cometary atmospheres. I. Models and equations. *Astron. Astrophys.* **95**, 69–79.

[13] Jewitt, D., and Luu, J. (1989). A ccd portrait of comet P/Tempel 2. *Astron. J.* **97**. in press.

[14] Jewitt, D. C., and Luu, J. (1988). Comet P/Tempel 2. IAU Circular 4582.

[15] Jewitt, D. C., and Meech, K. J. (1987). Surface brightness profiles of 10 comets. *Astrophys. J.* **317**, 992–1001.

[16] Jewitt, D. C., and Meech, K. J. (1988). Optical properties of cometary nuclei and a preliminary comparison with asteroids. *Astrophys. J.* **328**, 974–986.

[17] Marsden, B. G. (1985). Non-gravitational forces on comets: The first fifteen years. In *Dynamics of Comets: Their Origin and Evolution*, (A. Carusi and G. B. Valsecchi, Eds.), pp. 343–352, D. Reidel Publishing Co., Dordrecht. IAU Symposium.

[18] Millis, R. L., A'Hearn, M. F., and Campins, H. (1988). An investigation of the nucleus and coma of comet P/Arend-Rigaux. *Astrophys. J.* **324**, 1194–1209.

[19] Öpik, E. J. (1963). The stray bodies in the solar system. Part 1. Survival of cometary nuclei and the asteroids. *Advances in Astronomy and Astrophysics* **2**, 219–262.

[20] Sekanina, Z. (1979). Fan-shaped coma, orientation of rotation axis, and surface structure of a cometary nucleus. I. Test of a model on four comets. *Icarus* 37, 420–442.

[21] Sekanina, Z. (1987). Anisotropic emission form comets: Fans versus jets. II. Periodic comet Tempel 2. In *Symposium on the Diversity and Similarity of Comets*, (E. J. Rolfe and B. Battrick, Eds.), pp. 323–336, ESA Publications Division, Noordwijk. ESA SP-250.

[22] Sekanina, Z. (1988). Periodic comet Tempel 2 (1987g). IAU Circular 4624.

[23] Spinrad, H., Stauffer, J., and Newburn, Jr., R. L. (1979). Optical spectrophotometry of comet Tempel 2 far from the sun. *Pub. Astron. Soc. Pac.* 91, 707–711.

[24] Stellingwerf, R. F. (1978). Period determination using phase dispersion minimization. *Astrophys. J.* 224, 953–960.

[25] Thomas, N., and Keller, H. U. (1989). The colour of comet Halley's nucleus and dust. *Astron. Astrophys.*, in press.

[26] Tokunaga, A. T. (1986). *Photometry Manual*. NASA Infrared Telescope Facility.

[27] Weissman, P., A'Hearn, M. F., McFadden, L.-A., and Rickman, H. (1989). Evolution of comets into asteroids. In *Asteroids II*. (R. Binzel and M. S. Matthews, Eds.). University of Arizona Press, Tucson. in press.

[28] Wetherill, G. W. (1988). Where do the Apollo objects come from? *Icarus* 76, 1–18.

[29] Whipple, F. L. (1950). A comet model. I. The acceleration of comet Encke. *Astrophys. J.* 111, 375–394.

[30] Wisniewski, W. (1988). Periodic comet Tempel 2 (1987g). IAU Circular 4603.

FIGURE CAPTIONS

Figure 1. Observed lightcurve of comet P/Tempel 2 in reflected optical light and thermal infrared radiation on 1988 June 10 UT. The optical observations were made with a 10.1–arcsec aperture and the infrared observations were made with a 7.0–arcsec aperture.

Figure 2. Same as Figure 1 but for 1988 June 11.

Figure 3. Phase-dispersion-measure for the lightcurve of comet P/Tempel 2 as a function of period. The statistic is shown for each of the three wavelengths at which lightcurves were obtained, 4845 Å, 6840 Å, and 10.1 μm. All show their deepest minimum at 4.45 hours which yields a single-peaked light curve and we believe that the correct rotational period is the one indicated by the broad but shallower minimum at twice that period, 8.9 hours.

Figure 4. Phased lightcurves for comet P/Tempel 2 assuming a period of 8.9 hours including data from 1988 June 9 (4845 Å only; filled triangles), June 10 (open circles), and June 11 (filled circles). Zero phase is at 1988 June 9, 7.75 hrs UT.

Figure 5. Variation of flux with aperture at 10.1 μm. The data are consistent with the absence of any coma.

Figure 6. Variation of flux with aperture in the optical region. Straight lines have been fitted by least squares and indicate that a coma is definitely present. The average slope was used for removal of coma from the data.

Figure 7. Rotational lightcurve of the nucleus of comet P/Tempel 2. The optical observations have been corrected for the contribution by the coma. The difference in amplitude between the optical and infrared could be due to incomplete correction for coma but could also be an effect due to the enhanced amplitude of a prolate spheroid in its thermal emission. Zero phase is 1988 June 9, 7.75 hours UT.

Figure 8. Spectral reflectivity of the nucleus of comet P/Tempel 2. The two points at the shortest wavelengths differ from the extrapolated relationship from longer wavelengths by only about three standard deviations but appear to represent a real feature.

APPENDIX E

THEORETICAL PREDICTIONS OF VOLATILE BEARING PHASES AND VOLATILE RESOURCES IN SOME CARBONACEOUS CHONDRITES

Jibamitra Ganguly
Department of Geosciences
University of Arizona, Tucson, AZ 85721

Surendra K. Saxena
Department of Geology
Brooklyn College, Brooklyn, NY 11280

5/9-90

14655

N91-25222

Abstract

Carbonaceous chondrites are usually believed to be the primary constituents of near-Earth asteroids and Phobos and Diemos, and are potential resources of fuels which may be exploited for future planetary missions. In this work we have calculated the nature and abundances of the major volatile bearing and other phases, including the vapor phase, that should form in C1 and C2 type carbonaceous chondrites as functions of pressure and temperature. The results suggest that talc, antigorite ± magnesite are the major volatile bearing phases and are stable below 400°C at 1 bar in these chondritic compositions. Simulated heating of a kilogram of C2 chondrite at fixed bulk composition between 400 and 800°C at 1 bar yields about 135 gm of volatile, which is made primarily of H_2, H_2O, CH_4, CO_2 and CO. The relative abundances of these volatile species change as functions of temperature, and on a molar basis, H_2 becomes the most dominant species above 550°C. In contrast, C1 chondrites yield about 306 gm of volatile under the same condition, which consist almost completely of 60 wt% H_2O and 40 wt% CO_2. Preliminary kinetic considerations suggest that equilibrium dehydration of hydrous phyllosilicates should be attainable within a few hours at 600°C. These results provide the framework for further analyses of the volatile and economic resource potentials of carbonaceous chondrites.

Introduction

The near-Earth asteroids are potential resources of volatiles which can be used as propellants and life supporting purposes for planetary missions. As emphasized by Lewis and Lewis (1), these asteroids are at times the nearest bodies to Earth, and many of them can pass between Earth and Moon. These authors have also shown that within any arbitrary three-year period, there are roughly 300 and 90,000 launch opportunities to respectively kilometer and 100-meter sized asteroidal bodies as compared to 39 lunar launch windows. These facts and the potential volatile resources make the asteroids important candidates for detailed analyses for supporting future planetary missions.

Cost-effective or energy-efficient extraction of volatiles from the asteroids require knowledge of the nature and modal abundances of the constituent minerals in which the volatile components are structurally bound. There has been several studies on reflectance spectroscopy of near-Earth asteroids to characterize the nature of the volatile bearing minerals (2,3). While these studies report absorption band near 3 μm suggesting presence of hydrous phyllosilicates, more precise characterizations were equivocal. An obvious alternative approach to the resolution of the problem is to examine directly the asteroidal materials.

The spectral and density characteristics strongly suggest that a significant fraction of the near-Earth asteroids are made of carbonaceous chondrites (1,4). The most volatile rich of these meteorites are what are commonly known as C1 or (CI) and C2 (or CM) classes. However, the grain size of the volatile bearing phases are often too small (100 to 1000 A) (5) to permit identification under optical microscope, and are best observed under high resolution transmission electron microscopy (HRTEM). Zolensky and McSween (5) have recently presented a summary of volatile bearing phases identified in the carbonacous chondrites.

The primary objective of this work is to carry out theoretical calculations to predict modal abundances and compositions of the major mineral phases, along with the abundance and composition of the coexisting vapor phase, that could develop in the bulk compositions of C1 and C2 chondrites as functions of pressure and temperature. The results would provide the framework for engineering designs for the extraction of volatile components from asteroids as well as Phobos and Deimos, the two small natural satellites of Mars, which are also likely to be made of carbonaceous chondrites (1).

Theoretical Method

Principles

According to Duhem's theorem in classical thermodynamics (6,7), the equilibrium state of a closed system (i.e., a system of fixed composition and mass) is completely determined if any two variables are fixed regardless of whether these are intensive, extensive, or a combination of both. Ganguly and Saxena (7) have recently reviewed the various methods by which one may carry out the actual computation of the equilibrium assemblages. The

Table 1 Bulk chemical compositions of C1 and C2 carbonaceous chondrites

	C1	C2
Si	10.40	12.96
Ti	0.04	0.06
Al	0.84	1.17
Cr	0.23	0.29
Fe	18.67	21.56
Mn	0.17	0.16
Mg	9.60	11.72
Ca	1.01	1.32
Na	0.55	0.42
K	0.05	0.06
P	0.14	0.13
Ni	1.03	1.25
Co	0.05	0.06
S	5.92	3.38
H	2.08	1.42
C	3.61	2.30
O	45.61	41.74

method used in this study obtains the compositions and abundances of the equilibrium phase assemblages by minimizing the Gibbs Free Energy (G) of the system at fixed P-T conditions. The minimization is constrained to conserve the various elemental masses of the system through the method of Lagrangian multipliers (7). Because of the extremely small grain size of the phyllosilicates observed in carbonaceous chondrites, one should consider the effects of surface free energy on the formation of these phases. As a first approximation, we have, however, ignored this effect. Therefore, the actual equilibrium temperatures of volatile bearing phases could be lower than those predicted by our calculations.

System, Phases and Data Base

Table 1 shows the bulk compositions of C1 and C2 carbonaceous chondrites. These compositions are based on analyses of a number of fragments of Orgueil and

Table 2 Phases in the system Mg-Fe-Si-C-H-O-S considered in this work

The sources of thermochemical data are shown by reference numbers within parentheses. The Heat of Formation of the Fe-end members of the hydrous phyllosilicates are derived in this work.

Anhydrous Silicates and Oxides		
Olivine	$(Mg,Fe)_2SiO_4$	(8)
Orthopyroxene	$(Mg,Fe)SiO_3$	(8)
Periclase	$(Mg,Fe)O$	(23)
Quartz	SiO_2	(17)
Cristobalite	SiO_2	(17)
Hematite	Fe_2O_3	(23)
Magnetite	Fe_3O_4	(23)
Hydrous and Carbonate Phases		
Anthophyllite	$(Mg,Fe)_7Si_8O_{22}(OH)_2$	(8,27)
Talc	$(Mg,Fe)_3Si_4O_{10}(OH)$	(8)
Antigorite	$(Mg,Fe)_{48}Si_{34}O_{85}(OH)_{62}$	(8)
Chrysotile	$(Mg,Fe)_3Si_2O_5(OH)_4$	(8)
Brucite	$(Mg,Fe)(OH)_2$	(17,24)
Magnesite	$(Mg,Fe)CO_3$	(17,25)
Sulfides and Elements		
Troilite	FeS	(17)
Pyrite	FeS_2	(17)
Iron	Fe	(26)
Sulfur	S	(17)
Graphite	C	(17)
Vapor Phase	C-O-H-S	(15,16,17)

Species: H_2O, CO_2, CH_4, CO, O_2, H_2S, S_2, SO_2, COS

Murchison meteorites, respectively, and are summarized in Dodd (22). It can be easily seen from this table that the subsystem Mg-Fe-Si-C-H-O-S (MFCHOS) constitutes almost 96% by weight of the bulk compositions of C1 and C2 chondrites. In order to somewhat simplify the computational problem, we have confined the G minimization calculation to this subsystem, but evidently the phases whose compositions form outside of this subsystem cannot be major constituents of these chondrites.

Table 2 shows the list of phases that we have considered as possible crystallizing phases within the above subsystem along with the sources of the thermochemical data. The choice of these phases have been guided by the published reports of the mineralogy of carbonaceous chondrites whose compositions lie within the system MFCHOS (e.g., Zolensky and McSween (5)). The selection of thermochemical data in the system Mg-Si-O-H is based on the critical analysis of Chatterjee (8,11) for consistency with both calorimetric and experimentally determined phase equilibrium measurements. These data are similar to those of Berman (9). However, unlike those in Berman, the data are also consistent with high P-T experimental data involving distribution of Fe and Mg among coexisting silicates.

The heat capacities (C_p) and entropies (S^o) of the phases, if not available in any of the recent systematizations of self-consistent data set, are estimated by stoichiometric summation of the properties of oxides and structurally analogous compounds, as discussed in a number of publications (13,14).

There are no thermochemical data for the Fe-end members of the phyllosilicates listed in Table 2. The enthalpies of these phases are estimated according to the known relative properties of Fe- and Mg-end members of biotite, which is also a phyllosilicate. The data derived by Chatterjee (8) and Robie and Hemingway (10) for the Mg- and Fe^{2+}-end members (phlogopite and annite, respectively) yield an enthalpy difference of -359.566 KJ per mole of divalent cation at 1 bar, 298 K. We have used these values to estimate the enthalpies of formation from elements of Fe-end members of phyllosilicates at 1 bar, 298 K from the available data for the Mg-end members. The results are as follows (KJ/mol of Fe). Fe-talc: -1606.80; Fe-antigorite: -1127.53 and Fe-chrysotile: -1094.87. The corresponding values of the free energy of formation from elements (ΔG_f^o) for Fe-talc and Fe-antigorite at 1 bar, 298 K are -4477.18 and -4784.0 KJ/mol of Fe^{2+}, respectively.

The validity of the estimated thermochemical properties of the Fe-end members of the phyllosilicates may be tested as follows. The Fe-end members of talc and antigorite are unstable. Instead, the stable phases are closely analogous compounds, namely, minnesotite, which has a stoichiometry of $Fe_{27}Si_{36}O_{86}(OH)_{26}$ as compared to that of $Fe_{27}Si_{36}O_{90}(OH)_{18}$ for Fe-talc, and greenalite with a stoichiometry of $Fe_{48}Si_{32}O_{80}(OH)_{64}$ compared to $Fe_{48}Si_{34}O_{85}(OH)_{62}$ for Fe-antigorite. Anovitz et al. (12) have recently determined ΔG_f^o of minnesotite and greenalite from phase equilibrium data. Their results, ΔG_f^o (minnesotite) = -4577.78 KJ and ΔG_f^o (greenalite) = -4799.50 KJ, differ in the right direction from the corresponding values of Fe-talc and Fe-antigorite, considering the relative stabilities of the phases.

The stereochemical environments of divalent cations in biotite are quite similar to those in talc, both being 2:1 (TOT) layer silicates, and partly similar to those in antigorite, which is an 1:1 (TO) layer silicate (28). Thus, these phyllosilicates should have similar differences between the enthalpies of formation of the Fe- and Mg-end members. Further, since on the basis of observational data, the predicted compositions of the mineral phases in carbonaceous chondrites are expected to be Mg-rich, the effects of errors in the Fe-end member thermochemical properties and solid solution model will be relatively small. This can be easily understood by considering the form of G-X curve of a stable solution and evaluating the effects of errors in above properties near Mg-terminal segment.

The thermodynamic mixing properties of the Fe^{2+}- and Mg-end member components of the anhydrous silicates are taken from the self-consistent summary of Chatterjee (8), while those of the phyllosilicates are assumed to be ideal for the lack of any data. The latter assumption is likely to be approximately valid at $T \geq 600^oC$, since at these conditions biotite solid solution is found to behave approximately ideally (7). At lower temperature, the phyllosilicates may deviate from ideal solution behavior, but perhaps not too dissimilarly to significantly affect their relative stabilities. Magnesite is also assumed to be an ideal solution of Fe-Mg components. As emphasized by Ganguly and Saxena (7), the computed dehydration conditions are not very sensitive to errors in activity-composition relations since the devolatilization equilibria are characterized by large enthalpy changes. The iron oxides and sulfides are considered to be stoichiometric phases since the solid solutions of Mg are around a few percent at the temperatures of interest.

The fluid properties are taken from Saxena and Fei (15,16) and Robie et al. (17). The "corresponding state method" of estimating P-V-T relation, as discussed by these authors, is extended to include the sulfur species. For mixing data, we have assumed that H_2S behave as H_2O, S_2 as

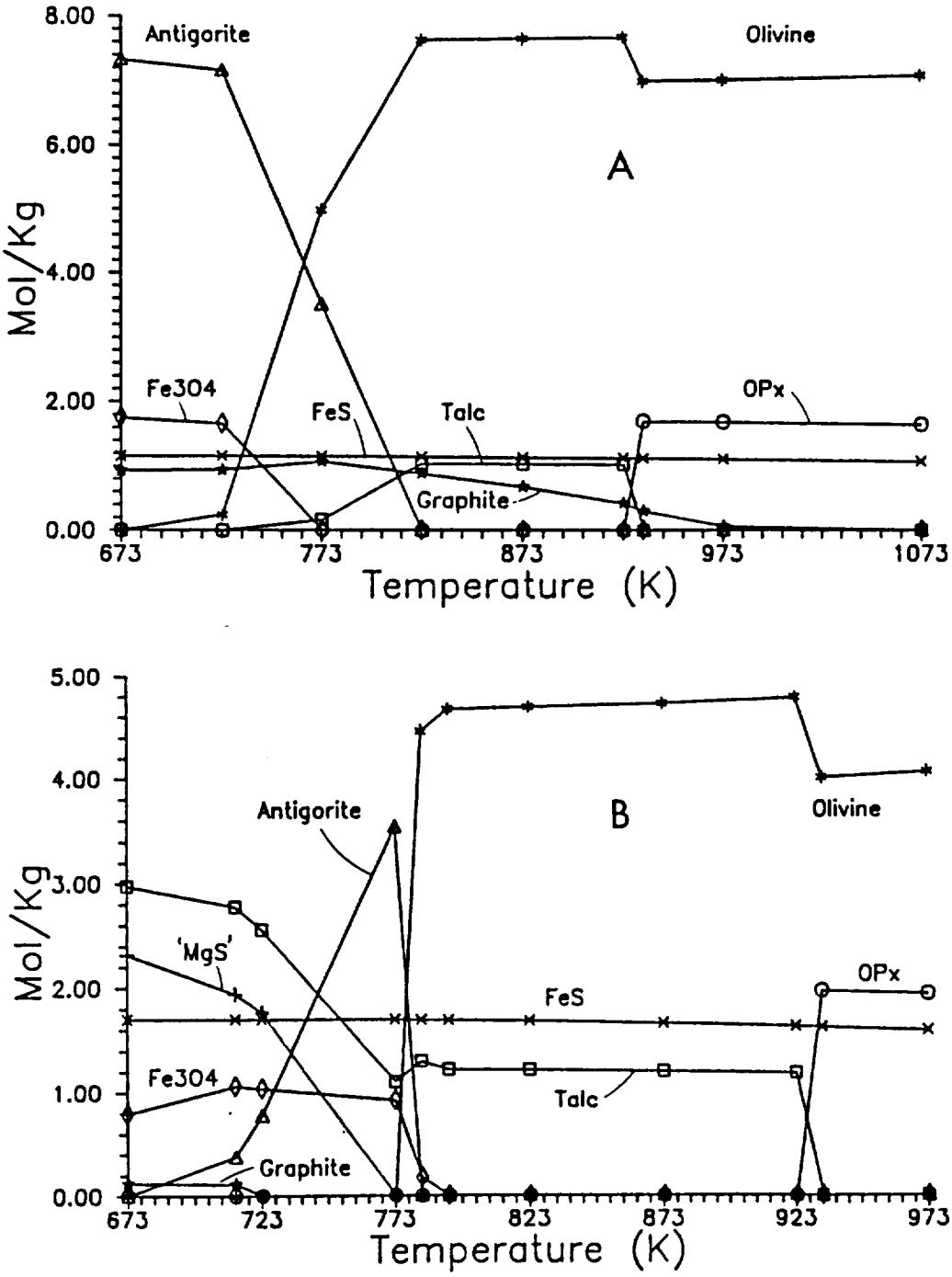

Fig. 1 Calculated modal abundances of minerals per kilogram of rock in (a) C1 and (b) C2 carbonaceous chondritic bulk compositions as functions of temperature at 2 Kb. The steps in the calculations are shown by symbols.

O_2, and SO_2 and COS as CO_2, and used the equivalent binary interaction parameters from Saxena and Fei (15).

Results

At 1 bar, the free energy minimization calculations do not yield any volatile bearing phase at $T \geq 400^{\circ}C$. At the present state of the thermochemical data, we do not believe that our calculations are reliable at lower temperatures. Indeed, we find results at lower temperatures which do not seem to follow the systematics of the results obtained at higher temperatures. Thus, we have calculated the equilibrium phase assemblages at a pressure of 2 Kb so that the volatile bearing phases appear at higher temperatures. This procedure at least permits recognition of the major volatile bearing phases. Some of these phases may be re-

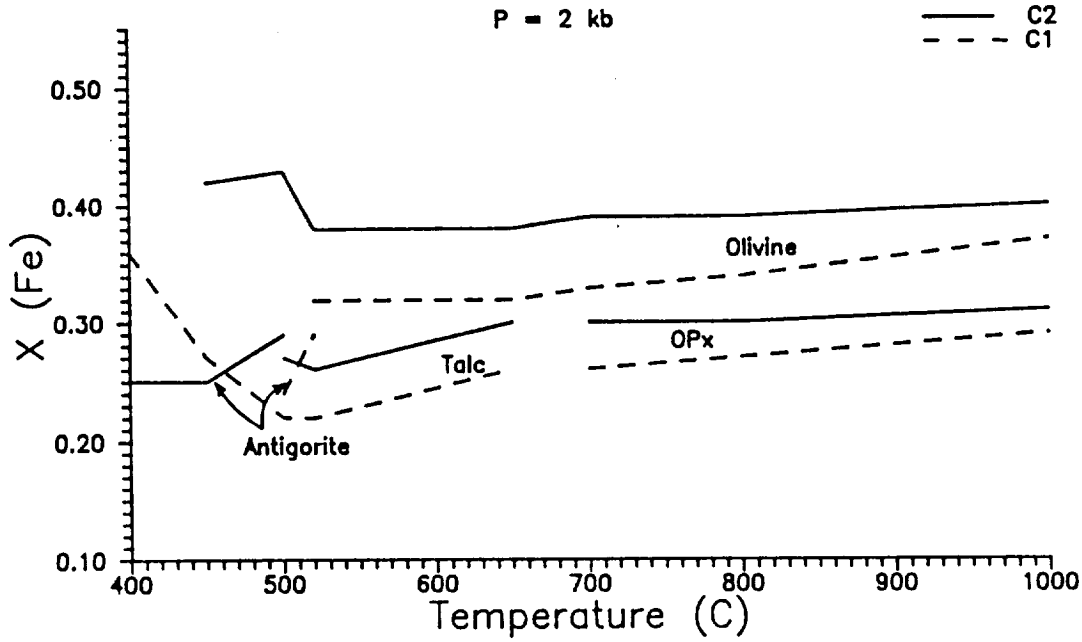

Fig. 2 Calculated compositions of the silicate phases in C1 and C2 carbonaceous chondrites as functions of temperature at 2 Kb.

placed by more stable assemblages at lower temperature, but should reappear during heating experiment. The results, which are illustrated in Figure 1, show that the primary volatile bearing phases in the C1 and C2 bulk compositions are talc, antigorite ± magnesite. Talc is stable to around 650°C at 2 Kb, and dehydrates to orthopyroxene (OPx) at higher temperature according to Tc + Ol = 5 OPx + H_2O. Antigorite and magnesite crystallize at T < 550°C, but magnesite is absent in C2 bulk composition at T ≥ 400°C. FeS is a stable phase at all temperatures investigated in this work. We, however, did not consider the formation of sulfate or pyrrhotite. Magnetite becomes a stable phase at T ≤ 500°C. Elemental sulfur found in C1 chondrite is invariably associated with pyrrhotite ($Fe_{1-x}S$) (5). This suggests decomposition of troilite (FeS) to pyrrhotite and sulfur.

Figure 2 shows the compositions of the ferromagnesian phases as function of temperature at 2 Kb for the C1 and C2 bulk compositions. Calculations at 1 bar also yield similar compositions. The observed compositions of these phases in the carbonaceous chondrites vary widely in Fe/Mg ratio. One way to achieve this diverse Fe/Mg ratio is by aqueous alteration which seems to be a characteristic of the carbonaceous chondrites. Fe^{2+} fractionates very strongly into an aqueous phase relative to the silicates (18). Thus, varying degrees of equilibration with an aqueous phase could lead to a spectrum of Fe/Mg compositions of the ferromagnesian silicates. Aqueous alteration may not be the sole reason, but is likely to be an important contributing factor in the development of variable Fe/Mg ratio of the ferromagnesian silicates in carbonaceous chondrites.

The abundances of volatile species in equilibrium with the solids per kilogram of total mass of C2 chondrites are illustrated in Figure 3. Figures 3a and 3b illustrate the molar and mass abundances, respectively, as functions of temperature at 1 bar. It should be noted that the total mass of the volatiles do not change above 400°C, which means that under equilibrium condition C2 chondritic material will completely devolatize if heated above 400°C. The total yield of the volatile is about 14% of the initial mass of C2 chondrites. The change in the abundance of various species above 400°C is due to homogeneous reactions within the fluid phase. Above 550°C, hydrogen has the highest molar concentration in the vapor phase. Hydrogen is a very good propellant and reducing agent which may thus be preferentially extracted by heating the C2 chondritic material to T > 550°C.

In contrast to the C2 chondrites, the volatiles given off by C1 material above 400°C consist essentially of H_2O and CO_2 at 1 bar pressure. Per kilogram of material, the total yield of volatile is about 306 grams of which nearly 60 wt% is H_2O.

The above results are subject to considerable uncertainties owing to the

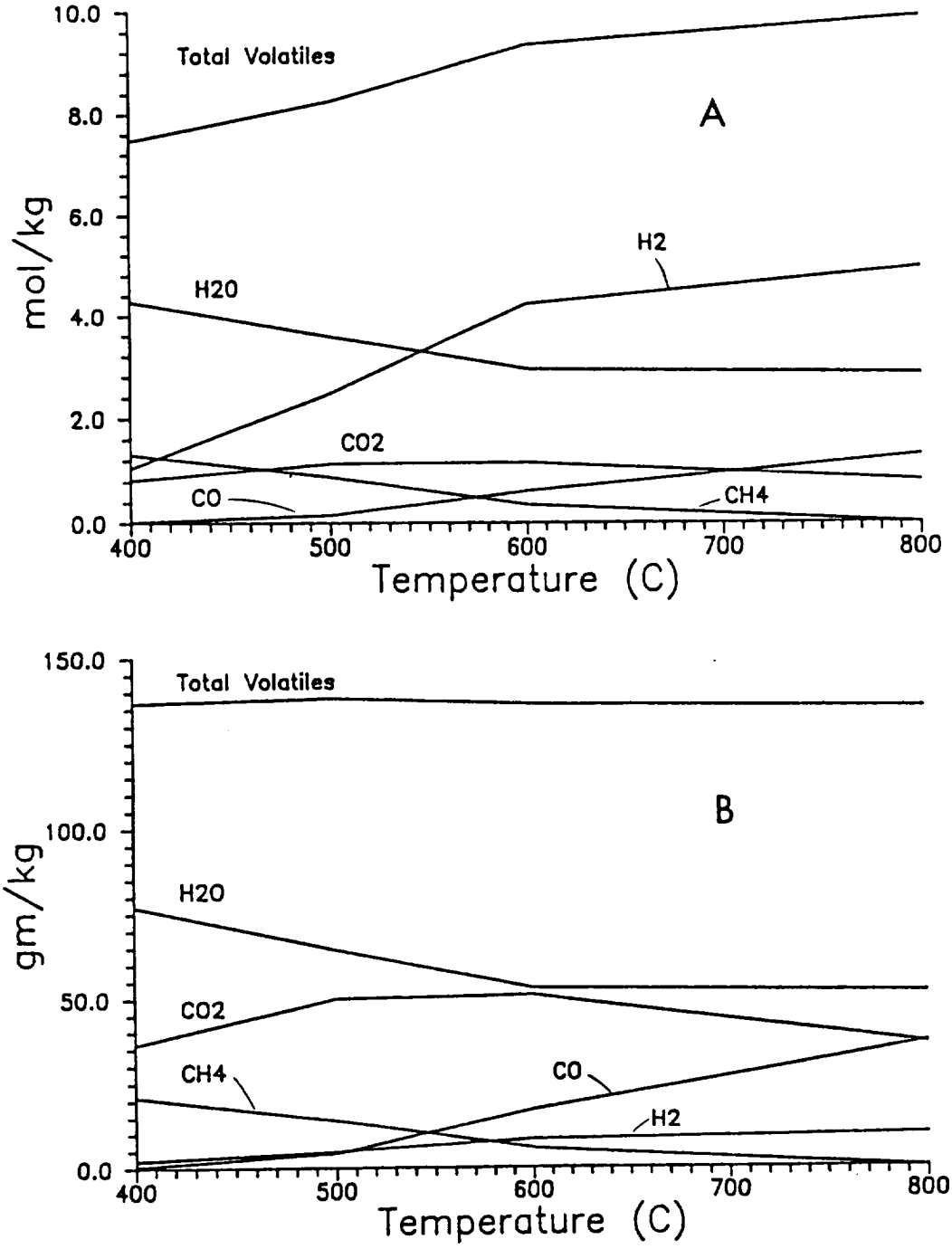

Fig. 3 Calculated equilibrium (a) molar and (b) mass abundances of the volatile species per kilogram of C2 chondritic material.

approximate nature of the thermochemical properties of the phyllosilicate solid solutions, and also since we have ignored the effects of surface free energy on the formation of extremely fine grained crystals. Further, carbonaceous chondrites of any given type do not have homogeneous compositions, but instead probably represent agglomeration of materials formed at different conditions at different parts of the solar system. However, these calculations are still useful in providing an idea of the relative stabilities, as well as upper stabilities of the volatile bearing phases and their average abundance. It is interesting to note that recent reflectance spectroscopic studies of carbonaceous chondrites seem to corroborate the predictions made above as to the nature of the most abundant hydrous phases (Gaffey, pers. comm.).

Kinetics of Devolatilization

The equilibrium calculations presented above provide a framework for the

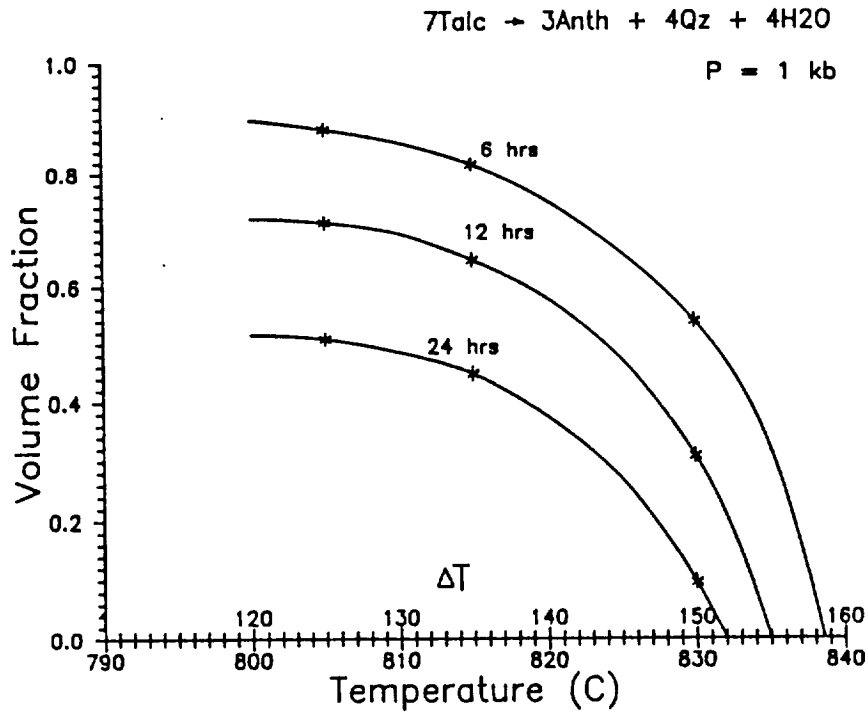

Fig. 4 Dehydration of talc as functions of time, temperature and extent of overstepping above the equilibrium dehydration boundary at 1 Kb. Volume fraction is that of talc remaining after reaction. Experimental data points, shown by asterisks, are from Greenwood (19).

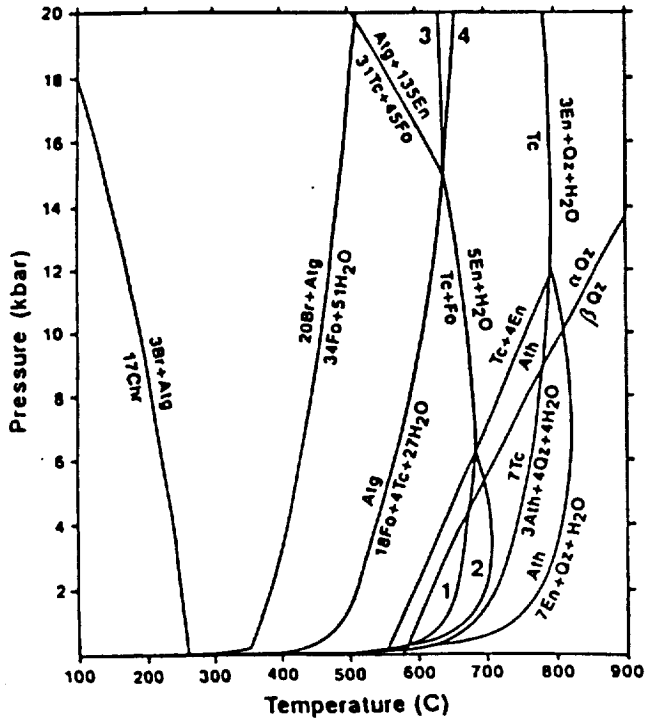

Fig. 5 Equilibrium relations of talc, antigorite and brucite along with other minerals in the system $MgO-SiO_2-H_2O$. Reproduced from Evans and Guggenheim (21).

evaluation of the volatile as well as some mineralogical resource potential of C1 and C2 carbonaceous chondrites. The actual extraction of volatiles as a function of temperature and heating rate, however, depends on the kinetics of the devolatilization process. For kinetic analysis, it is essential to identify the minerals in which the volatiles are most likely to be structurally bound. The above results suggest that talc, antigorite and magnesite are likely to be the major volatile bearing phases in carbonaceous chondrites.

Except for pure Mg-talc, there are no kinetic data for the other volatile bearing phases. The dehydration kinetics of talc was determined by Greenwood (19). At a given temperature, the rate of reaction depends on the rate constant, $K^{\ddagger}$, and the extent of departure from the equilibrium boundary. This is expressed in transition state theory (20) according to the relation $\text{Rate} = K^{\ddagger}(1-\exp(n\Delta G/RT))$, where n is a constant, commonly assumed to be unity, and ΔG is the Gibbs free energy of the reaction at the P,T condition of interest. Figure 4, which is constructed from Greenwood's experimental data, illustrates the dehydration kinetics of talc as functions of time, temperature and extent of overstepping (ΔT) above the equilibrium dehydration boundary at 1 Kb. It is evident from this figure that essentially complete dehydration of talc can be achieved within

6 hours at about 160°C above the equilibrium boundary.

The stability fields of the pure Mg-end members of various phyllosilicates of interest in this study are summarized for the condition of $P_{total} = P_{H2O}$ in Figure 5, which is reproduced from Evans and Guggenheim (21). According to our results, talc and other phyllosilicates completely dehydrate at $\geq 400^{\circ}C$ at 1 bar in C1 and C2 bulk compositions. This is compatible with the phase relations shown in Figure 5. Thus, based on the results shown in Figure 4, one would anticipate that essentially complete dehydration of all phyllosilicates in C1 and C2 chondritic material is likely to be achieved in a matter of a few hours at $T \geq 600^{\circ}C$. Detailed studies of the devolatilization kinetics of both phyllosilicates and carbonates as functions of temperature, fluid composition, and grain size are currently under way to evaluate the practical limitations of the extraction of volatiles from carbonaceous chondritic materials.

Acknowledgments

This research was supported by a NASA grant NAGW-1332 administered through the Center for Utilization of Local Planetary Resources at the University of Arizona. Thanks are due to Professor John Lewis for his invitation to join the NASA project and helpful discussions, to Dr. Larry Anovitz for making available his thermochemical data for minnesotite and greenalite before publication, and to Dr. Nilanjan Chatterjee and Kunal Bose for their help in the preparation of the manuscript. The skillful production of the manuscript in camera ready form by Jo Ann Overs is greatly appreciated.

References

1. Lewis, J.S., and Lewis, R.A. (1987) Space resources: Breaking the bonds of Earth. Columbia University Press, New York.

2. Jones, T., Lebofsky, L., and Lewis, J.S. (1989) Asteroidal H_2O and the hydration state of terrestrial raw materials. EOS Trans. Amer. Geophys. Union 70, 379.

3. Gaffey, M.J., and McCord, T.B. (1979) Mineralogical and petrological characterizations of asteroid surface materials, in Gehrels, T. (ed.) Asteroids, pp. 688-723, University of Arizona, Tucson.

4. Lewis, J.S., and Prinn, R.G. (1984) Planets and their atmospheres. Academic Press.

5. Zolensky, M., and McSween, H.S. (1988) Aqueous alteration, in Kerridge, J.F., and Mathews, M.S. (eds.) Meteorites and the early solar system, University of Arizona Press, Tucson.

6. Prigogine, I., and Defay, R. (1954) Chemical thermodynamics. Longman, London.

7. Ganguly, J., and Saxena, S.K. (1987) Mixtures and mineral reactions. Springer-Verlag.

8. Chatterjee, N. (1989) An internally consistent thermodynamic data base on minerals. Ph.D. thesis, City University of New York.

9. Berman, R.G. (1988) Internally consistent thermodynamic data for minerals in the system Na_2O-K_2O-CaO-MgO-FeO-Fe_2O_3-Al_2O_3-SiO_2-TiO_2-H_2O-CO_2. J. Petrology 29, 445-552.

10. Robie, R.A., and Hemingway, B.S. (1984) Heat capacities and entropies of phlogopite and paragonite between 5 and 900 K and estimates of enthalpies and Gibbs free energy of formation. Amer. Mineralogist 69, 858-868.

11. Chatterjee, N. (1987) Evaluaton of thermochemical data on Fe-Mg olivine, orthopyroxene, spinel and Ca-Fe-Mg-Al garnet. Geochim. Cosmochim. Acta 51, 2515-2525.

12. Anovitz, L.M., Essene, E., and Hemingway, B.S. (1989) Self-consistent thermodynamic data for the system Fe-Si-C-O-H: Applications to metamorphosed banded iron formations and iron-rich blueschists. Geochim. Cosmochim. Acta, in submission.

13. Lewis, G.N., and Randall, M. (1961) Thermodynamics. McGraw-Hill.

14. Helgeson, H.C., Delaney, J.M., Nesbitt, H.W., and Bird, D.K. (1978) Summary and critique of the thermodynamic properties of rock-forming minerals. Amer. J. Sci. 278A, 1-229.

15. Saxena, S.K., and Fei, Y. (1988) Fluid mixtures in the C-H-O system at high pressure and temperature. Geochim. Cosmochim. Acta 52, 505-512.

16. Saxena, S.K., and Fei, Y. (1987) High pressure and high temperature fluid fugacities. Geochim. Cosmochim. Acta 51, 783-791.

17. Robie, R.A., Hemingway, B.S., and Fisher, J.R. (1978) Thermodynamic properties of minerals and related substances at 298.15 K and 1 bar (10^5 pascals) pressure and higher temperatures. U.S. Geol. Survey Bull. 1452.

18. Eugster, H.P., and Ilton, E.S. (1983) Mg-Fe fractionation in metamorphic environments, in Saxena, S.K. (ed.)

Kinetics and equilibrium in mineral ractions, Springer-Verlag.

19. Greenwood, H.J. (1963) The synthesis and stability of anthophyllite. J. Petrology 4, 317-351.

20. Lasaga, A.C. (1981) Transition state theory, in Lasaga, A.C., and Kirkpatrick, R.J. (eds.) Kinetics of geochemical processes, Reviews in Mineralogy 8, 135-169.

21. Evans, B.W., and Guggenheim, S. (1988) Talc, pyrophyllite, and related minerals, in Bailey, S.W. (ed.) Hydrous phyllosilicates (exclusive of micas), Reviews in Mineralogy 19, 225-294.

22. Dodd, R.T. (1981) Meteorites: A petrological-chemical synthesis. Cambridge University Press.

23. Fei, Y., and Saxena, S.K. (1986) A thermochemical data base for phase equilibrium in the system Fe-Mg-Si-O at high pressure and temperature. Phys. Chem. Minerals 13, 311-324.

24. Babushkin, V.I., Matreyev, G.M., Mohedlov-Petrossyan, O.P. (1985) Thermodynamics of silicates. Springer-Verlag.

25. Barin, I., and Knacke, O. (1978) Thermochemical properties of inorganic substances. Springer-Verlag.

26. Gustafsson, P. (1984) A thermodynamic evaluation of Fe-C system. TRITA-MAC, Royal Inst. of Tech., Stockholm, Sweden.

27. Anovitz, L.M., Essene, E.J., Hemingway, B.S., Komada, N.L., and Westrum, E.F. (1988) The heat capacities of grunerite and deerite: Phase equilibria in the system Fe-Si-C-O-H and implications for the metamorphism of banded iron formations. EOS Trans. Amer. Geophys. Union 69, 515.

28. Bailey, S.W. (1988) Introduction, in Bailey, S.W. (ed.) Hydrous phyllosilicates (exclusive of micas), Reviews in Mineralogy 19, 1-8.